

STRUCTURE AND DYNAMICS OF SEVERAL RARE
GAS-HALOGEN VAN DER WAALS MOLECULES

Thesis by

Dwight David Evard

In Partial Fulfillment of the Requirements
for the Degree of
Doctor of Philosophy

California Institute of Technology
Pasadena, California

1988

(Submitted 21 September 1987)

To the Memory of
My Father

ACKNOWLEDGMENTS

I would like to express my appreciation to my research advisor, Ken Janda, for his patience and guidance throughout my graduate student years. His ideas, insight and excitement about science have helped to make the time fly, or so it seems. Alberto Beswick and Nadine Halberstadt gave me some appreciation for theoretical work, and I will certainly remember their cooking.

I have enjoyed working and sharing with many people the past five years at Caltech and Pitt. The postdocs and fellow graduate students I have worked with have helped to make life enjoyable usually, and bearable always. Some of them are Dave Brinza, Joe Cline, Sally Hair, Brian Reid, N. Sivakumar, Fritz Thommen and the youngest, Craig Bieler. Thank you Fritz, for introducing the group to the wonders of raclette. I greatly enjoyed associating with the Beauchamp group, the Sparks group, and the Pratt lads. Joey, Craig, Sally, Siva and Brian deserve special credit for helping to read, type and tape this thesis. I would also like to thank Rob Coalson for the kind use of his laser printer to print the "final" copy of this thesis.

Finally, I would like to thank my family for their love, understanding and support. And that's the way it is.

ABSTRACT

The structure and dynamics of several rare gas-halogen van der Waals molecules have been studied in the six laser-free jet expansion experiments which are described in this thesis. High resolution (0.01 cm^{-1}) spectra were obtained for one $B \leftarrow X$ transition of both NeBr_2 and NeCl_2 , in order to determine the structure and lifetime of these complexes in the ground and excited states. NeCl_2 was studied extensively at moderate resolution (0.05 cm^{-1}) to probe the potential energy surface and the correlation of the van der Waals bond with the covalent bond. The lifetime of metastable vibrationally excited NeBr_2 $X(v = 1)$ was determined directly by measuring its concentration as a function of distance from the source to the detection region. A pump-probe technique was used to study ArCl_2 to probe the structure and dynamics of the complex. Ar_nCl_2 ($n = 1, 2, 3$) was studied to test the validity of the bond-bond additivity model of binding for the complex. This set of experiments has provided a great deal of information on the nature of the structure and dynamics of the complexes.

TABLE OF CONTENTS	Page
Dedication	ii
Acknowledgements	iii
Abstract	iv
List of Figures	vii
List of Tables	ix
Chapter I.	
Introduction	1
Chapter II.	
Rotational Resolution of the NeBr_2 $B \leftarrow X$ ($10 \leftarrow 0$) Transition	20
Chapter III.	
Rotational Resolution of the NeCl_2 $B \leftarrow X$ ($9 \leftarrow 1$) Transition	30
Chapter IV.	
Molecular Beam-Laser Spectroscopy of the NeCl_2 van der Waals Molecule	51
Chapter V.	
Direct Measurement of the Vibrational Predissociation Lifetime of NeBr_2 in the Ground Electronic State	82

TABLE OF CONTENTS, continued	Page
CHAPTER VI.	
The Structure and Dynamics of the ArCl_2 van der Waals Molecule	103
CHAPTER VII.	
A Test of Atom-Atom Additive Interactions: Ar_nCl_2 , $n = 1, 2, 3$	147
APPENDIX I.	
SHAPE: A Working Manual	164

LIST OF FIGURES

Chapter II.	Rotational Resolution of NeBr₂ (10←0)	
Figure 1.	The B←X (10←0) LIF spectrum	25
Chapter III.	Rotational Resolution of NeCl₂ (9←1)	
Figure 1.	LIF spectrum of Cl ₂ B←X (9←1)	37
Figure 2.	LIF spectrum of NeCl ₂ B←X (9←1)	42
Chapter IV.	Spectroscopy of NeCl₂	
Figure 1.	Cl ₂ B←X (11←1) region	63
Figure 2.	NeCl ₂ near Cl ₂ (7←0)	67
Figure 3.	NeCl ₂ near Cl ₂ (10←0)	69
Figure 4.	NeCl ₂ near Cl ₂ (13←0)	70
Figure 5.	Momentum gap plot for NeCl ₂	73
Chapter V.	Lifetime Measurement for NeBr₂	
Figure 1.	Br ₂ and NeBr ₂ X(v=1) 4 and 11 mm	90
Figure 2.	Intensity ratio NeBr ₂ /Br ₂ vs r	93
Figure 3.	Energy gap plot for NeBr ₂	97
Chapter VI.	Structure and Dynamics of ArCl₂	
Figure 1.	Experimental apparatus	110
Figure 2.	ArCl ₂ (6←0) excitation spectra	114
Figure 3.	Cl ₂ Δv = -1 fragment spectrum	119
Figure 4.	Odd (7←0) excitation spectrum	121
Figure 5.	Even (7←0) excitation spectrum	122
Figure 6.	ArCl ₂ rotational energy levels	124
Figure 7.	Δv = -1 rotational distributions	130

LIST OF FIGURES, continued

Figure 8.	Cl_2 $\Delta v = -2$ fragment spectrum	133
Figure 9.	$\Delta v = -2$ rotational distributions	135
Figure 10.	$\Delta v = -2$ energy levels	139
Figure 11.	$\Delta v = -2$ energy levels in detail	141
Chapter VII. Atom-Atom Additive Interactions		
Figure 1.	Ar_2Cl_2 fragment Cl_2 spectrum	154
Figure 2.	Ar_3Cl_2 fragment Cl_2 spectrum	157
Appendix. SHAPE: A Working Manual		
Figure 1.	Axis system for an asymmetric top	168

LIST OF TABLES

Chapter II.	Rotational Resolution of NeBr_2 ($10 \leftarrow 0$)	
Table I.	Spectral Constants for NeBr_2	26
Chapter III.	Rotational Resolution of NeCl_2 ($9 \leftarrow 1$)	
Table I.	Spectral Constants for Cl_2	39
Table II.	Spectral Data for NeCl_2 ,	46
Chapter IV.	Spectroscopy of NeCl_2	
Table I.	Data for NeCl_2 Transitions	66
Chapter VI.	Structure and Dynamics of ArCl_2	
Table I.	Structure of ArCl_2	118
Table II.	Bond Energies for ArCl_2	127
Chapter VII.	Atom-Atom Additive Interactions	
Table I.	Ar_nCl_2 Bond Energies	159
Appendix I.	SHAPE: A Working Manual	
Table I.	Rotational Constants for ArCl_2	169
Table II.	Character Table for D_2	172
Table III.	Asymmetric Rotor Symmetries	172

CHAPTER I

Introduction

Introduction

The purpose of chemical physics is to explain the basic nature of physical phenomena at a fundamental level. Originally this was done by observing the behavior of bulk material and basing explanations upon the statistical nature of largely unobserved atoms and molecules. More recently, the availability of experimental and theoretical techniques has allowed scientists to directly study the microscopic molecular interactions which are responsible for the macroscopic observations of the bulk properties of matter. There are still many difficulties associated with the study of chemical reactions on the microscopic level, but a variety of model systems provide examples where experiment and theory may meet to explain physical phenomena at a basic level.

Van der Waals molecules provide a convenient model system to test theory against experiment, so the study of their structure and dynamics has become very popular. Several groups are studying triatomic van der Waals molecules consisting of a rare gas atom bound to a diatomic halogen molecule,^{1,2} for which the comparison between experiment and theory can be made with only a few adjustable parameters.³ These triatomic complexes are easily formed in molecular beam expansions and may be probed spectroscopically^{1,2} or by molecular beam resonance techniques.^{4,5} The van der Waals bond in the rare

gas-halogen complex is very weak; typically less than the energy of a quantum of vibration of the halogen stretch for He and Ne compounds. Vibrational predissociation will occur if energy from the vibrational mode of the halogen molecule is transferred to the van der Waals modes. The vibrational predissociation process is thought to proceed on a single adiabatic potential energy surface which makes the predissociation process a theoretically accessible example of intramolecular vibrational relaxation (IVR). Studies of the rare gas-chlorine complexes indicate that for the progression from HeCl_2 to NeCl_2 to ArCl_2 the dynamics may span the range from simple $V \rightarrow T$ vibrational predissociation to IVR.

Background

The first studies of rare gas-halogen van der Waals molecules by Klemperer et al. involved detection of ArClF^4 and KrClF^5 by molecular beam resonance techniques. These ClF complexes have a linear geometry with the rare gas atom bound to the Cl atom. They rationalize the structure by considering the rare gas atom to be a Lewis acid which donates electrons into the lowest unoccupied molecular orbital (LUMO), which is mainly localized at the Cl end of the molecule. Although this model rationalizes the linear geometry of the interhalogen van der Waals molecules, it fails to predict the geometries of the observed rare

gas-homonuclear diatomic halogen complexes. These homonuclear halogen dimers are T-shaped,² indicating a van der Waals atom-atom additive model for the binding. It is apparent that more experimental data is necessary for the development of appropriate theories to determine which is the most important interaction in the formation of the van der Waals bond.

Levy et al. were the first to study the structure of rare gas-homonuclear van der Waals complexes and to directly monitor the vibrational predissociation dynamics. They carried out a detailed study, probing the HeI₂ complex by laser induced fluorescence.⁶⁻⁹ The strong fluorescence of the B←X system of I₂ made possible the detection of both total laser induced fluorescence and dispersed fluorescence. The van der Waals molecule HeI₂ was shown to be responsible for spectral features appearing 3.4 - 4.0 cm⁻¹ to the blue of the (3←0) to (29←0) bandheads of free I₂.⁶ Analysis of the rotational band contours yielded a T-shaped structure for the complex with a 4.5 Å distance from the He to the I₂ center of mass. Homogeneous linewidths were found to vary with the vibrational state excited, corresponding to predissociation lifetimes ranging from 220 picoseconds for v' = 12 to 38 picoseconds for v' = 26.⁷ The vibrational predissociation rates showed a quadratic plus linear dependence on the upper state vibrational quantum number. A study of the

dispersed fluorescence spectrum of HeI_2 excited to the $B(v')$ state showed that the fluorescence was dominated by I_2 in the $B(v' - 1)$ state.⁸ This led to a statement of the propensity rule $\Delta v = -1$ for this predissociative process.

Brinza et al. studied the van der Waals complexes of Cl_2 with Ne.¹⁰ The structure of the NeCl_2 van der Waals molecule was determined to be T-shaped in both the ground and excited states. There was no homogeneous broadening observed in the low resolution (0.2 cm^{-1}) spectroscopy of the complex. However, the observation of NeCl_2 $X(v'' = 1, 2)$ in metastable vibrationally excited states was very interesting. NeCl_2 lives for more than 10^{-5} seconds in the $X(v'' = 1)$ state even though the complex contains over ten times the energy necessary to dissociate the van der Waals bond. This was the first observation of a long lived metastable vibrationally excited complex.

Janda and coworkers studied the van der Waals molecule NeBr_2 using laser induced fluorescence techniques.¹¹ Spectra were recorded at low resolution (0.2 cm^{-1}) for the van der Waals molecule associated with the $(11 \leftarrow 0)$ through the $(30 \leftarrow 0)$ $B^3\Pi(0_u^+) \leftarrow X^1\Sigma_g^+$ transitions of Br_2 . The NeBr_2 bands showed increasing spectral shifts of the complex from the free Br_2 with increasing v' , ranging from 5.5 to 8.8 cm^{-1} . The natural linewidths of the van der Waals features increased from the laser bandwidth limited value of 0.10 cm^{-1} for NeBr_2 $(16 \leftarrow 0)$ to 3.1 cm^{-1} for the $(27 \leftarrow 0)$

band, corresponding to vibrational predissociation lifetimes of 84 and 1.7 picoseconds, respectively. They estimated the dissociation energy in the B state to be $64 \pm 4 \text{ cm}^{-1}$ from the apparent closing of the one quantum predissociation channel near $v' = 27$. The data follow the trends predicted by the gap models discussed below.

Heaven and coworkers¹² observed the van der Waals molecule HeBr_2 B \leftarrow X system at moderate resolution (0.05 cm^{-1}) in a free jet expansion. Spectra were obtained for the (11 \leftarrow 0) through (38 \leftarrow 0) bands and rotational structure for several bands was resolved with analysis consistent with a T-shaped structure. The He to Br_2 center of mass distances are 3.7 Å and 3.8 Å in the ground and excited states, respectively. Lifetimes ranged from > 100 picoseconds to 1.8 ± 0.2 picoseconds for the (12 \leftarrow 0) and (38 \leftarrow 0) bands of $\text{He}^{79}\text{Br}_2$, respectively. An upper limit of 23 cm^{-1} for the HeBr_2 dissociation energy in the B state was provided by observation of rapid predissociation from the $v' = 40$ vibrational level. The lifetimes reported are again consistent with a simple energy gap model for vibrational predissociation.

The first laser induced excitation study of a rare gas-interhalogen van der Waals complex was reported by Skene and Lester.¹³ A spectroscopic feature approximately 3.6 cm^{-1} to the blue of the expected band origin of the ICl B($v' = 3$) \leftarrow X($v'' = 0$) transition was attributed to HeICl .

This is particularly interesting because no fluorescence from uncomplexed ICl was observed for this vibrational level because of subnanosecond electronic predissociation of the ICl. This indicates that the vibrational predissociation of the HeICl van der Waals bond is competitive with the electronic predissociation of the ICl molecule. Analysis yields a lower bound estimate of 550 ± 150 picoseconds for the vibrational predissociation lifetime. Drobits et al.¹⁴ report the use of optical-optical double resonance techniques to study the dynamics of the vibrational predissociation process in the NeICl van der Waals complex. A pump laser excites the $A \leftarrow X$ transition, then at a time up to 15 nanoseconds later a probe laser scans through several $E \leftarrow A$ transitions of ICl while the fluorescence from the E state is collected. The lifetime for NeICl in the A state ($v_A = 14$) is 3 ± 2 nanoseconds based on experimental and theoretical ratios of the complex signal to free ICl as a function of time. The A state ($v_A = 14$) binding energy was determined to be 44 cm^{-1} .

The theoretical treatment of the vibrational predissociation in rare gas-halogen van der Waals complexes is based on the assumption that the stretch vibration of the halogen molecule and the van der Waals stretching mode are only weakly coupled. Beswick and Jortner^{15,16} calculated the vibrational predissociation of T-shaped

complexes where the interaction between the diatomic halogen molecule and the rare gas atom was represented by a sum of Morse atom-atom potentials. The resulting close-coupling scattering equations could not be solved analytically, but numerical solutions gave vibrational predissociation rates from the widths of the resulting resonances. The model predicts that the predissociation rates have a strong inverse dependence on the energy difference between the initially bound complex and the final dissociated state. This energy gap model correctly describes the $\Delta v = -1$ propensity rule and the superlinear dependence of the rate on the vibrational quantum number, but did not correctly predict the absolute predissociation rates observed in HeI_2 . Ewing has proposed a momentum gap model¹⁷ for vibrational predissociation which contains many features of the Beswick and Jortner analysis and clearly shows the qualitative basis of the momentum gap constraint on the $V \rightarrow T$ rate. In both models the $V \rightarrow T$ rate is limited by the ability of the intermode perturbation part of the Hamiltonian to couple the nodeless $v = 0$ wavefunction of the van der Waals stretch to the oscillating plane wave that represents dissociated products. Since the plane wave frequency is proportional to the product momentum, higher momentum in the products leads to rapid dephasing of the coupling matrix element integrand and a slower $V \rightarrow T$ rate. For both models, any rotational excitation of the

dissociation products would serve to lower the energy or momentum gap and thereby increase the dissociation rate, but rotational excitation would also be limited by angular momentum constraints. The final dynamics will be determined by the interplay between momentum gap, angular momentum gap and IVR constraints.

Current Work

The experimental and theoretical work discussed above provided the original motivation for much of the work presented in this thesis. Chapter II describes a high resolution (0.001 cm^{-1}) experiment performed on the $B \leftarrow X$ ($10 \leftarrow 0$) transition of NeBr_2 . Detailed rotational structure in the spectrum was observed which allowed us to determine the structure of the complex and the vibrational predissociation lifetime precisely. The experimental resolution was limited to 0.017 cm^{-1} by Doppler broadening, but the spectrum was fit to a rigid T-shaped model with a natural linewidth of 0.015 cm^{-1} . The entire spectrum was well fit to this linewidth, which corresponds to a vibrational predissociation lifetime of 355 picoseconds.

The NeCl_2 $B \leftarrow X$ ($9 \leftarrow 1$) transition was also studied at high resolution, as described in Chapter III. This study confirmed the previously reported observation of a metastable vibrationally excited ground state of NeCl_2 ,¹⁰ and provided a more precise geometrical structure of the

molecule. Although the energy in the X state Cl_2 stretching vibration is an order of magnitude larger than the Ne-Cl_2 dissociation energy, no dissociation is observed on the microsecond time scale. Despite Doppler and homogeneous broadening, several rovibronic transitions were nearly unblended and a detailed rotational assignment was made which allowed the structure of the complex to be accurately determined. The structure of the NeCl_2 van der Waals molecule is T-shaped and the Ne to Cl_2 center of mass distance is $3.565 \pm 0.035 \text{ \AA}$ in the ground state and $3.536 \pm 0.036 \text{ \AA}$ in the excited state. The vibrational predissociation lifetime in the $B(v' = 9)$ state was found to be 258 ± 42 picoseconds on the basis of homogeneous broadening.

Chapter IV describes an experiment using moderate resolution (0.06 cm^{-1}) in which we studied eleven bands of the $B \leftarrow X$ system of NeCl_2 in a free jet expansion. We were able to determine the vibrational predissociation lifetime as a function of vibrational level and to set upper limits on the intermode coupling and the effect of angular momentum on the lifetime. As was seen previously, the rotational structure of NeCl_2 was well simulated by a T-shaped rigid Hamiltonian model for both the ground and excited states. Homogeneous broadening was observed and the lifetimes ranged from 258 ± 42 picoseconds for $B(v' = 9)$ to 33 ± 2 picoseconds for $B(v' = 13)$. The

$B(v' = 7, 8)$ levels have longer lifetimes since the spectra were not broadened at the resolution of the experiment. Another goal of the experiment was to evaluate the extent of coupling between the van der Waals mode and the halogen covalent stretching mode. This coupling could be measured as a change in the van der Waals bond length as a function of halogen vibrational quantum number. Analysis of the data showed that the intermode coupling and angular momentum effects on the dynamics are quite small. The lifetime trends for NeCl_2 could be fit to the gap laws, but showed a very different behavior than HeCl_2 .¹⁸ For a given energy gap, NeCl_2 dissociates much faster than HeCl_2 . This result has subsequently been determined to be due to the fact that product rotational excitation is much more efficient for NeCl_2 than HeCl_2 .^{19,20}

Chapter V describes an experiment which we performed to directly measure the vibrational predissociation lifetime of NeBr_2 in the ground electronic state with one vibrational quantum in the halogen stretch. The pump-probe technique was employed to monitor the decrease in the population of the vibrationally excited level as a function of distance from a supersonic nozzle source where the metastable state is prepared. We measured the ratio of the fluorescence signal due to excitation of NeBr_2 ($X, v = 1$) to that due to Br_2 ($X, v = 1$) as a function of distance from the nozzle. This ratio cancels the effects of the

geometrical expansion of the molecular jet, so that the rate of vibrational predissociation of NeBr_2 can be measured. Analysis of the data showed that the lifetime for NeBr_2 ($X, v = 1$) is 8 ± 3 microseconds. This lifetime is in fairly good agreement with a prediction based on the energy gap extrapolation of lifetimes of several vibrational levels of the B electronic state. Apparently, both the vibrational predissociation mechanisms and the van der Waals potential energy surfaces are similar for the two electronic states.

Chapter VI describes a laser pump-probe experiment designed to study the structure and dynamics of the ArCl_2 van der Waals molecule. We were able to determine the structure and the bond energy of the complex. Also, the rotational state distributions of the Cl_2 molecule product of vibrational predissociation were measured for a number of initial excited states. The rotational distributions were quite complex, particularly those due to $\Delta v = -2$ channels. An interesting aspect of the rare gas-homonuclear halogen complexes is that parity is a good quantum number which is conserved throughout the vibrational predissociation. Cl_2 is produced with even j rotational quantum numbers when the initially prepared state of the ArCl_2 complex is symmetric with respect to a two-fold rotation about the figure axis, i.e., an exchange of the Cl atoms. Conversely, Cl_2 is produced with odd j

when the initially excited state of ArCl_2 is antisymmetric with respect to an exchange of the Cl atoms. This symmetry selection makes it possible to record greatly simplified excitation spectra by detecting only even or odd product states. This provides easier identification of individual rovibronic transitions. Spectra were taken of the ArCl_2 $B \leftarrow X$ ($6 \leftarrow 0$) transition with the probe laser detecting Cl_2 $E \leftarrow B$ ($0 \leftarrow 5$) $j = 9$ or $j = 10$ to obtain odd and even parity-selected excitation spectra. The spectra were modeled with a rigid asymmetric top fitting routine. The structure of the ArCl_2 molecule is T-shaped with an Ar to Cl_2 center of mass distance of 3.72 Å in the ground state and 3.70 Å in the excited state.

The structure of the ArCl_2 van der Waals molecule is similar to HeCl_2 , but the dynamics are very different. The vibrational predissociation mechanism in ArCl_2 is $V \rightarrow T, R$ with a significant amount of energy going into rotation of the Cl_2 product. The $\Delta v = -1$ channel, which is open for HeCl_2 and NeCl_2 at all vibrational levels studied, closes between $v = 8$ and $v = 9$ in the B state. The bond energy, D_0 , for the Ar-Cl_2 van der Waals molecule is determined to be $178.4 \pm 0.3 \text{ cm}^{-1}$ in the $B(v = 7)$ state and $187.9 \pm 0.4 \text{ cm}^{-1}$ in the $X(v = 0)$ state, because of the $9.5 \pm .3 \text{ cm}^{-1}$ blue shift from free Cl_2 . The rotational distributions for Cl_2 formed in the $\Delta v = -2$ predissociation process are not at all statistical in nature. The

distributions may show some signs of resonance effects with the intermediate $\Delta v = -1$ bound level. The lifetime of the ArCl_2 ($B, v = 11$) van der Waals molecule is 83 ± 10 picoseconds based on homogeneous broadening. The gap laws are not applicable here where the $\Delta v = -1$ channel is closed.

The study of Ar_nCl_2 ($n = 1, 2, 3$), described in Chapter VII, enabled us to examine the nature of the bonding which is dominant in larger complexes. We tested the validity of the atom-atom additive interaction by determining the bond energy of these three Ar_nCl_2 van der Waals molecules. In the Ar_nCl_2 case the cut off between the highest observed Cl_2 fragment level and the lowest unobserved level is quite sharp, so we believe that the cutoff is due strictly to conservation of energy and not kinematic constraints. The bond energies which were obtained experimentally were compared to the approximation that the intermolecular potential is given by the sum of the Ar-Ar and Ar- Cl_2 interactions. For Ar_2Cl_2 the product state distribution shows that the dynamics can proceed through either of two paths: $\text{Ar}_2\text{Cl}_2 \rightarrow (1) 2\text{Ar} + \text{Cl}_2$ or (2) $\text{Ar}_2 + \text{Cl}_2$. The experimental bond energy for Ar_2Cl_2 which gives $2\text{Ar} + \text{Cl}_2$ as the products is $458 \pm 3 \text{ cm}^{-1}$ in the $X(v = 0)$ state, while the pair-pair additive model predicts a value of $460.6 \pm 0.4 \text{ cm}^{-1}$. The bond energy for Ar_2Cl_2 is predicted by the simple bond-bond additivity, so

this model appears to accurately describe the bonding in this system.

Suggested Future Work

The rare gas-halogen van der Waals molecules have provided a model system for the experimental and theoretical study of energy transfer from a covalent bond to a weak van der Waals bond. However, the complexes which have been studied by optical spectroscopy have all been shown to have a T-shaped structure in both the ground and excited states.² It would be interesting to study a complex which is linear, because the coupling between the covalent and van der Waals modes should be much more efficient. ArClF and KrClF both have linear structures in the ground state, but the structure is not known in the excited electronic state.^{4,5} The dynamics of a linear van der Waals molecule should be quite different from that of the T-shaped complexes. The $B \leftarrow X$ transition of the T-shaped van der Waals complexes of He, Ne and Ar with Cl_2 are blue-shifted approximately 3, 6 and 12 cm^{-1} , respectively, from the corresponding halogen bands.¹ The shift is due to the difference in the well depths between the ground and the excited states and it is not known if the potentials will be similar for the linear complexes. This experiment may require a great deal of searching to

find the transitions, but the results should be well worth the effort.

The triatomic rare gas-halogen complexes have only one covalent vibrational mode and van der Waals stretch and bend modes. The substitution of a second covalently bonded species as the van der Waals partner would add a great deal of complexity to the experimental and theoretical considerations. The van der Waals complexes NOCl_2 and COCl_2 could be studied in experiments analogous to those discussed previously, exciting the $B \leftarrow X$ transition of Cl_2 . However the second covalent bond could participate in the predissociation process. A study of this vibrational predissociation as a function of stretching frequency of the partner would help to elucidate the important features of the process. The pump-probe technique could be used to probe the final vibrational and rotational state of each partner of the complex.

A great deal of information has been obtained by studying the rare gas-halogen van der Waals molecules. The potential energy surfaces of several of these molecules have been studied through determination of the structure and the bond energy. Pump-probe experiments have given detailed information on the dynamics of the dissociation process. It is interesting that the complexes which have been studied using LIF and pump-probe techniques have been T-shaped even though the first complexes studied, ArClF and

KrClF, were linear. Certainly these molecules should be studied using pump-probe techniques to examine the different dynamics. The difference in lifetimes and dynamics seen already in the rare gas-halogen van der Waals molecules is intriguing. NeBr₂ and NeCl₂ have lifetimes varying over five orders of magnitude, apparently due simply to the difference in the vibrational frequency of the halogen. In conjunction with studies performed by several colleagues it is clear that the vibrational predissociation dynamics of HeCl₂, NeCl₂ and ArCl₂ are very different despite their superficially similar structures. A great deal of progress has been made in recent years, but it is clear that there is more exciting research to be done by the next generation of graduate students.

References

1. D.H. Levy, *Adv. Chem. Phys.* **47**, 323 (1981).
2. K.C. Janda, *Adv. Chem. Phys.* **60**, 201 (1985).
3. J.A. Beswick, and J. Jortner, *Adv. Chem. Phys.* **47**, 363 (1981).
4. S.J. Harris, S.E. Novick, W. Klemperer, and W.E. Falconer, *J. Chem. Phys.* **61**, 193 (1974).
5. S.E. Novick, S.J. Harris, K.C. Janda, and W. Klemperer, *Can. J. Phys.* **53**, 2007 (1975).
6. R.E. Smalley, D.H. Levy, and L.J. Wharton, *J. Chem. Phys.* **64**, 3266 (1976).
7. K.E. Johnson, L. Wharton, and D.H. Levy, *J. Chem. Phys.* **69**, 2719 (1978).
8. W. Sharfin, K.E. Johnson, L. Wharton, and D.H. Levy, *J. Chem. Phys.* **71**, 1292 (1979).
9. K.E. Johnson, W. Sharfin, and D.H. Levy, *J. Chem. Phys.* **74**, 163 (1981).
10. D.E. Brinza, C.M. Western, D.D. Evard, F. Thommen, B.A. Swartz, and K.C. Janda, *J. Phys. Chem.* **88**, 2004 (1984).
11. B.A. Swartz, D.E. Brinza, C.M. Western, and K.C. Janda, *J. Phys. Chem.* **88**, 984 (1984).
12. L.J. van de Burgt, J.P. Nicolai, and M.C. Heaven, *J. Chem. Phys.* **81**, 5514 (1984).

13. J.M. Skene, and M.I. Lester, Chem. Phys. Lett. 116, 93 (1985).
14. J.C. Drobits, J.M. Skene, and M.I. Lester, J. Chem. Phys. 84, 2896 (1986).
15. J.A. Beswick, and J.J. Jortner, J. Chem. Phys. 69, 512 (1978).
16. N. Halberstadt, and J.A. Beswick, Faraday Discuss. Chem. Soc. 73, 357 (1982).
17. G.E. Ewing, Faraday Discuss. Chem. Soc. 73, 325 (1982).
18. J.I. Cline, D.D. Evard, F. Thommen, and K.C. Janda, J. Chem. Phys. 84, 1165 (1986).
19. J.I. Cline, N. Sivakumar, D.D. Evard, and K.C. Janda, J. Chem. Phys. 86, 1636 (1987).
20. J.I. Cline, N. Sivakumar, D.D. Evard, and K.C. Janda, Phys. Rev. A 36, 1944 (1987).

CHAPTER II

Rotational Resolution of the NeBr_2
 $B \leftarrow X$ ($10 \leftarrow 0$) Transition

Rotational Resolution of the NeBr_2
 $B \leftarrow X$ ($10 \leftarrow 0$) Transition^{a)}

Fritz Thommen, Dwight D. Evard and
Kenneth C. Janda^{b)}

Arthur Amos Noyes Laboratory of Chemical Physics
California Institute of Technology
Pasadena, California 91125^{c)}

- a) This manuscript was published in modified form in J. Chem. Phys. **82**, 5295 (1985).
- b) A.P. Sloan Research Fellow, Camille and Henry Dreyfus Teacher-Scholar.
- c) Contribution No. 7115.

Abstract

The $B \leftarrow X$ ($10 \leftarrow 0$) transition of the NeBr_2 van der Waals molecule was studied at high resolution (0.01 cm^{-1}). Detailed rotational structure in the spectrum was observed which allowed us to determine the geometrical structure of the complex. The Ne to Br_2 center of mass distance is $3.67 \pm 0.01 \text{ \AA}$ in the ground state and $3.65 \pm 0.01 \text{ \AA}$ in the B state. Homogeneous broadening was observed which corresponds to a vibrational predissociation lifetime of 355 picoseconds.

Since the first observation of the HeI_2 laser excited fluorescence spectrum by Wharton, Smalley, and Levy,¹ rare gas-halogen vibrational predissociation has become a valuable model system for understanding intramolecular energy redistribution. The dissociation of these molecules is a process for which detailed state-to-state cross sections can be obtained from both experiment and theory. Recently, however, it has become apparent that the potential energy surfaces for these systems are not known well enough for accurate calculations of the dynamics.²

Smalley, Wharton, and Levy reported well resolved P, R branches characteristic of an a-type near prolate top for the $(10 \leftarrow 0)$, $B \leftarrow X$ transition of HeI_2 .³ They noted that the spectrum suggests a T-shaped molecule. Further resolution of the spectrum is precluded by the large I atomic mass and the homogeneous linewidth of the transition.

Unlike HeI_2 , a T-shaped NeBr_2 molecule produces a highly asymmetric oblate top spectrum. Resolving the details of this spectrum can both remove any ambiguity about the structure of the molecule and lead to refined information on the potential energy surface. In addition, detailed rotational structure allows us to determine the homogeneous linewidth as a function of the rotational quantum numbers. As discussed below a single linewidth, characteristic of a 355 picosecond lifetime, fits both the

low J and high J data.

The observed spectrum, illustrated in Figure 1, was recorded on a spectrometer described elsewhere.⁴ A Coherent CR 599-21 dye laser, obtained from the San Francisco Laser Center, was used as the excitation source. The Rhodamine 6G dye was pumped with an Ar⁺ laser to obtain a bandwidth of 0.001 cm⁻¹ tunable over 1 cm⁻¹ segments. The 1 cm⁻¹ segment was divided into 1024 data points and was recorded in 9 minute sequences. Overlapping segments of the NeBr₂ spectrum were recorded simultaneously with an I₂ spectrum for frequency calibration. Twenty such scans were combined to produce the spectrum as shown in Figure 1.

The model used to simulate the NeBr₂ spectrum consists of a T-shaped rigid rotor Hamiltonian for both the ground and excited electronic states. The Br₂ bond lengths are taken to be unchanged from those of uncomplexed Br₂.⁵ Thus, the only free parameters are the Ne-Br₂ center of mass separation in each state, the bandhead position, the rotational temperature, and a single homogeneous linewidth for the transition. The values obtained for these parameters are given in Table I.

The Ne-Br₂ bond length is remarkably similar in the two different electronic states. The Br₂ bond length increases by about 30% in the electronic excitation while the Ne-Br₂ bond decreases by 0.5%. The Ne-Br atomic separation increases from 3.80 Å to 4.10 Å, or 8%, upon

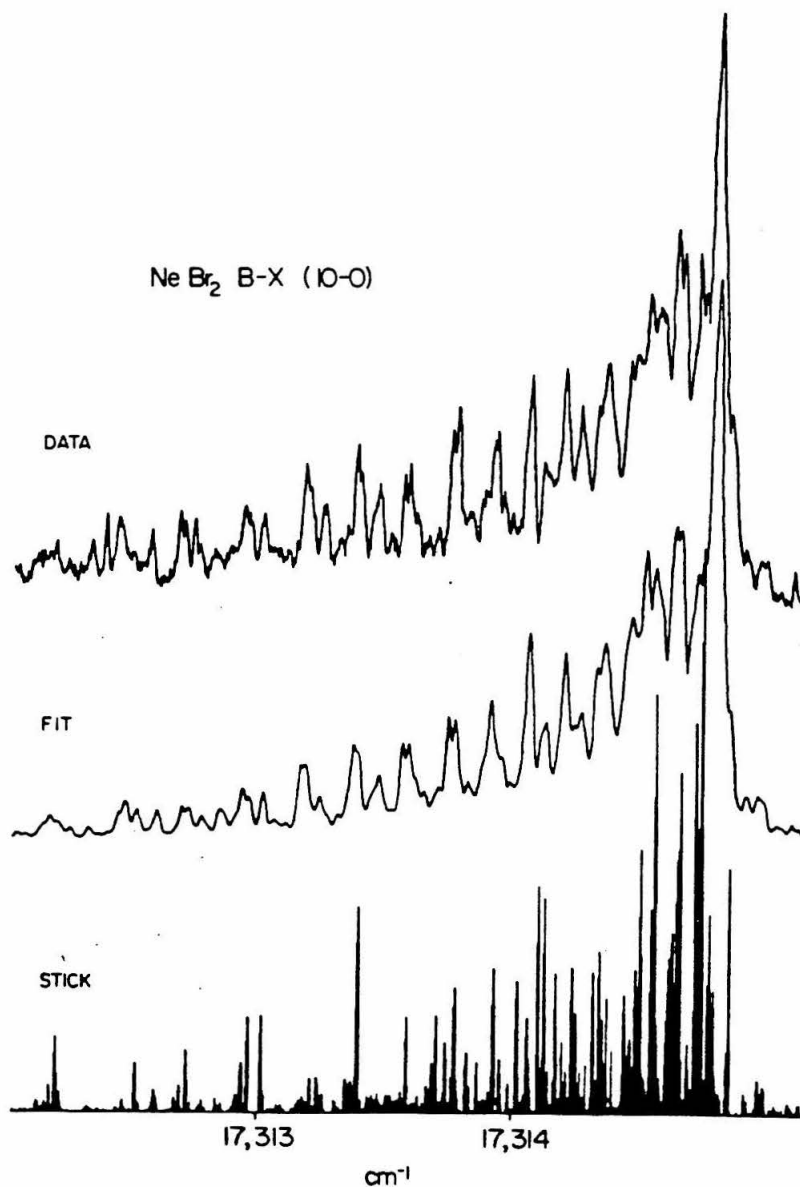


Figure 1. The NeBr₂ B←X (10←0) laser excited fluorescence spectrum. The stick spectrum is the same as the fitted spectrum except that the homogeneous and Doppler widths have been removed from the calculation.

Table I. Spectral constants for NeBr_2 $B \leftarrow X$, ($10 \leftarrow 0$)

R_0 , Br_2 X state (Reference 5)	2.284 Å
R_{10} , Br_2 B state (Reference 5)	2.821 Å
R_0 , Ne-Br_2 X state	3.67 ± 0.01 Å
R_0 , Ne-Br_2 B state	3.65 ± 0.01 Å
Γ (homogeneous linewidth)	0.015 ± 0.005 cm^{-1}
T (rotational temperature)	3.345 K
Bandhead shift from free Br_2	6.045 cm^{-1}

transition. The atom separation in both states is somewhat larger than the 3.58 Å NeKr equilibrium distance measured in scattering experiments.⁶ The similarity of the ground and excited state bond lengths accounts for the weakness of vibronic bands involving the van der Waals stretching motion. We searched for such bands to the blue of the reported transition without success.

The observed spectrum allows us to assert that the homogeneous linewidth of this transition is at most weakly dependent on the J and K quantum numbers of the molecule. The entire spectrum is well simulated by a single homogeneous linewidth, 0.015 cm^{-1} . (The laser bandwidth was negligible in comparison, the Doppler width was 0.017 cm^{-1} , as measured on adjacent Br_2 transitions.) Although the homogeneous linewidth and Doppler width are comparable, the shape of the convoluted spectrum is still very dependent on the homogeneous width. By reducing the Doppler contribution to future spectra it will be possible to study this effect in more detail. The homogeneous linewidth corresponds to a lifetime of 355 picoseconds. This agrees well with an extrapolation of data from higher vibrational levels obtained from spectra of much lower resolution.⁷

Spectra such as those reported here will be most useful if accurate potential energy surfaces can be extracted from them. Not only is it necessary to obtain

the shape of the potential, but also detailed cross terms for the interaction of the two bond lengths. The results presented here show that this goal can be reached, but perhaps not easily. First, the T-shaped structure of these molecules results in a highly congested spectrum. Second, the observed spectrum is surprisingly well fitted by a rigid rotor model. This indicates that zero point vibrations probably span a limited range of the potential. Third, the weak dependence of the van der Waals bond length on the halogen bond length results in very weak vibronic overtone transitions.

This work was supported by the United States Department of Energy. The laser was obtained from the San Francisco Laser Center funded by the National Science Foundation. Acknowledgement is made to the donors of the Petroleum Research Fund, administered by the American Chemical Society, for partial support of this work.

References

1. R.E. Smalley, D.H. Levy, and L. Wharton, *J. Chem. Phys.* **64**, 3266 (1976).
2. D.W. Schwenke and D.G. Truhlar, *Chem. Phys. Lett.* **98**, 217 (1983).
3. R.E. Smalley, L. Wharton, and D.H. Levy, *J. Chem. Phys.* **68**, 671 (1978).
4. D.E. Brinza, C.M. Western, D.D. Evard, F. Thommen, B.A. Swartz, and K.C. Janda, *J. Phys. Chem.* **88**, 2004 (1984).
5. R.F. Barrow, T.C. Clark, J.A. Coxon, and K.K. Yee, *J. Mol. Spectrosc.* **51**, 428 (1974).
6. C.Y. Ng, Y.T. Lee, and J.A. Barker, *J. Chem. Phys.* **61**, 1996 (1974).
7. B.A. Swartz, D.E. Brinza, C.M. Western, and K.C. Janda, *J. Phys. Chem.* **88**, 6272 (1984).

CHAPTER III

Rotational Resolution of the NeCl_2

$B \leftarrow X$ ($9 \leftarrow 1$) Transition

Rotational Resolution of the NeCl_2
 $B \leftarrow X$ ($9 \leftarrow 1$) Transition^{a)}

Dwight D. Evard, Fritz Thommen^{b)}
and Kenneth C. Janda^{c)}

Department of Chemistry
California Institute of Technology
Pasadena CA, 91125

- a) This manuscript was published in modified form in J. Chem. Phys. 84, 3630 (1986).
- b) Present address: CIBA-Geigy, Basel, Switzerland.
- c) A.P. Sloan Research Fellow, Camille and Henry Dreyfus Teacher-Scholar.

Abstract

High resolution (0.01 cm^{-1}) laser induced fluorescence spectra of the ($9 \leftarrow 1$) rovibronic band of the $B^3\Pi(0_u^+) \leftarrow X^1\Sigma_g^+$ system of Cl_2 and the associated van der Waals molecule NeCl_2 have been obtained in a free jet expansion. The spectrum of NeCl_2 associated with the ($9 \leftarrow 1$) transition of the free Cl_2 molecule was observed 5.46 cm^{-1} to the blue of the band origin of uncomplexed Cl_2 . This study confirms the previously reported observation of a metastable vibrationally excited ground electronic state of NeCl_2 . Although the energy in the Cl_2 stretching vibration is an order of magnitude larger than the Ne-Cl_2 dissociation energy, no dissociation is observed on the microsecond time scale. Rotational resolution was achieved and a detailed rotational assignment was made which allowed the Ne to Cl_2 center of mass distance to be determined. This distance is $3.565 \pm 0.035 \text{ \AA}$ in the ground state, and $3.536 \pm 0.036 \text{ \AA}$ in the excited state. The structure of the NeCl_2 van der Waals molecule is T-shaped, with the dipole transition moment lying along the Cl_2 bond axis, giving a b-type asymmetric top spectrum. The vibrational predissociation lifetime in the $B(v' = 9)$ state was found to be 258 ± 42 picoseconds on the basis of homogeneous broadening.

Introduction

We recently reported a low resolution laser excited fluorescence spectrum of NeCl_2 in which the initial state contains one quantum of Cl_2 stretching excitation.^{1,2} The state is metastable, with $\tau > 10^{-5}$ seconds, even though the molecule contains over ten times the vibrational energy necessary to dissociate the van der Waals bond. The existence of the metastable state of NeCl_2 $X(v' = 1)$ strongly supports the current theories of vibrational predissociation which predict long lived vibrationally excited triatomic van der Waals molecules.^{3,4} In the present paper, we report the high resolution spectroscopy of the NeCl_2 $B \leftarrow X$ ($9 \leftarrow 1$) transition, which gives more detailed information of the structure and dynamics of this van der Waals molecule. The rotational structure serves to remove any doubt as to the assignment of the spectrum to the vibrationally excited metastable state. Analysis of the spectrum also determines the average distance of the Ne atom from the Cl_2 center of mass to 1% precision.

Experimental

The free jet expansion apparatus employed in these measurements is similar to the system described previously.² The spectra were obtained by passing a 90%/10% Ne/He gas mixture at a total pressure of 200 psi

over liquid Cl_2 with a vapor pressure of 60 torr (-70 C) through a 35 micron nozzle. The Ne/He gas mixture and Cl_2 gas were used as supplied by Matheson with no further purification. A Coherent Innova 18 argon ion laser supplied 6 W of continuous power at 488 nanometers to pump a Coherent 599-21 continuous wave (cw) high resolution dye laser. The dye laser, on loan from the San Francisco Laser Center, was actively stabilized to provide radiation with a bandwidth of 0.001 cm^{-1} , continuously tunable over 1 cm^{-1} segments. The laser was operated with Coumarin 6 dye, which gave 100 mW of power throughout the spectral region of interest. The dye laser was directed through light baffles into the vacuum apparatus to intersect the molecular beam at a right angle. The laser radiation was tuned to excite the $(9 \leftarrow 1)$ transition of the $B^3\Pi(0_u^+) \leftarrow X^1\Sigma_g^+$ band of Cl_2 , and the associated van der Waals molecule NeCl_2 . The total fluorescence was collected at right angles to the laser and molecular beams by a 75 mm diameter aspheric lens ($f/0.7$), which projects the fluorescence to variable defining slits approximately 35 centimeters from the point of intersection for the laser and molecular beams. The defining slits and a Schott OG-530 cut off filter served to reduce the scattered laser light.

The laser and data acquisition system are controlled by an IBM PC microcomputer through a Tecmar Labmaster interface card. The microcomputer operates in an

interrupt-driven mode using the PC-Forth system from Laboratory Microsystems, Inc. A cooled RCA 7265 photomultiplier operating in the photon counting mode was used to detect the total fluorescence. The number of photons counted during a preset time, typically 0.5 seconds, was stored in the microcomputer and the laser frequency was incremented. The total 1 cm^{-1} segment was separated into 1024 points, so that a single scan took about 9 minutes. Approximately 80 scans were averaged to obtain each 1 cm^{-1} segment of the spectrum. The spectrum shown in Figure 2 was obtained by scanning three overlapping 1 cm^{-1} regions, piecing the individual spectra together and averaging the intersecting portions.

Absolute wavelength calibration was achieved by simultaneously recording the absorption spectrum of iodine. A small fraction of the laser beam was diverted with a beam splitter and passed through an iodine cell at ambient temperature. The beam was detected by a photodiode, and the signal was stored concurrently with the molecular beam fluorescence in the computer. The experimental absorption spectrum of iodine was matched with the published spectrum,⁶ which gave the absolute wavelength of the individual iodine transitions. A miniature train wavemeter similar in design to one described by Hui-Rang et al.⁷ was used to monitor the laser frequency while setting up a scan. This method required a large fraction of the cw

laser light, so it was not used while data was being collected.

Results and Discussion

The laser induced fluorescence spectrum of the $B^3\Pi(O_u^+) \leftarrow X^1\Sigma_g^+$ ($9 \leftarrow 1$) vibronic transition of $^{35}\text{Cl}_2$ in a continuous expansion of Cl_2 , Ne, and He is shown in Figure 1. The transition moment for the $B \leftarrow X$ system of the halogens lies along the axis of the bond and the transition is allowed due to spin-orbit coupling.⁸ The strength of the $B \leftarrow X$ transition is several orders of magnitude larger in I_2 than in Cl_2 because of the greater spin-orbit coupling in the heavier molecule. The chlorine spectrum was modeled to a rigid rotor Hamiltonian using a nonlinear least squares fitting routine. The literature values of 0.2417 and 0.1342 cm^{-1} for the rotational constants for the X and B states,⁹ respectively, and 18963.43 cm^{-1} for the band origin⁵ for the $^{35}\text{Cl}_2$ were used as initial estimates for the fit. The rotational temperature, laser bandwidth, band origin, and both rotational constants were allowed to vary during the fitting process. The band origins of the three isotopic forms of Cl_2 are separated by nearly 20 cm^{-1} , allowing excitation of any one species. This paper deals only with $^{35}\text{Cl}_2$, the most abundant isotope, because of the extensive signal averaging necessary to obtain a high quality spectrum.

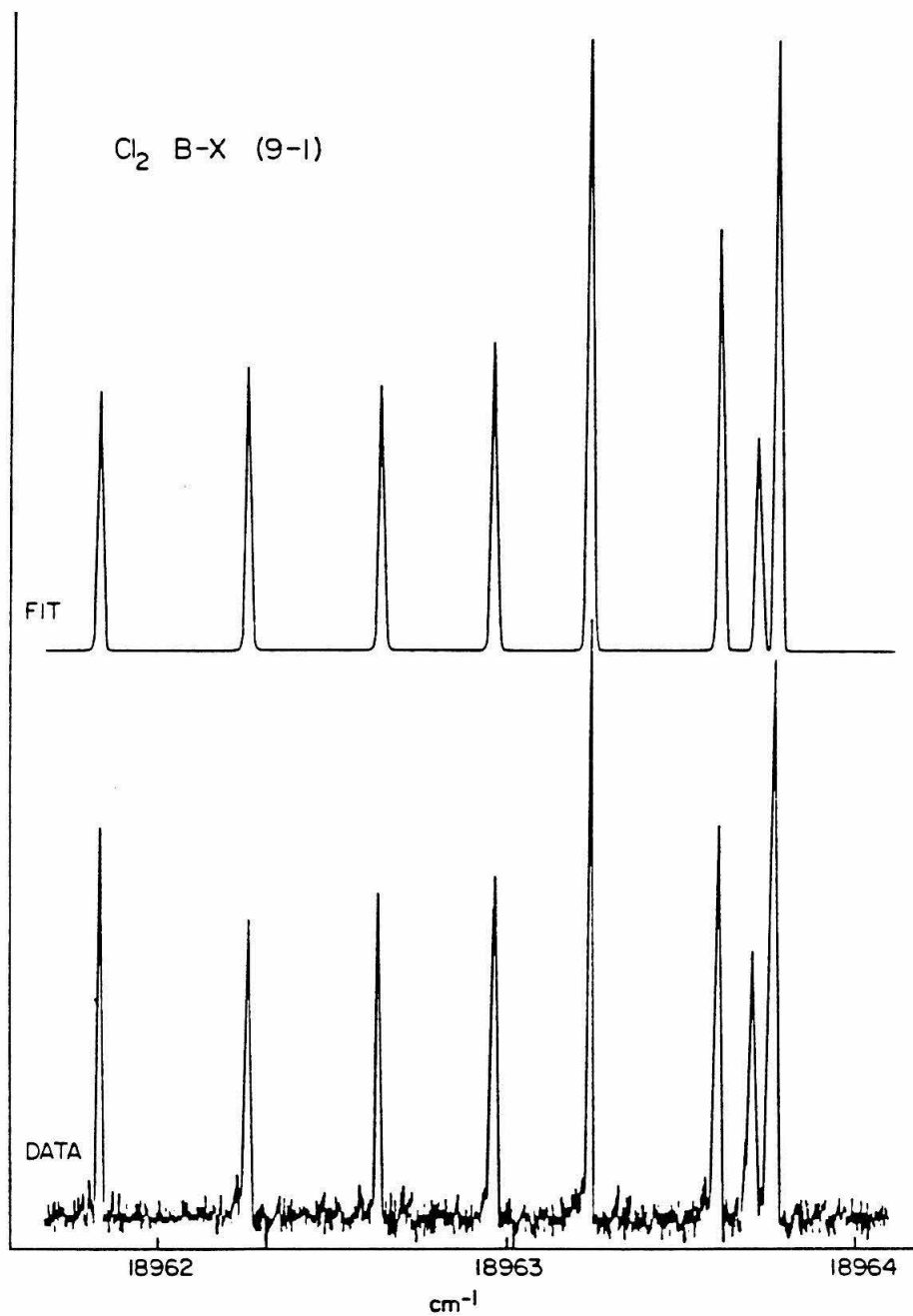


Figure 1. Laser excited fluorescence spectrum of the $B \leftarrow X$ (9 \leftarrow 1) vibronic band for Cl_2 . The upper line is the fit to the experimental data, which is shown in the lower trace.

The rotational constants determined by fitting the high resolution Cl_2 spectrum in Figure 1 are obtained from a different rotational regime than the literature values of Coxon.⁹ Rather than employing the method of combination differences, Coxon performed direct least squares fitting of the observed line frequencies for Cl_2 . He found it necessary to include a second centrifugal distortion term, $H_v J^3(J+1)^3$, to fit the higher vibrational levels of the B state. Thus, the molecular constants are extracted from the high J region where the rotational energy levels are strongly influenced by centrifugal distortion. The molecular beam experiment discussed in this paper produces Cl_2 with low rotational temperatures, so a large fraction of the population is in the low J region near the band origin. Figure 1 shows the spectrum of Cl_2 with $J < 4$, though it is clear that some higher rotational states are also populated. The rigid rotor approximation is valid within the accuracy of this experiment, so the determination of the rotational constants is a much simpler process. The values for the rotational constants obtained in this work are compared to the literature values in Table I. It is seen that the literature values and our experimental values are the same within experimental error although they are obtained by different means using data from different portions of the spectrum.

Table I. Spectral Constants for Cl_2 , $B \leftarrow X$ ($9 \leftarrow 1$).

	Literature	Experimental ^{a)}
B, Cl_2 X State	0.2417 cm^{-1} b)	0.2419 cm^{-1}
B, Cl_2 B State	0.1342 cm^{-1} b)	0.1344 cm^{-1}
Band Origin	18 963.47 cm^{-1} c)	18 963.44 cm^{-1}

a) From this work.

b) From reference 9.

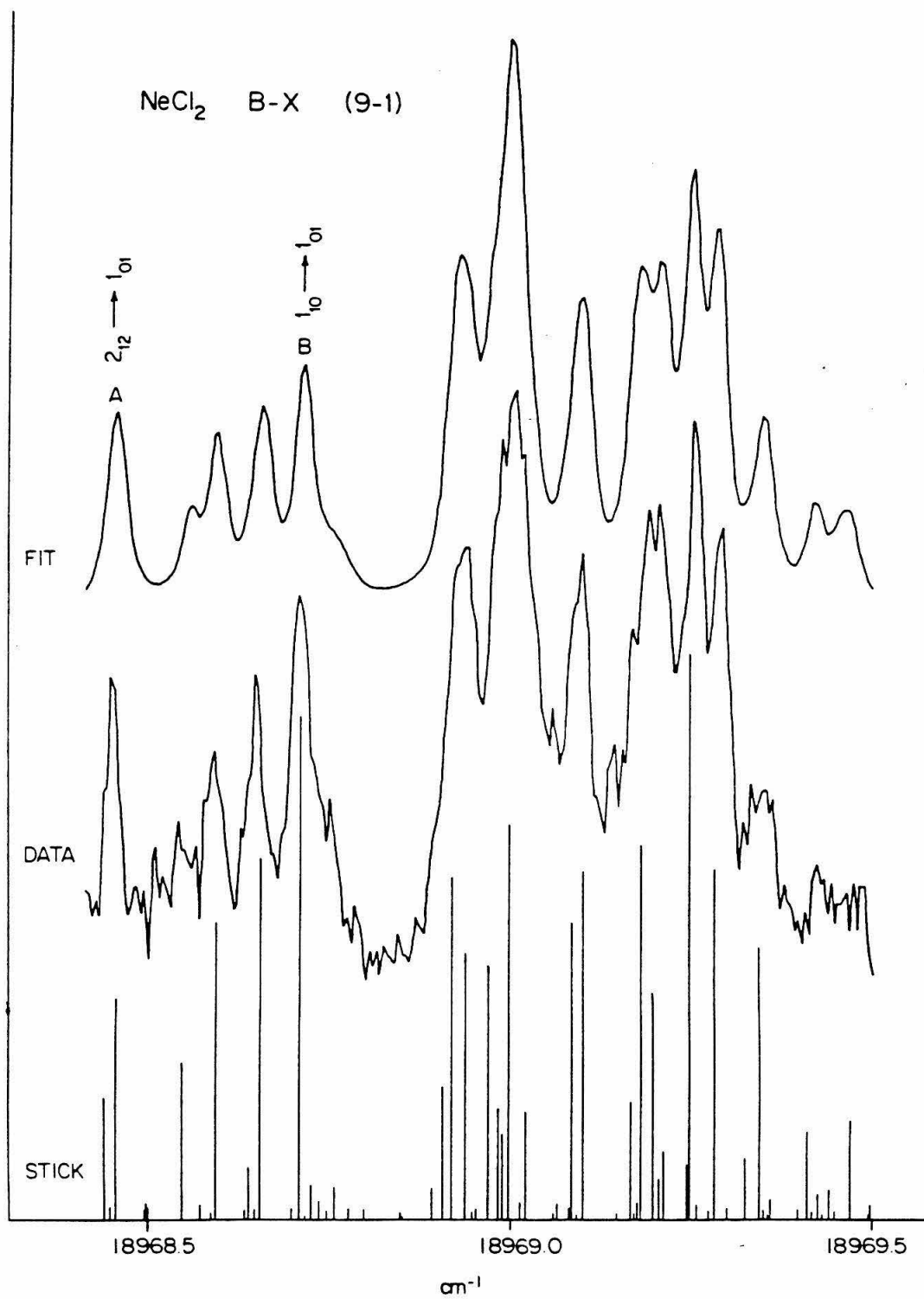
c) From reference 5.

The rotational temperature of the Cl_2 spectrum could not be fit accurately using this generalized fitting routine. The mass 35 isotope of chlorine is a fermion with nuclear spin $I = 3/2$, which should lead to a 5:3 alternation of degeneracies for the odd and even j rotational levels of the homonuclear $^{35}\text{Cl}_2$ molecule. This effect was clearly visible in spectra taken using lower resolution lasers,² however, it is not readily apparent here. A reasonable fit to the experimental data could be obtained by starting with any temperature from 3 to 7 K, and the final temperature reached by the fitting routine was never significantly different from the initial temperature. There are several possible explanations for this behavior. The data for the spectrum in Figure 1 were taken over a one week period, during which time the experimental conditions, in particular the laser power and expansion conditions, varied. The reported spectrum is an average over any such variations in experimental conditions. The premise that the rotational temperature of a molecular beam expansion may be modeled by a Boltzmann distribution has been contested by a number of experiments where non-Boltzmann distributions of rotational states have been observed.^{10,11} Typically, the higher j states are more heavily populated than would be predicted by a Boltzmann population distribution. Finally, we have the problem that we are sampling different portions of the

expansion. With only limited spatial filtering the spectrum consists of contributions from molecules in a number of different expansion conditions. However, the agreement in Table I between our data and Coxon's values demonstrates that precise knowledge of the population distribution is not critical to the determination of spectroscopic constants of interest.

The high resolution spectrum of a feature observed 5.46 cm^{-1} to the blue of the band origin of the $B^3\Pi(0_u^+) \leftarrow X^1\Sigma_g^+$ ($9 \leftarrow 1$) transition of Cl_2 is shown in Figure 2. This feature is observed only in expansions of gas mixtures containing Ne, as well as He and Cl_2 , and has previously been attributed to NeCl_2 .^{1,2} The individual transitions are not well enough resolved to avoid having to use spectral simulation to extract the individual transition frequencies. In fitting the NeCl_2 spectrum we assume that the van der Waals bond has little effect on the Cl_2 ground state potential energy surface so the transition moment remains along the Cl-Cl bond axis. The spectrum was fit using a model consisting of a T-shaped rigid rotor Hamiltonian for both the ground and excited states. The bond lengths for the Cl-Cl distance in the complex were taken to be identical to those in the free Cl_2 molecule. The Ne was assumed to lie on the line perpendicular to the Cl-Cl bond passing through the center of mass of the Cl_2 species. In our previous work, the spectrum of the free

Figure 2. Laser excited fluorescence spectrum of NeCl_2 associated with the $B \leftarrow X$ ($9 \leftarrow 1$) transition of Cl_2 . The stick spectrum is the same as the fitted spectrum, but the linewidth has been artificially removed to show the frequency of each individual transition. The peaks labeled A and B were used to determine the ground state rotational constants. See the text for details.



Cl₂ was used to determine the rotational temperature in fitting the associated van der Waals molecule. In the present situation, the temperature must be fit independently, since the Cl₂ could not be adequately fit to a single rotational temperature. The major contributions to the linewidth of the transition are from the homogeneous linewidth and the Doppler broadening. The laser bandwidth was negligible in comparison with the Doppler width of 0.0125 cm⁻¹, taken from the Cl₂ spectrum. The Doppler width was generated using a Gaussian line shape, while the natural linewidth was convoluted using a Lorentzian line shape. The spectrum was fit by varying five parameters, the rotational temperature, the natural linewidth, the band origin, and the Ne to Cl₂ center of mass distance in both the ground and excited states defined as R_X and R_B, respectively.

The rotational constants obtained from this procedure were used to generate a stick spectrum similar to that in Figure 2 to show which transitions contributed to each peak in the spectrum. For the symmetric T-shaped molecular structure of the NeCl₂ van der Waals molecule the moments of inertia are

$$I_A = \mu_m r^2; \quad I_B = \mu_M R^2; \quad I_C = I_A + I_B$$

where μ_m is the Cl₂ reduced mass, r is the Cl₂ bond length, μ_M is the Ne-Cl₂ reduced mass and R is the Ne atom to Cl₂ center of mass distance. The rotational energy levels are

labeled as J_{K_{-1}, K_1} , where K_{-1} is the K quantum number in the prolate top limit and K_1 is the quantum number in the oblate top limit. For $J < 4$, these energy levels for the X and B states can be written in closed form in terms of the rotational constants A, B, and C for each state. The transition moment lies along the Cl-Cl bond, the b inertial axis, and follows b-type asymmetric top selection rules. Assignment of the individual rotational transitions shows that the two lines, marked A and B in Figure 2, are due primarily to unblended transitions which have a common excited rotational state. Since the splitting between A and B could be measured accurately, this was used to determine the ground state rotational constants. The entire spectrum was then least squares fitted varying the four remaining parameters to determine the excited state van der Waals bond length. The final values for the parameters are given in Table II.

The Ne to Cl_2 center of mass distance is similar in the ground and excited electronic states, decreasing by only 8% while the Cl_2 bond length increases by 34% upon electronic excitation. The Ne-Cl atomic separation is 3.70 Å in the ground state and increases to just 3.78 Å in the excited state. These atomic separations are both larger than the r_m value of 3.43 Å for Ne-Ar obtained from scattering data.¹² The r_m value corresponds to the minimum

Table II. Spectral Constants for NeCl_2 $B \leftarrow X$ ($9 \leftarrow 1$).

R_0 , Ne- Cl_2 X State	$3.565 \pm 0.035 \text{ \AA}$
R_0 , Ne- Cl_2 B State	$3.536 \pm 0.036 \text{ \AA}$
Γ (homogeneous linewidth)	$0.02186 \pm 0.0022 \text{ cm}^{-1}$
T (rotational temperature)	0.949 K
Bandhead shift from free Cl_2	5.460 cm^{-1}

of the potential well, while the Ne-Cl atomic separations reported here are vibrationally averaged distances.

The vibrational predissociation lifetime may be estimated from the natural linewidth if the spectrum is homogeneously broadened. The vibrational predissociation lifetime is

$$\tau = [2\pi c\Gamma]^{-1}$$

where Γ is the full width at half maximum of the natural linewidth. Using the natural linewidth of $0.0219 \pm 0.0022 \text{ cm}^{-1}$ from the fit to the entire spectrum we obtain the vibrational predissociation lifetime of 243 ± 24 picoseconds. The fitting routine appears to compensate for small errors in the line frequencies of individual transitions by broadening the natural linewidth further than is correct, which gives a low estimate for the lifetime. A more accurate determination of the lifetime may be obtained by fitting the area of the spectrum between, and including, the points labeled A and B. The natural linewidth obtained by fitting this region is $0.0196 \pm 0.0020 \text{ cm}^{-1}$ which gives a lifetime of 272 ± 28 picoseconds for the B state. We conservatively report the average of these two lifetimes giving a vibrational predissociation lifetime of 258 ± 42 picoseconds for the NeCl_2 van der Waals molecule in the $B(v' = 9)$ state.

Conclusions

The $B \leftarrow X$ ($9 \leftarrow 1$) transition of the NeCl_2 van der Waals molecule has been studied by laser induced fluorescence techniques at 0.001 cm^{-1} resolution. The transitions in the rotationally resolved spectrum were assigned and two unblended lines were used to accurately determine the absolute value of the Ne to Cl_2 center of mass distance in the ground state. The structure is T-shaped and the Ne to Cl_2 center of mass distance is $3.565 \pm 0.035 \text{ \AA}$ in the ground state and $3.536 \pm 0.036 \text{ \AA}$ in the excited state. The vibrational predissociation lifetime in the $B(v' = 9)$ state is 258 ± 42 picoseconds based on the homogeneous broadening of the spectrum.

Acknowledgments

This work was supported by the United States Department of Energy. The dye laser was obtained from the San Francisco Laser Center funded by the National Science Foundation. Acknowledgment is made to the donors of the Petroleum Research Fund, administered by the American Chemical Society, for partial support of this work.

References

1. D.E. Brinza, B.A. Swartz, C.M. Western, and K.C. Janda, *J. Chem. Phys.* **79**, 1541 (1983).
2. D.E. Brinza, C.M. Western, D.D. Evard, F. Thommen, B.A. Swartz, and K.C. Janda, *J. Phys. Chem.* **88**, 2004 (1984).
3. J.A. Beswick, and J. Jortner, *J. Chem. Phys.* **69**, 512 (1978).
4. G.E. Ewing, *Faraday Discuss. Chem. Soc.* **73**, 325 (1982).
5. J.A. Coxon, *J. Quant. Spectrosc. Radiat. Transfer.* **11**, 1355 (1971).
6. S. Gerkenstorn, and P. Luc, *Atlas du Spectre D'Absorption de la Molecule D'Iode* (CNRS, Paris, 1978).
7. X. Hui-Rang, S.V. Benson, and T.W. Hansch, *Laser Focus March*, **54** (1981).
8. R.S. Mulliken, *Phys. Rev* **36**, 699 (1930).
9. J.A. Coxon, *J. Mol. Spectrosc.* **82**, 264 (1980), and references therein.
10. R.E. Smalley, D.H. Levy, and L. Wharton, *J. Chem. Phys.* **64**, 3266 (1976).
11. S.G. Kubolich, D.E. Oates, and J.H.S. Wang, *J. Chem. Phys.* **61**, 4686 (1974).

12. C.Y. Ng, Y.T. Lee, and J.A. Barker, J. Chem. Phys 61, 1996 (1974).
13. F. Thommen, D.D. Evard, and K.C. Janda, J. Chem. Phys. 82, 5295 (1985).

CHAPTER IV

**Molecular Beam-Laser Spectroscopy of
the NeCl_2 van der Waals Molecule**

Molecular Beam-Laser Spectroscopy
of the NeCl_2 van der Waals Molecule^{a)}

Dwight D. Evard, Fritz Thommen,^{b)} Joseph I. Cline^{c)}
and Kenneth C. Janda^{d)}

Arthur Amos Noyes Laboratory of Chemical Physics
California Institute of Technology, Pasadena CA 91125

and

Department of Chemistry, University of Pittsburgh
Pittsburgh, PA 15260

- a) This manuscript was published in modified form in J. Phys. Chem. 91, 2508 (1987).
- b) Present address: CIBA-Geigy, Basel, Switzerland.
- c) National Science Foundation Predoctoral Fellow.
- d) Camille and Henry Dreyfus Teacher-Scholar.

Abstract

Laser-induced fluorescence excitation spectra for eleven bands of the $B^3\Pi(0_u^+) \leftarrow X^1\Sigma_g^+$ system of Cl_2 and the associated van der Waals molecule $NeCl_2$ have been obtained at 0.06 cm^{-1} resolution in a free jet expansion of Ne, Cl_2 , and He. The observed rotational structure of the spectra of $NeCl_2$ are well simulated by a T-shaped, rigid Hamiltonian model for both the ground and excited states. The vibrational predissociation lifetimes ranged from 258 ± 42 picoseconds for $B(v' = 9)$ to 33 ± 2 picoseconds for $B(v' = 13)$. The intermode coupling and angular momentum effects were too small to be determined with the resolution achieved in this experiment.

Introduction

The study of the structure and dynamics of van der Waals molecules has become an active area for research in chemical physics. The triatomic van der Waals molecules, particularly those consisting of a rare gas atom bound to a diatomic halogen molecule, have been of both experimental and theoretical interest because their relative simplicity may allow a quantitative comparison between experiment and theory with few adjustable parameters. These triatomic complexes are easily formed in molecular beam expansions and may be probed spectroscopically by laser induced fluorescence or by molecular beam resonance techniques. The van der Waals bond in the rare gas-halogen complex is very weak; less than the energy of a quantum of vibration of the halogen stretch for He and Ne compounds. Vibrational predissociation will occur if energy from the vibrational mode of the halogen molecule is transferred to the van der Waals mode. The vibrational predissociation process is thought to proceed on a single adiabatic potential energy surface which makes the predissociation a theoretically accessible example of intramolecular vibrational relaxation (IVR).

The first studies of these molecules by Klemperer et al. involved detection of ArClF^1 and KrClF^2 by molecular beam resonance techniques. These ClF complexes have a

linear geometry with the rare gas atom bound to the Cl atom. They rationalize the structure by considering the rare gas atom to be a Lewis acid which donates electrons into the halogen σ orbital, which is the lowest unoccupied molecular orbital (LUMO) of ClF. This model correctly predicts the linear geometry of the interhalogen van der Waals molecules, but fails to predict the geometries of the observed rare gas-homonuclear diatomic halogen complexes. These homonuclear halogen complexes are T-shaped, indicative of a van der Waals additive model of the binding. It is apparent that more experimental data are necessary for the development of appropriate theories to determine which is the most important interaction in the formation of the van der Waals bond.

A detailed study probing the HeI_2 complex by laser induced fluorescence was carried out by Levy and coworkers.³⁻⁶ The strong fluorescence of the $B \leftarrow X$ system of I_2 made possible the detection of both total laser induced fluorescence and dispersed fluorescence. The van der Waals molecule HeI_2 was shown to be responsible for structural features appearing $3.4 - 4.0 \text{ cm}^{-1}$ to the blue of the $(3 \leftarrow 0)$ to $(29 \leftarrow 0)$ bandheads of free I_2 .³ Analysis of the rotational band contours yielded a T-shaped structure for the complex with 4.5 \AA He to I_2 center of mass distance. Homogeneous linewidths were found to vary with the vibrational state excited, corresponding to

predissociation lifetimes ranging from 220 picoseconds for $v' = 12$ to 38 picoseconds for $v' = 26$.⁴ The vibrational predissociation rates showed a quadratic plus linear dependence on the upper state vibrational quantum number. A study of the dispersed fluorescence spectrum of HeI_2 excited to the $B(v')$ state showed that the fluorescence was dominated by I_2 in the $B(v' - 1)$ state.⁵ This led to a statement of the propensity rule $\Delta v = -1$ for this predissociative process.

The theoretical treatment of the vibrational predissociation in rare gas-halogen van der Waals complexes is based on the assumption that the normal vibration of the halogen molecule and the van der Waals stretching mode are only weakly coupled. Beswick and Jortner^{7,8} studied the vibrational predissociation of T-shaped complexes where the interaction between the diatomic halogen molecule and the rare gas atom was represented by a sum of Morse atom-atom potentials. The resulting close-coupling scattering equations could not be solved analytically, but numerical solutions gave vibrational predissociation rates from the widths of the resulting resonances. The model predicts that the predissociation rates have a strong inverse dependence on the energy difference between the initially bound complex and the final dissociated state. This energy gap model correctly describes the $\Delta v = -1$ propensity rule and the superlinear dependence of the rate on the

vibrational quantum number, but did not correctly predict the absolute predissociation rates observed in HeI_2 . The potential energy surface used by Beswick and Jortner has been shown to be quite unrealistic.⁹ Ewing has proposed a momentum gap model¹⁰ for vibrational predissociation which contains many features of the Beswick and Jortner analysis and gives a qualitative understanding for the basis of the momentum gap constraint on the $V \rightarrow T$ rate. In both models the $V \rightarrow T$ rate is limited by the ability of the intermode perturbation part of the Hamiltonian to couple the nodeless $v = 0$ wavefunction of the van der Waals stretch to the oscillating plane wave that represents dissociated products. Since the plane wave frequency is proportional to the product momentum, higher momentum in the products leads to rapid dephasing of the coupling matrix element integrand and a slower $V \rightarrow T$ rate. For both the Ewing and the Beswick and Jortner models any rotational excitation of the dissociation products would serve to lower the momentum (or energy) gap and thereby increase the IVR rate.

Janda and coworkers have studied the van der Waals molecule NeBr_2 using laser induced fluorescence techniques.^{11,12} Spectra were recorded at low resolution ($0.1\text{-}0.2 \text{ cm}^{-1}$) for the van der Waals molecule associated with the $(11 \leftarrow 0)$ through the $(30 \leftarrow 0)$ $B^3\Pi(0_u^+) \leftarrow X^1\Sigma_g^+$ transition of Br_2 .¹¹ The NeBr_2 bands showed increasing spectral shifts of the complex from the free Br_2 with

increasing ν' , ranging from 5.5 to 8.8 cm^{-1} . The natural linewidths of the van der Waals features increased from the laser bandwidth limited value of 0.10 cm^{-1} for NeBr_2 ($16\leftarrow 0$) to 3.1 cm^{-1} for the ($27\leftarrow 0$) band, corresponding to vibrational predissociation lifetimes of 84 and 1.7 picoseconds, respectively. They estimate the dissociation energy in the B state to be $64 \pm 4 \text{ cm}^{-1}$ from the apparent closing of the one quantum predissociation channel near $\nu' = 27$. One transition, the $B\leftarrow X$ ($10\leftarrow 0$), was studied at high resolution.¹² The homogeneous linewidth was found to be $0.015 \pm 0.005 \text{ cm}^{-1}$, giving an estimate of 355 ± 120 picoseconds for the vibrational predissociation lifetime of $\nu' = 10$. This lifetime agrees well with an extrapolation of the low resolution data. The data follow the trends predicted by the gap models discussed above.

Heaven and coworkers¹³ observed the van der Waals complex HeBr_2 using laser induced fluorescence of the Br_2 $B\leftarrow X$ system at moderate resolution (0.05 cm^{-1}) in a free jet expansion. Spectra were obtained for the ($11\leftarrow 0$) through ($38\leftarrow 0$) bands and rotational structure for several bands was resolved with analysis consistent with a T-shaped structure. The He to Br_2 center of mass distances are 3.7 Å and 3.8 Å in the ground and excited states, respectively. Lifetimes ranged from > 100 picoseconds to 1.8 ± 0.2 picoseconds for the ($12\leftarrow 0$) and ($38\leftarrow 0$) bands of $\text{He}^{79}\text{Br}_2$, respectively. An upper limit of 23 cm^{-1} for the

He-Br₂ dissociation energy in the B state was provided by observation of rapid predissociation from the $v' = 40$ vibrational level. The lifetimes reported are again consistent with a simple energy gap model for vibrational predissociation.

The first laser induced excitation study of a rare gas-interhalogen van der Waals molecule was reported by Skene and Lester.¹⁴ A spectroscopic feature approximately 3.6 cm^{-1} to the blue of the expected band origin of the ICl $B(v' = 3) \leftarrow X(v'' = 0)$ transition was attributed to HeICl. This is particularly interesting because no fluorescence from uncomplexed ICl was observed for this vibrational level because of subnanosecond electronic predissociation. This indicates that the vibrational predissociation of the He-ICl van der Waals bond is competitive with the electronic predissociation of the ICl molecule. Analysis yields a lower bound estimate of 550 ± 150 picoseconds for the vibrational predissociation lifetime. Drobits, et al.,¹⁵ report the use of optical-optical double resonance techniques to study the dynamics of the vibrational predissociation process in the NeICl van der Waals complex. A pump laser excites the $A \leftarrow X$ transition, then at a time up to 15 nanoseconds later a probe laser scans through several $E \leftarrow A$ transitions of ICl while the fluorescence from the E state is collected. The lifetime for NeICl in the A state ($v_A = 14$) is 3 ± 2 nanoseconds based on experimental and

theoretical ratios of the complex signal to free ICl as a function of time. The A state ($v_A = 14$) binding energy was determined to be 44 cm^{-1} .

Previously, we have studied the van der Waals complexes of Cl_2 with He ¹⁶ and Ne .^{17,18} No lifetime information was obtained in the low resolution (0.2 cm^{-1}) spectroscopy of the NeCl_2 complex. However, the observation of NeCl_2 $X(v'' = 1, 2)$ in metastable vibrationally excited states was very interesting. The NeCl_2 exists for more than 10^{-5} seconds in the $X(v'' = 1)$ state even though the complex contains over ten times the energy necessary to dissociate the van der Waals bond. High resolution (0.01 cm^{-1}) spectra of the $B \leftarrow X$ ($9 \leftarrow 1$) rovibronic bands of Cl_2 and the associated NeCl_2 van der Waals molecule were obtained. The experimental resolution was limited by lifetime and Doppler broadening, with analysis leading to an estimate of 258 ± 42 picoseconds for the $B(v' = 9)$ state. The Ne to Cl_2 center of mass distance in the ground state, R_X , is $3.565 \pm 0.035 \text{ \AA}$ based on the experimental line positions of two rotationally assigned, nearly unblended lines in the spectrum. The structure of both the HeCl_2 and NeCl_2 van der Waals complexes is T-shaped in both the ground and excited electronic states.

In this paper we report the dependence of the NeCl_2 B state lifetimes as a function of vibrational excitation. The observed trends are compared to HeCl_2 and to the energy

gap and momentum gap laws. That the basic notion of energy gap laws applies to the rare gas-halogens seems to be beyond doubt. What remains is to obtain both potential energy surface parameters and predissociation rates as a function of vibrational and rotational quantum numbers which are accurate enough to test the details of presently available theory. Ideally, we want to have experimental measurements to evaluate the extent of coupling between the van der Waals bond and the covalent bonds in these molecules. This would be measured as a change in the van der Waals bond length upon excitation of the halogen vibration. Also, we want to be able to measure lifetimes of individual rotational levels. In this paper we report progress toward meeting those goals via 0.06 cm^{-1} laser band width spectra of the NeCl_2 $B \leftarrow X$ ($7 \leftarrow 0$) to ($13 \leftarrow 0$) and ($9 \leftarrow 1$) to ($12 \leftarrow 1$) vibronic bands. The spectra for the lowest excited electronic state vibrational levels show clearly resolved rotational transitions which can be used to extract the desired information. Analysis of this data shows that both the intermode coupling and the angular momentum effects on the dynamics are quite small.

Experimental Section

The basic design of the molecular beam apparatus as used in these experiments has been described previously,¹⁷ therefore only a brief summary is given here. A supersonic

beam was formed by passing a mixture of Ne and He at pressures varying from 100 to 300 psi over liquid Cl_2 at 200 K where the vapor pressure of Cl_2 is approximately 60 torr. The mixture was expanded through a 35μ pinhole into the vacuum chamber maintained below 10^{-4} torr by a 10,000 liter/second diffusion pump backed by a roots blower and mechanical pump.

Molecules were excited with a pulsed dye laser (Lambda Physik FL2002E) which was pumped by an XeCl excimer laser (Lumonics 861-S). This dye laser, which is equipped with an air spaced Fabry-Perot etalon, is continuously tunable over a range of 20 cm^{-1} with a bandwidth of 0.05 cm^{-1} and a pulse energy of 1-3 millijoules using Coumarin 503. The total fluorescence was detected by an S-20 photomultiplier and appropriate cutoff filters were used to reduce the stray laser light. The data were recorded on line by means of a multi-channel signal averager connected to an IBM-PC microcomputer. The experiment consists of scanning the laser through a transition of Cl_2 and further to the blue while detecting the total fluorescence from the halogen and associated van der Waals molecules.

Results

The laser-induced fluorescence spectrum of the $^{35}\text{Cl}_2$ $B \leftarrow X$ ($11 \leftarrow 1$) transition is shown in Figure 1. The feature observed $\approx 5.5 \text{ cm}^{-1}$ to the blue of the $^{35}\text{Cl}_2$ band is

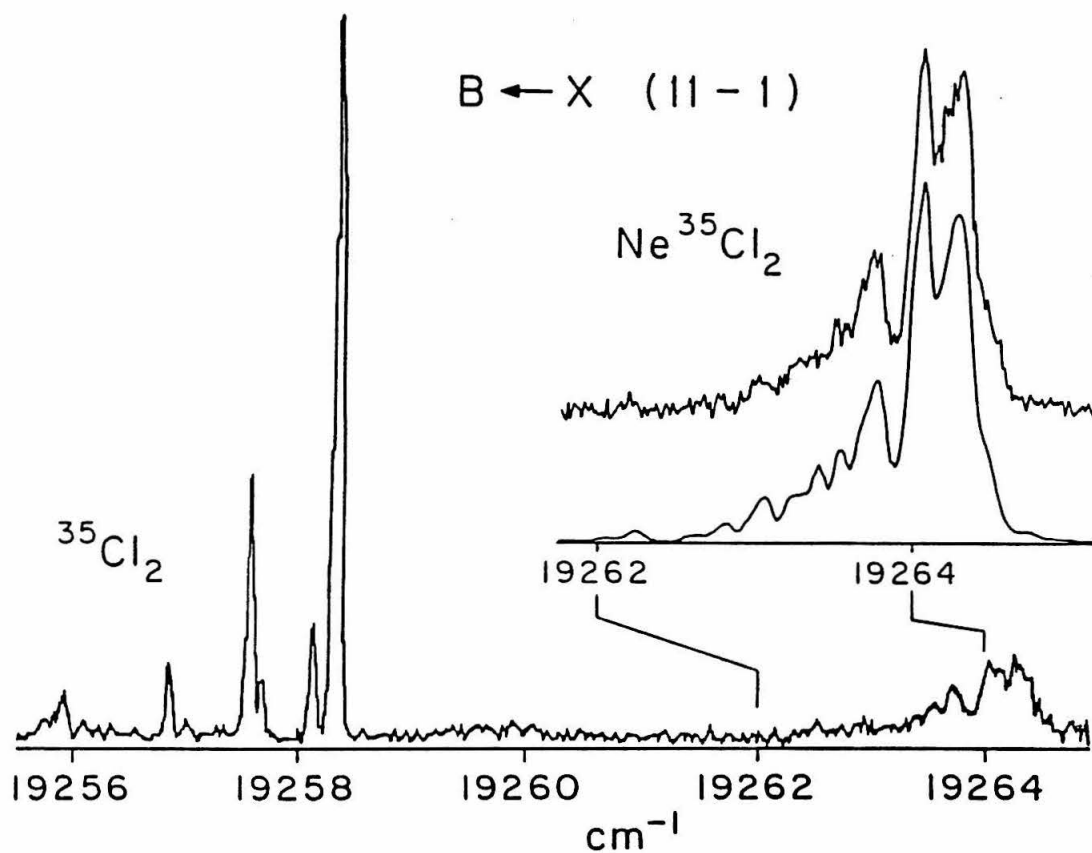


Figure 1. Laser excited fluorescence spectrum of the $B \leftarrow X$ ($11 \leftarrow 1$) vibronic band for Cl_2 and the associated van der Waals molecule NeCl_2 . The inset shows an expanded view of the transition for NeCl_2 with the fit to the data.

attributed to the $\text{Ne}^{35}\text{Cl}_2$ van der Waals molecule on the basis of pressure dependence studies.^{17,18} The feature shows a nearly quadratic dependence upon backing pressure and disappears entirely in expansions consisting of only He and Cl_2 . Excitation spectra were obtained for the $(7\leftarrow 0)$ through $(13\leftarrow 0)$ and $(9\leftarrow 1)$ through $(12\leftarrow 1)$ band of the $B\leftarrow X$ system of $^{35}\text{Cl}_2$ and the associated $\text{Ne}^{35}\text{Cl}_2$ van der Waals molecule.

The $^{35}\text{Cl}_2$ $B\leftarrow X$ excitation spectra were fit to a rigid rotor model, which included nuclear spin statistics. The temperature and the inhomogeneous linewidth were fit by a nonlinear least squares routine while the rotational constants for both the ground and excited states and the band origin were held constant at the literature values.¹⁹ The Cl_2 transitions have inhomogeneous linewidths of about 0.06 cm^{-1} which consist of a convolution of the laser bandwidth (0.05 cm^{-1}) with the Doppler width (0.01 cm^{-1}).

The NeCl_2 spectra were fit to a model consisting of a rigid T-shaped Hamiltonian for both the ground and excited states. The Cl-Cl bond distances, R_X and R_B , were assumed to be unchanged by the presence of the Ne and were held constant at the free Cl_2 literature values.¹⁹ The inhomogeneous linewidths, with laser bandwidth and Doppler contribution, were held at the values obtained from fitting the spectra of uncomplexed $^{35}\text{Cl}_2$. From the high resolution

spectrum of the NeCl_2 $B \leftarrow X$ ($9 \leftarrow 1$) transition previously reported¹⁸ we know that the portion of the spectrum which contains the most structural information is in the region to the red of the band origin. The portion of the spectrum to the blue of the band origin consists of a blend of many individual transitions and is less useful for extracting rotational constants. Since the ($7 \leftarrow 0$) and ($8 \leftarrow 0$) spectra were best resolved, they were fitted to obtain $R_X(v'' = 0) = 3.532 \pm 0.040$ Å. This value was then used in fitting all other spectra originating at $v'' = 0$. $R_X(v'' = 1) = 3.536 \pm 0.035$ as previously determined¹⁸ was used in fitting of each spectrum originating at $v'' = 1$. The fitted parameters were the rotational temperature, the natural linewidth, the band origin and $R_B(v')$. R , Γ and τ are given in Table I. The quality of the fits is shown in Figures 2, 3 and 4.

The natural linewidths for the ($7 \leftarrow 0$) and ($8 \leftarrow 0$) are too small to be determined from these spectra. For the other bands, the linewidth can be converted to a vibrational predissociation lifetime via the formula

$$\tau = (2\pi c \Gamma(\text{FWHM}))^{-1}$$

The effect of lifetime broadening is readily seen in Figures 3 and 4 as decreased resolution of the spectra. We are limited to estimating the vibrational predissociation rates for levels in the B state with $v' < 13$ because higher levels are dominated by electronic predissociation.²²

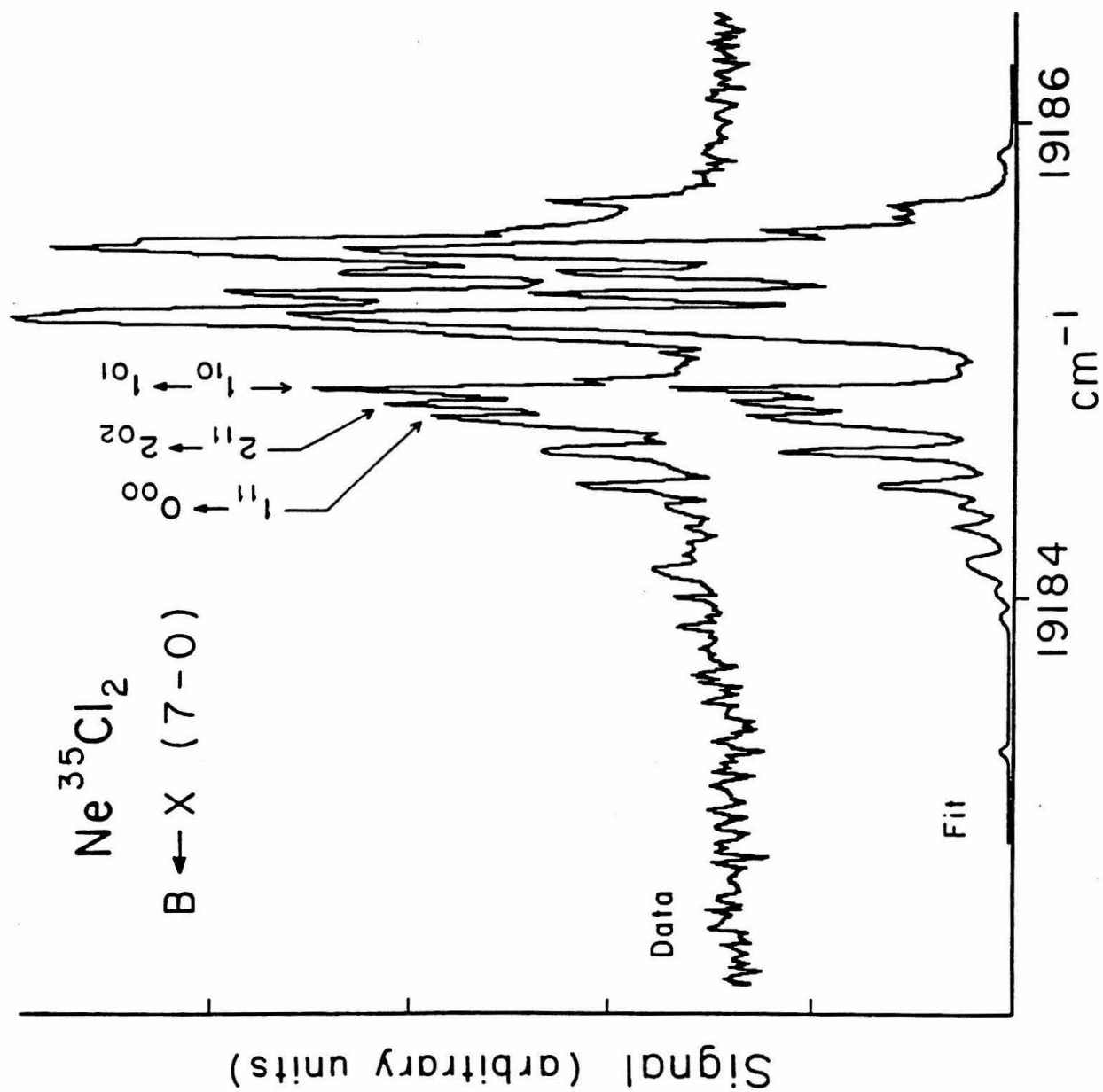
Table I. NeCl_2 Bond lengths, linewidths and lifetimes^{a)}

Band	R_B (Å)	Γ (cm^{-1})	τ (ps)
7←0	3.52 ± 0.05	-----	-----
8←0	3.51 ± 0.05	-----	-----
9←0	3.53 ± 0.05	0.022 ± 0.003	240 ± 30
10←0	3.51 ± 0.05	0.029 ± 0.003	180 ± 20
11←0	3.51 ± 0.05	0.052 ± 0.003	100 ± 6
12←0	3.51 ± 0.05	0.081 ± 0.005	66 ± 4
13←0	3.55 ± 0.05	0.16 ± 0.01	33 ± 2
9←1	$3.55 \pm 0.04^{\text{b)}}$	$0.021 \pm 0.003^{\text{b)}}$	$258 \pm 42^{\text{b)}}$
10←1	3.54 ± 0.06	-----	-----
11←1	3.51 ± 0.06	0.053 ± 0.003	100 ± 6
12←1	3.54 ± 0.06	0.070 ± 0.004	76 ± 4
<hr/>			
$R_X(v''=0)$:	3.57 ± 0.04 Å		
$R_X(v''=1)$:	3.53 ± 0.04 Å ^{b)}		

a) In each case the rotational temperature used to fit the spectrum was 0.67 ± 0.03 K.

b) From reference 18.

Figure 2. Laser excited fluorescence spectrum of NeCl_2 associated with the $B \leftarrow X$ ($7 \leftarrow 0$) transition of Cl_2 . The lower trace is the fit and the upper trace is the data. The labeled transitions give the $J_{K_{-1}K_1}$ rotational energy levels for the ground and excited states. The similar linewidths demonstrate the apparent independence of lifetime on rotational quantum number. See the text for details.



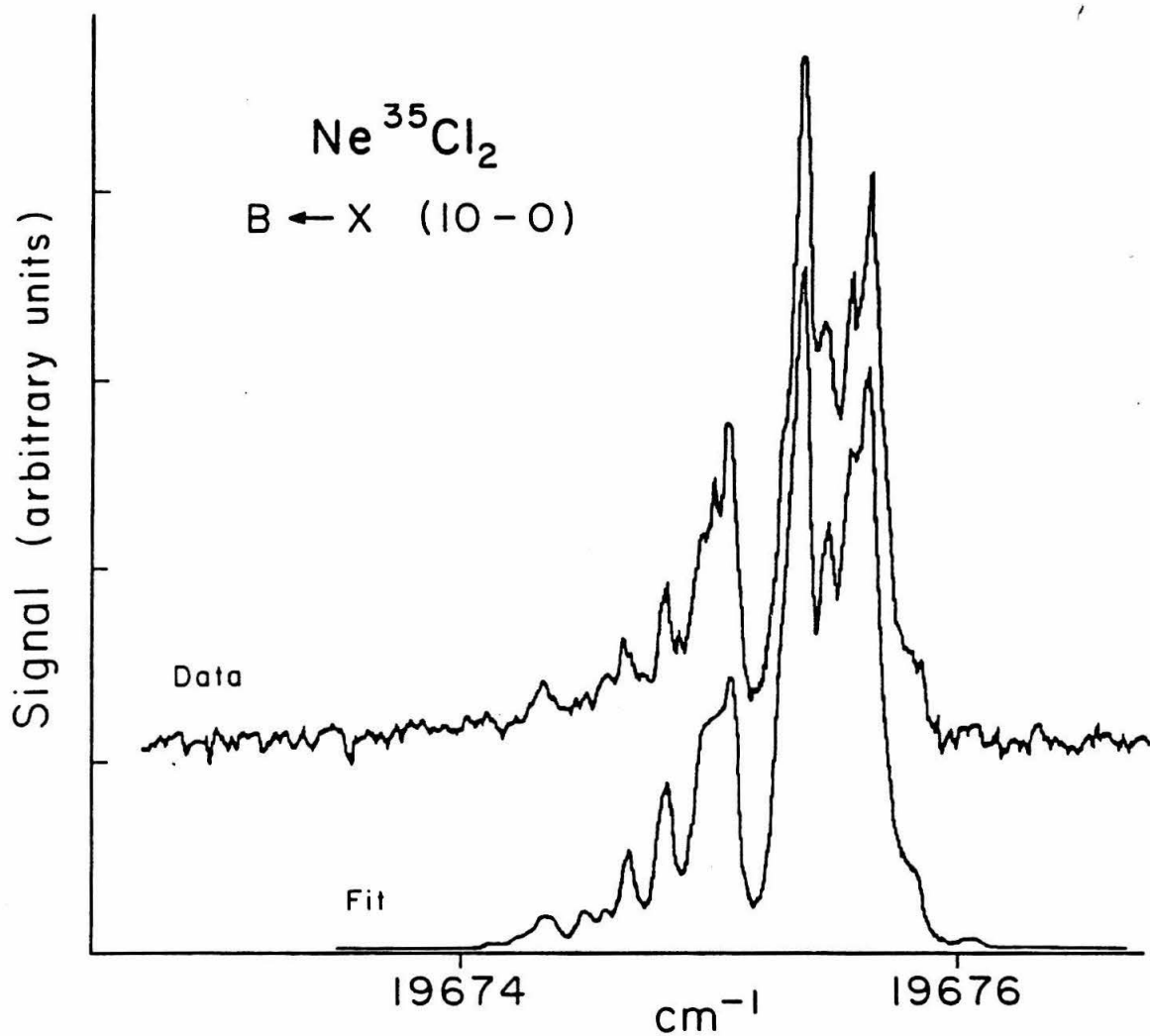


Figure 3. Laser excited fluorescence spectrum of NeCl_2 associated with the $B \leftarrow X$ ($10 \leftarrow 0$) transition of Cl_2 . The lower trace is the fit and the upper trace is the data.

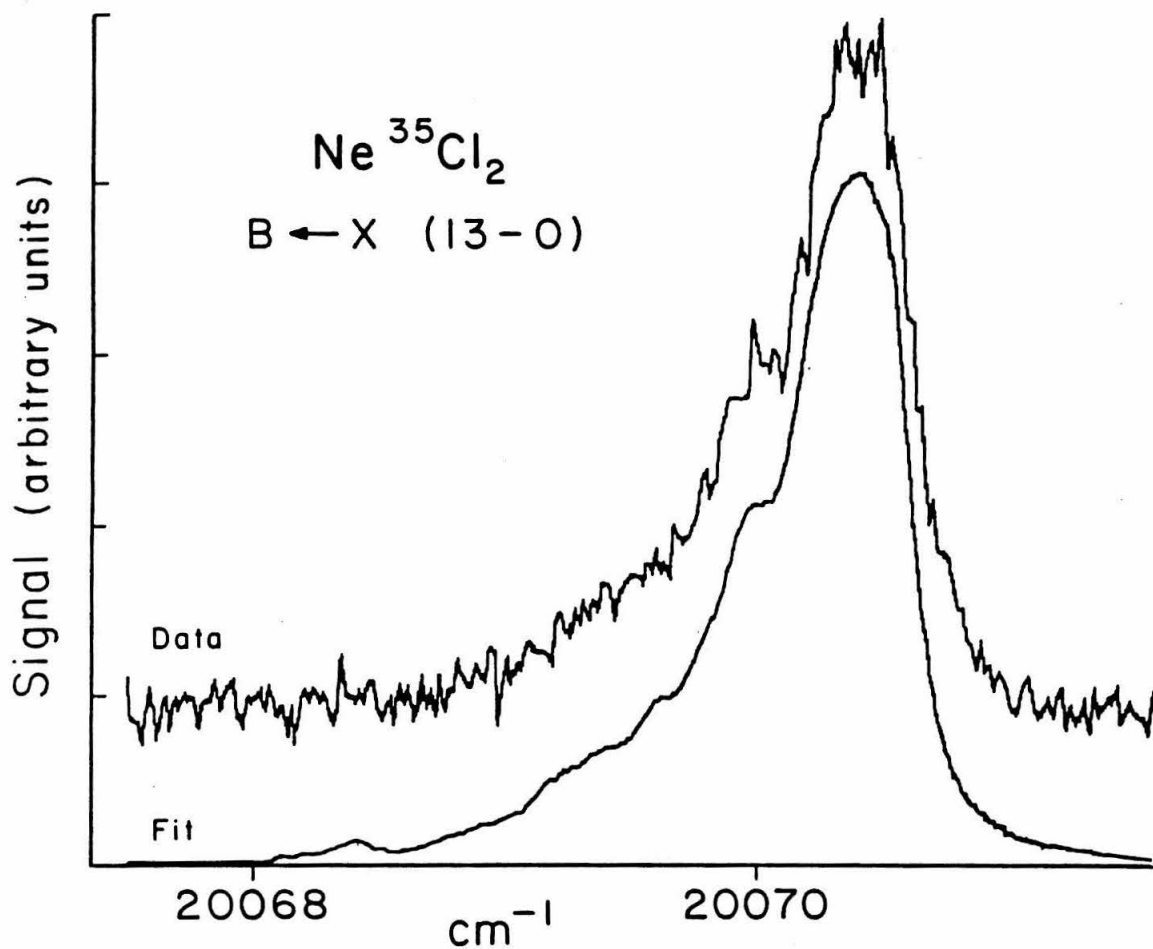


Figure 4. Laser excited fluorescence spectrum of NeCl_2 associated with the $B \leftarrow X (13 \leftarrow 0)$ transition of Cl_2 . The decreased rotational structure compared to Figures 2 and 3 is due to homogeneous lifetime broadening.

Discussion

The vibrational predissociation of rare gas-halogen dimers is particularly interesting because the combination of high resolution spectroscopy and inelastic scattering data for the isovalent series of molecules provides a more detailed test of IVR theories than for other classes of molecules. The dependence of the vibrational predissociation rate of NeCl_2 on the vibrational quantum number which we report here completes the matrix of possible combinations of He and Ne with Cl_2 ^{17,18}, Br_2 ^{11,12} and I_2 ³⁻⁶. We can now see how well the general trends predicted by gap models are obeyed by this group of molecules. The next phase of this project will be to make more quantitative predictions based on realistic intermode coupling parameters and understanding of angular momentum effects on the IVR dynamics. Analysis of the present data puts limits on the magnitude of these effects discussed below.

Ewing's analysis¹⁰ of vibrational predissociation dynamics indicates that vibrational state lifetimes should be correlated by the formula

$$-\log(\tau) = b(2\mu\Delta E_{V \rightarrow T})^{1/2}/\alpha\hbar + c$$

where τ is the lifetime, $(2\mu\Delta E_{V \rightarrow T})^{1/2}$ is the relative momentum of the dissociated products and α is the Morse range parameter for the dimer bond. The constants b and c

should be independent of the molecule at this level of approximation. Figure 5 shows how the NeCl_2 data reported here compare to the previously reported HeCl_2 data¹⁶ when correlated in this manner. D_0 for the complexes have been estimated by a one dimensional zero point energy correction of the D_e values reported by Reid, et al.²³ Values for the excited electronic state were obtained by subtracting the dimer band origin shift from the free halogen band origin.

As predicted by Ewing's model, the data for each molecule has a nearly linear dependence of $\log(\tau)$ on the momentum gap. Although the slopes of the two sets of data are somewhat different, this could be corrected by a slight adjustment of the Morse range parameters of the molecules. For a given momentum gap, however, the predissociation rates of NeCl_2 and HeCl_2 are different by several orders of magnitude. In fact, the lifetime is better correlated with the vibrational state quantum number than with the momentum gap.

By examining specific vibrational levels of I_2 , Br_2 and Cl_2 , we can compare the lifetimes of the Ne complexes of the halogens in states for which the product energy (and less accurately, momentum) is nearly independent of which halogen is bonded to the Ne atom. For instance I_2 , $v = 12$ has $\omega = 107 \text{ cm}^{-1}$, Br_2 , $v = 16$ has $\omega = 108 \text{ cm}^{-1}$ while Cl_2 , $v = 14$ has $\omega = 110 \text{ cm}^{-1}$. The vibrational predissociation lifetimes for Ne bonded to each halogen in the stated

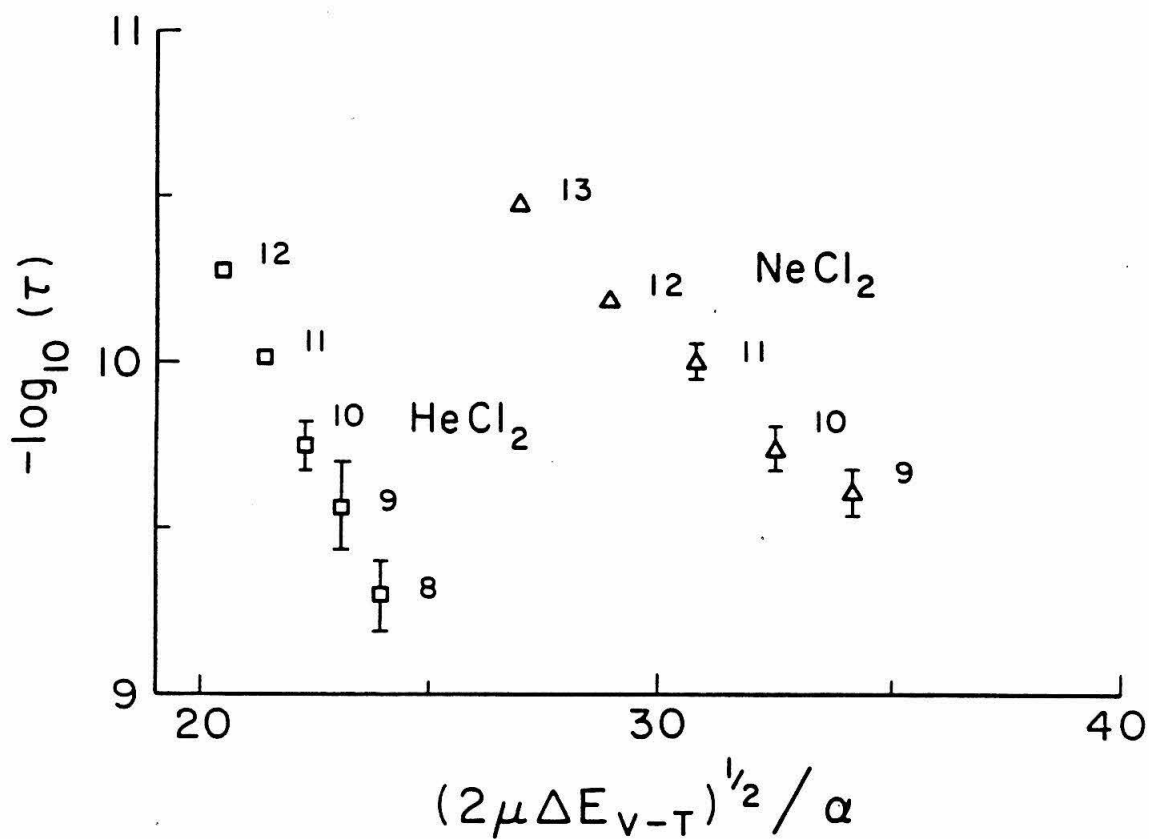


Figure 5. Plot of $-\log(\tau)$ versus $(2\mu\Delta E_{V-T})^{1/2}/\alpha$ as a test of the momentum gap law for NeCl₂ and a comparison to HeCl₂.¹⁶ 95% confidence limits are shown. See the text for details.

vibrational levels are 229 ± 118 picoseconds,²⁴ 93 ± 10 picoseconds²⁵ and 30 ± 10 picoseconds,²⁶ respectively. Thus, when compared in this fashion the correlation of lifetime with the vibrational energy which might have been inferred from Figure 5 is no longer evident, even though the energy gap should be similar for the three molecules.

Several explanations for the deviations from simple gap law correlation of the data are possible. Most obviously, we have been treating the vibrational predissociation as a simple, one dimensional process. Not only does this ignore the role of angular momentum on the dissociation dynamics, it also ignores the wide amplitude van der Waals motions within the molecules. In fact, for a rigid T-shaped structure Ewing's analysis would predict that the dissociation rate would be zero;¹⁰ only deviations from that geometry allow the weak and strong bonds to couple. It is not hard, in principle, to see how to improve the models to account for both realistic potential energy surfaces and angular momentum effects. At this time, however, we have insufficient data to proceed with such corrections. The remainder of the discussion is intended to outline what data is needed and to illustrate the experiments necessary to obtain such data.

A fairly realistic representation of the NeCl_2 X state $v = 0$ potential energy surface can be obtained from the

analysis of differential inelastic scattering data with constraints on the well position imposed by spectroscopy.²³ What remains is to determine the intermode coupling terms which relate the van der Waals bond to the Cl_2 covalent bond. One experimental source of such information would be to determine the dependence of the van der Waals bond length on the Cl_2 vibrational quantum number. As can be seen in Table I, such a dependence is too small to be measured with the present data which only determines R_X and R_B to 0.04 Å at best.

To estimate the extent to which this precision must be improved, consider the approximation that the Ne to Cl atom distance is independent of vibrational level. The increase in the Cl_2 bond length in going from the $v = 7$ level ($r_7 = 2.612$ Å)¹⁹ of the B state to the $v = 10$ level ($r_{10} = 2.722$ Å) would lead to a decrease of the van der Waals bond length of 0.02 Å between the two vibrational levels. Thus, to the extent that atom atom properties determine the potential, modest improvements in the precision of rotational constant determination will start to provide the desired coupling information.

Another source of complexity in the vibrational predissociation is the effect of angular momentum. Angular momentum may help couple the IVR process via coriolis effects as have been postulated for IVR in covalent molecules like formaldehyde.²¹ The present data show that

angular momentum is not a dominating effect in determining the IVR rate for the NeCl_2 molecule. Each of the calculated spectra in Figures 2, 3 and 4 assumes that the natural linewidth is independent of J . If the linewidth were to increase as some strong function of J , e.g., J^2 , one would expect the calculated spectrum to be too narrow for the lowest frequency transitions of Figures 2 and 3. The same J dependence would lead to a sharp, intense spike for the $J = 0$ line near the origin of Figure 4. Neither of these effects is observed in NeCl_2 or the other rare gas-halogens.

Finally, the deviation from simple gap laws which are observed may be due to rotational excitation of the halogen molecule during dissociation. Such rotational excitation, which might be considered more probable for the light halogens due to mass matching of the "half collision" partners, would serve to lower the momentum gap and thereby also reduce the predissociation lifetime. Levy reported little rotational excitation of the I_2 upon dissociation of HeI_2 and ArI_2 .⁶ Preliminary measurements in our laboratory indicate slight rotational excitation of Br_2 upon dissociation of NeBr_2 . Such measurements have yet to be reported for NeCl_2 . Thus the role of product rotation remains open.

It is interesting to note that Drobits et al., observe substantial rotational excitation of the ICl product of

vibrational predissociation of the NeICl A state $v = 14$ even though the lifetime is quite long, 3 nanoseconds.¹⁵ Unfortunately, little information is available on the potential energy surface of this molecule. It is obviously considerably more anisotropic than that of the homonuclear halogen dimers.

Summary

In this paper we reported the vibrational state dependence of the IVR rate for NeCl₂ in the B electronic state. Comparison of this data to the momentum gap law shows that while the law predicts the correct dependence of lifetime on vibrational level for individual rare gas-halogen molecules, the comparison of rates between molecules will require a more sophisticated analysis. The type of measurements necessary for more complete analysis have been discussed. Better measurements of high J line positions and lifetimes are necessary to obtain the intermode coupling terms in the potential energy surface and the angular momentum effects on the IVR rate. Product state measurements are necessary to determine the role of product angular momentum in lowering the momentum gap.

Acknowledgements

This work was supported by the National Science Foundation. Acknowledgement is made to the donors of the Petroleum Research Fund administered by the American Chemical Society for partial support of this work.

References

1. S.J. Harris, S.E. Novick, W. Klemperer, and W.E. Falconer, *J. Chem. Phys.* **61**, 193 (1974).
2. S.E. Novick, S.J. Harris, K.C. Janda, and W. Klemperer, *Can. J. Phys.* **53**, 2007 (1975).
3. R.E. Smalley, D.H. Levy, L.J. Wharton, *J. Chem. Phys.* **64**, 3266 (1976).
4. K.E. Johnson, L. Wharton, and D.H. Levy, *J. Chem. Phys.* **69**, 2719 (1978).
5. W. Sharfin, K.E. Johnson, L. Wharton, and D.H. Levy, *J. Chem. Phys.* **71**, 1292 (1979).
6. K.E. Johnson, W. Sharfin, and D.H. Levy, *J. Chem. Phys.* **74**, 163 (1981).
7. J.A. Beswick, and J.J. Jortner, *J. Chem. Phys.* **69**, 512 (1978).
8. N. Halberstadt, and J.A. Beswick, *Faraday Discuss. Chem. Soc.* **73**, 357 (1982).
9. D.W. Schwenke, and D.G. Truhlar, *Chem. Phys. Lett.* **98**, 217 (1983).
10. G.E. Ewing, *Faraday Discuss. Chem. Soc.* **73**, 325 (1982).
11. B.A. Swartz, D.E. Brinza, C.M. Western, and K.C. Janda, *J. Phys. Chem.* **88**, 6272 (1984).
12. F. Thommen, D.D. Evard, and K.C. Janda, *J. Chem. Phys.* **82**, 5295 (1985).

13. L.J. van de Burgt, J.P. Nicolai, and M.C. Heaven, *J. Chem. Phys.* **81**, 5514 (1984).
14. J.M. Skene, and M.I. Lester, *Chem. Phys. Lett.* **116**, 93 (1985).
15. J.C. Drobits, J.M. Skene, and M.I. Lester, *J. Chem. Phys.* **86**, 2896 (1986).
16. J.I. Cline, D.D. Evard, F. Thommen, and K.C. Janda, *J. Chem. Phys.* **84**, 1165 (1986).
17. D.E. Brinza, C.M. Western, D.D. Evard, F. Thommen, B.A. Swartz, and K.C. Janda, *J. Phys. Chem.* **88**, 2004 (1984).
18. D.D. Evard, F. Thommen, and K.C. Janda, *J. Chem. Phys.* **84**, 3630 (1986).
19. J.A. Coxon, *J. Mol. Spec.* **82**, 264 (1980).
20. M.A.A. Clyne, and S.I. McDermid, *J. Chem. Soc. Faraday Trans. II* **75**, 1677 (1979).
21. H.L. Dai, C.L. Korpa, J.L. Kinsey, and R.W. Field, *J. Chem. Phys.* **82**, 1688 (1985).
22. M.C. Heaven, and M.A.A. Clyne, *J. Chem. Soc. Faraday Trans. II* **78**, 1339 (1982).
23. B.P. Reid, M.J. O'Loughlin, and R.K. Sparks, to be published.
24. J.E. Kenny, K.E. Johnson, W. Sharfin, and D.H. Levy, *J. Chem. Phys.* **72**, 1109 (1980).

25. Unpublished data.
26. The value given for Cl_2 $v = 14$ is extrapolated from the data in Table I. The extrapolation ignores the electronic predissociation which affects this level.

CHAPTER V

Direct Measurement of the Vibrational Predissociation
Lifetime of NeBr_2 in the Ground Electronic State

Direct Measurement of the Vibrational Predissociation
Lifetime of NeBr_2 in the Ground Electronic State^{a)}

N. Sivakumar, D.D. Evard, J.I. Cline, and K.C. Janda

Department of Chemistry
University of Pittsburgh
Pittsburgh, PA 15260

a) This manuscript was published in modified form in
Chem. Phys. Lett. 137, 403 (1987).

Abstract

The vibrational predissociation lifetime of NeBr_2 in the ground electronic state with one vibrational quantum in the halogen stretch was measured directly in a free jet expansion. $\text{NeBr}_2(X, v = 1)$ was detected by optical-optical double resonance to monitor the population as a function of distance from the nozzle to the laser interaction region. The vibrational predissociation lifetime for $\text{NeBr}_2(X, v = 1)$ was determined to be 8 ± 3 microseconds.

Introduction

The vibrational predissociation of van der Waals molecules has proved to be a simple and theoretically tractable process for studying the rate of intramolecular energy transfer.^{1,2} The systems for which the vibrational predissociation dynamics is perhaps best characterized are the electronically excited metastable levels of the rare gas-halogen van der Waals molecules.^{1,3-9} The vibrational predissociation rates in the ground electronic states of these molecules have not been measured, aside from a lower limit of 10 microseconds for NeCl_2 .³ Direct excitation of the stretch of the halogen covalent bond within these complexes is difficult because the infrared frequencies lie in an inconvenient region of the spectrum and the transitions are expected to be very weak for complexes containing the homonuclear halogens. We report here the vibrational predissociation lifetime of the $\text{Ne}^{79}\text{Br}_2$ molecule in the ground electronic state with one vibrational quantum in the Br-Br stretching mode. This measurement was performed by monitoring the decrease in the population of the vibrationally excited level as a function of the distance from a supersonic nozzle source where the metastable state is prepared.

Experimental

A gas mixture of $\approx 0.05\%$ Br_2 in 90% Ne and 10% He (natural isotopic abundances) was expanded through a 50 micron nozzle at a backing pressure of ≈ 175 psi, into a vacuum system previously described.³ The $\text{Ne}^{79}\text{Br}_2(X, v = 1)$ molecules formed in the expansion were detected downstream from the nozzle by an optical-optical double resonance technique. The symbol X indicates the electronic state of NeBr_2 associated with the ground $X^1\Sigma_g^+$ state of Br_2 and v is the number of vibrational quanta in the Br-Br stretching mode. A pump laser pulse promotes $\text{NeBr}_2(X, v = 1)$ to an electronically excited state, which correlates with the $B^3\Pi(O_u^+)$ electronic state of Br_2 , with 10 vibrational quanta in the Br-Br stretch. The absorption of the van der Waals molecule $\text{Ne}^{79}\text{Br}_2 B \leftarrow X (10 \leftarrow 1)$ is observed $\approx 6 \text{ cm}^{-1}$ to the blue of the $^{79}\text{Br}_2 B^3\Pi(O_u^+) \leftarrow X^1\Sigma_g^+ (10 \leftarrow 1)$ transition.¹⁰ The $\text{NeBr}_2 (B, v = 10)$ molecules dissociate to Ne and $\text{Br}_2(B, v = 9)$. The lifetime of $\text{NeBr}_2(B, v = 10)$ is 355 picoseconds, as determined by the homogeneous linewidth.¹⁴ Approximately 10 nanoseconds after the pump pulse, a probe laser pulse excites the product $\text{Br}_2(B, v = 9)$ to the $v = 2$ level of the $E(O_g^+)$ electronic state.¹¹ The intensity of the ultraviolet (UV) $E \rightarrow B$ fluorescence is then a measure of the number of

NeBr₂(X, v = 1) molecules in the collection volume within the expansion.

The number density of a stable molecule such as Br₂ will decrease roughly with $1/r^2$ as the distance from the nozzle, r , increases. Vibrational predissociation of NeBr₂(X, v = 1) to form Ne and Br₂(X, v = 0) will result in its number density falling off faster than $1/r^2$ with increasing r . Measuring the ratio of the populations of NeBr₂(X, v = 1) to Br₂(X, v = 1) as a function of r yields the vibrational predissociation rate. Comparison of the NeBr₂(X, v = 1) UV fluorescence signal to the Br₂(X, v = 1) fluorescence signal as a function of distance from the nozzle separates the effect of dissociation from the decrease due to the geometrical expansion of the jet.

Two dye lasers (Lambda Physik FL2002) pumped by a XeCl excimer laser (Lambda Physik EMG 201 MSC) generated pump and probe laser pulses. The output of one dye laser was frequency doubled in KDP to generate the UV probe pulse. The pump and probe laser beams propagated colinearly through the vacuum chamber 90° to the axis of the jet. The probe pulse was delayed approximately 10 nanoseconds from the pump pulse. A UV sensitive photomultiplier tube (EMI 9558QA) detected fluorescence. The signal was preamplified (LeCroy VT100B) and averaged by a boxcar integrator (Stanford Research Systems SR250) using

a 300 nanosecond wide gate. The UV laser intensity was monitored by a photodiode viewing a dye cell illuminated by a reflection from the laser beam. A second boxcar integrator averaged the photodiode signal. The dye lasers and doubling crystal were scanned by a microcomputer which also controlled the synchronization of the laser trigger and detection electronics and stored the data.

Fluorescence was collected at 90° to the plane of the laser beams and jet axis by a quartz lens (75 millimeter focal length, $f/0.7$). The scattered light from the visible laser beam was filtered by a Corning 7-54 filter. An adjustable aperture placed between the photomultiplier and lens defined the area from which fluorescence was collected and also rejected scattered UV light. Fluorescence was collected from a 2 millimeter diameter cylinder defined by the probe laser beam. The aperture defined the cylinder to be 5 millimeters in length.

The probe laser wavelength was tuned to the R branch head of the $^{79}\text{Br}_2 E(0_g^+) \leftarrow B^3\Pi(0_u^+)$ ($2 \leftarrow 9$) band and the pump laser wavelength was scanned through the $^{79}\text{Br}_2 B \leftarrow X$ ($10 \leftarrow 1$) band and the $\text{Ne } ^{79}\text{Br}_2 B \leftarrow X$ ($10 \leftarrow 1$) transition. Since the 7-54 filter transmits a fraction of the visible fluorescence from the excited $v = 10$ vibrational level of $\text{Br}_2(B)$, the $\text{Br}_2(X, v = 1)$ excitation spectrum could be recorded with the double resonance spectrum of

NeBr₂(X, v = 1) in the same scan. Negligible visible fluorescence due to the decomposition product Br₂(B, v = 9) was observed. Visible fluorescence excitation spectra of the reference Br₂(X, v = 1) and double resonance spectra of NeBr₂(X, v = 1) were obtained at distances ranging from 4 to 11 millimeters from the nozzle. Double resonance spectra were normalized to the probe laser intensity.

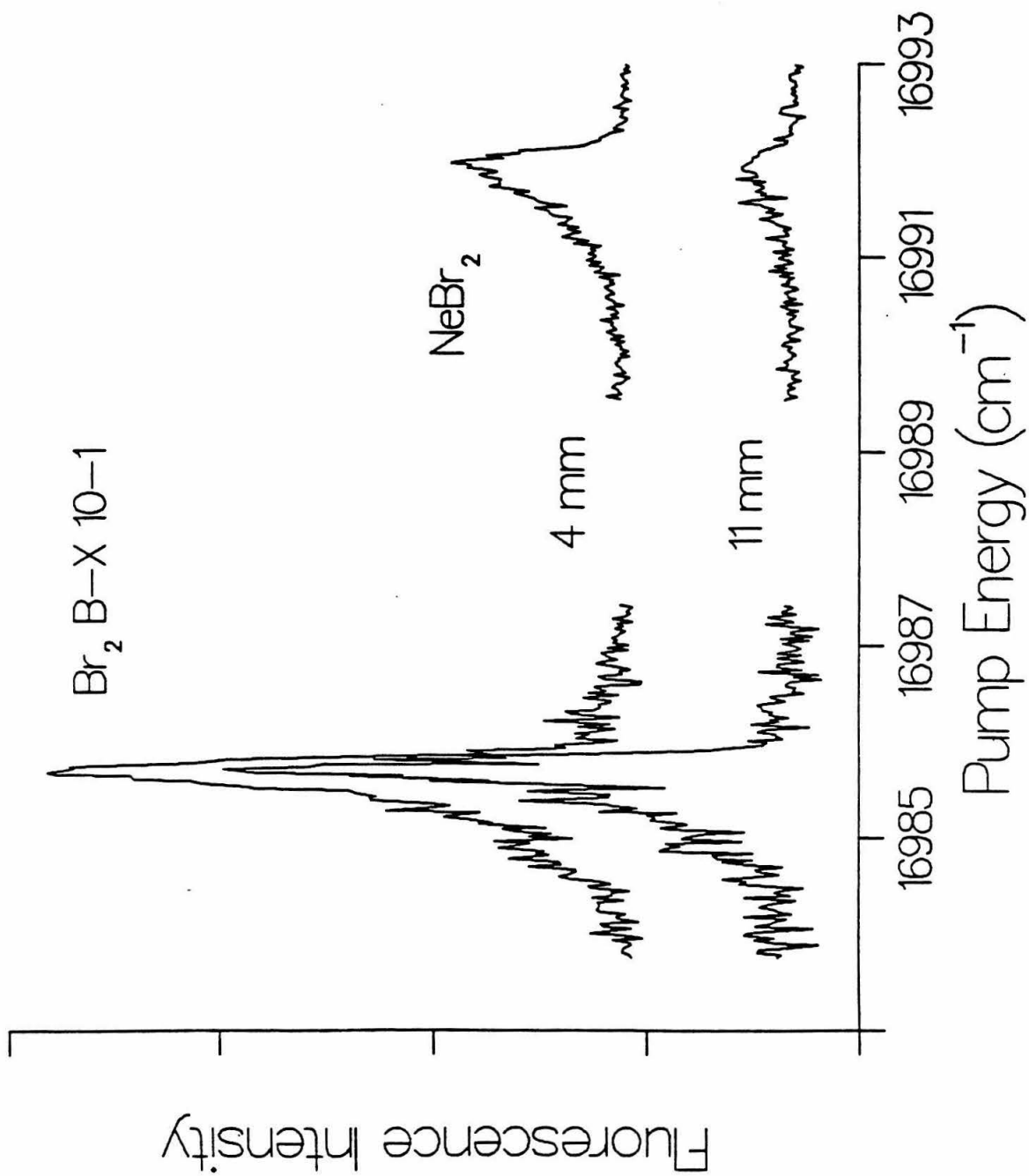
Results

Figure 1 shows spectra obtained at two different distances, 4 and 11 millimeters from the nozzle. These show the decrease in the NeBr₂(X, v = 1) population relative to the Br₂(X, v = 1) population. In order to confirm that the change in relative intensities indicates only a decay in the NeBr₂(X, v = 1) population, similar spectra were recorded for the uncomplexed Br₂ B←X (10←0) band and the corresponding NeBr₂ B←X (10←0) band. The probe laser transition used was the same as that used in the study of NeBr₂(X, v = 1). No change in the relative intensity of the NeBr₂(X, v = 0) to that of Br₂(X, v = 0) is observed over the range of distances for which NeBr₂(X, v = 1) was studied.

The density of NeBr₂(X, v = 1) molecules in the jet at a distance r from the nozzle can be written as

$$\rho(r) = \rho_0(r) \exp(-rk/u) \quad (1)$$

Figure 1. The spectra in this figure are of Br_2 and NeBr_2 taken at a distance of 4 and 11 millimeters from the nozzle to the laser interaction region. The Br_2 spectra are obtained by laser induced fluorescence while the NeBr_2 spectra are taken using optical-optical double resonance. The spectra are normalized such that the Br_2 peaks are of equal intensity. The observed decrease in the ratio of NeBr_2 to Br_2 is due to the vibrational predissociation of $\text{NeBr}_2(X, v = 1)$.



where $\rho_0(r)$ is the density of the NeBr_2 molecules at a distance r in the absence of dissociation, u is the velocity of NeBr_2 in the jet, and k is the first order rate constant for the dissociation. To correct for the decrease in $\rho_0(r)$ as the distance from the nozzle is increased, the integrated intensity of the NeBr_2 feature at r is divided by the ratio of the Br_2 integrated fluorescence intensity at r to that at the smallest distance studied. Figure 2 shows a plot of the logarithm of the corrected intensity versus the distance from the nozzle to the laser interaction region. The slope of the best straight line fit to this plot gives a value for k/u . The velocity of the jet is determined to be approximately 7.4×10^5 millimeters/second using the equation

$$\langle \text{K.E.} \rangle = \frac{1}{2}mu^2 = \frac{5}{2}k_b T \quad (2)$$

and assuming that the temperature of the gas has equilibrated to room temperature after travelling 7 meters from the Br_2 trap to the nozzle. This equation should be fairly accurate since the extent of cluster formation is small. The lifetime $\tau = 1/k$ is found to be 8 ± 3 microseconds. The quoted error reflects the spread obtained using different sets of data for the distance dependence.

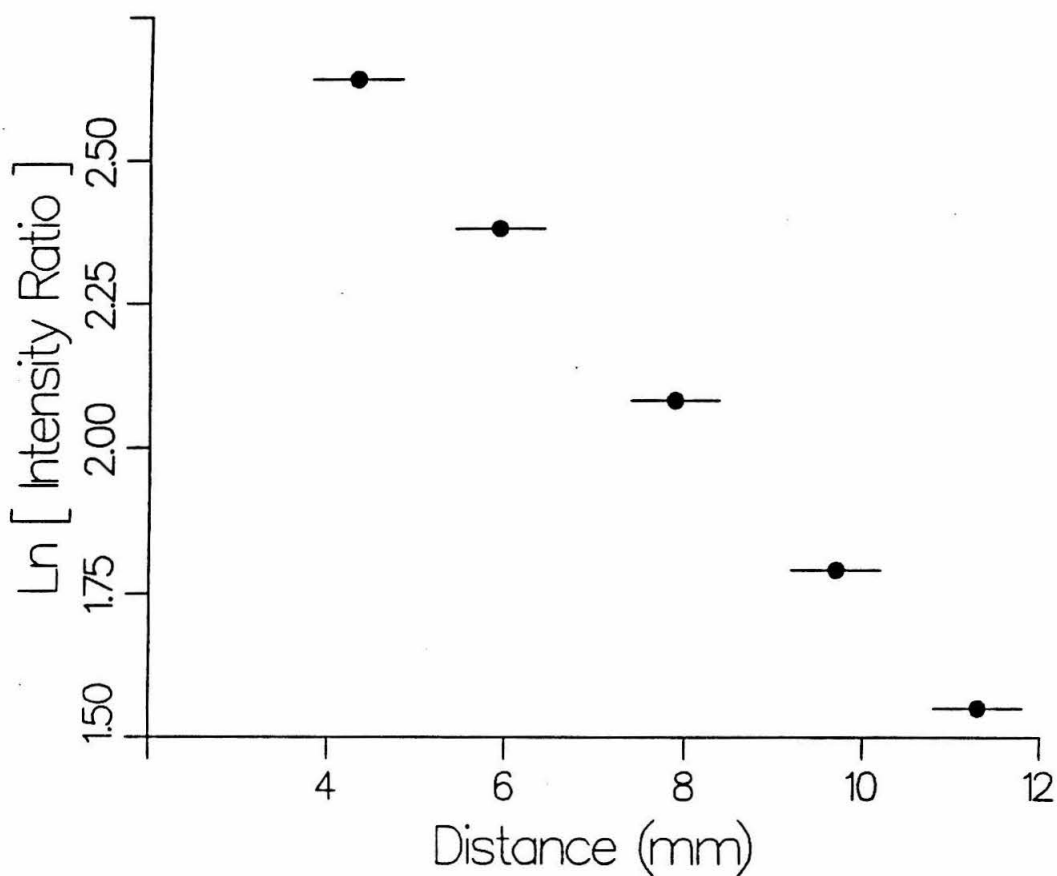


Figure 2. The intensity ratio of the NeBr₂ feature to the Br₂ feature, normalized to the Br₂ intensity at 4 millimeters, is plotted versus the distance from the nozzle to the laser interaction region. The slope gives a value for k/u where u is the velocity of the molecules in the expansion and k is the rate constant for the vibrational predissociation.

Discussion

Several experimental factors introduce error into the lifetime determination. There is an uncertainty of ± 0.5 millimeters in the distance at which the intensity ratios were determined. The correction for the decrease in $\rho_0(r)$ should include the fact that the photomultiplier does not view a point source of fluorescence. The pump and probe beam diameters which determine the volume of the jet from which fluorescence is detected are a large fraction of the distance from the nozzle. The intensity of the NeBr_2 feature should be given by

$$I \sim \int_V \rho_0(r) \exp(-rk/u) dV \quad (3)$$

where V is the collection volume in the jet.

Another source of error is that the rotational and vibrational temperature as well as the degree of cluster formation may be a function of position in the jet. However, the Br_2 rotational temperature distributions were constant over the range of distances used. This indicated that the smallest distance used is far enough downstream from the nozzle source that no further cooling occurs. The same value for the lifetime is obtained using different apertures which change the dimension of the collection

volume perpendicular to the plane of the axis of the lens. Since the above analysis applied to $\text{NeBr}_2(X, \nu = 0)$ does not result in any artifactual decay, these factors do not contribute greatly to the observed decay of $\text{NeBr}_2(X, \nu = 1)$.

The vibrational predissociation lifetime may also be estimated from a comparison of the intensity ratio of $I[\text{Br}_2(X, \nu = 0)]/I[\text{NeBr}_2(X, \nu = 0)]$ to the intensity ratio of $I[\text{Br}_2(X, \nu = 1)]/I[\text{NeBr}_2(X, \nu = 1)]$ assuming that these ratios for a given distance from the nozzle would be the same if the $\text{NeBr}_2(X, \nu = 1)$ molecules did not dissociate. Use of the ratios (≈ 0.04 and ≈ 2.5 respectively) measured for the smallest distance studied, gives a value for the lifetime of ≈ 1 microsecond. However, the assumption that $\text{NeBr}_2(X, \nu = 0)$ and $\text{NeBr}_2(X, \nu = 1)$ concentrations should be the same fraction of $\text{Br}_2(X, \nu = 0)$ and $\text{Br}_2(X, \nu = 1)$, respectively, need not be valid. Therefore, we view 8 microseconds to be closer to the actual value of the lifetime.

In view of the difficulties discussed above, the reported lifetime should be regarded as an order of magnitude determination. Even at this level of precision, this result is an interesting test of the energy gap law^{2,12} which adequately predicts the observed trends in vibrational predissociation rates for the rare gas-halogens

in excited electronic states. Beswick and Jortner have presented an intriguing correlation of the homogeneous linewidth of an observed transition with several parameters, including the amount of energy which must be deposited into product translational kinetic energy.¹² The resonance half-width, Γ , may be expressed as

$$\Gamma \propto \nu \hbar \omega \exp[-(2\mu\Delta E)^{1/2}/\alpha\hbar] \quad (4)$$

In this equation ν is the vibrational quantum number of the halogen, $\hbar\omega$ is the harmonic oscillator vibrational energy, ΔE is the energy of the vibrational quantum expended in the dissociation minus the energy required to break the van der Waals bond, μ is the reduced mass of the atom-diatom system, and α is the Morse range parameter for the atom-diatom stretching coordinate. The vibrational predissociation lifetime, τ , can be related to the homogeneous linewidth, Γ , by the equation

$$\tau = (2\pi c\Gamma)^{-1} \quad (5)$$

where c is the speed of light. Homogeneous linewidth measurements have been used to study the lifetimes of NeBr_2 with various quanta of excitation in the Br-Br stretch. Increasing vibrational excitation corresponds to decreasing values of ΔE because of the anharmonicity of the Br-Br stretching potential.^{4,13,14} The lifetimes range from a value of 355 ± 100 picoseconds for $\nu = 10$ to 2.8 ± 0.3 picoseconds for $\nu = 30$. Figure 3 shows a plot of

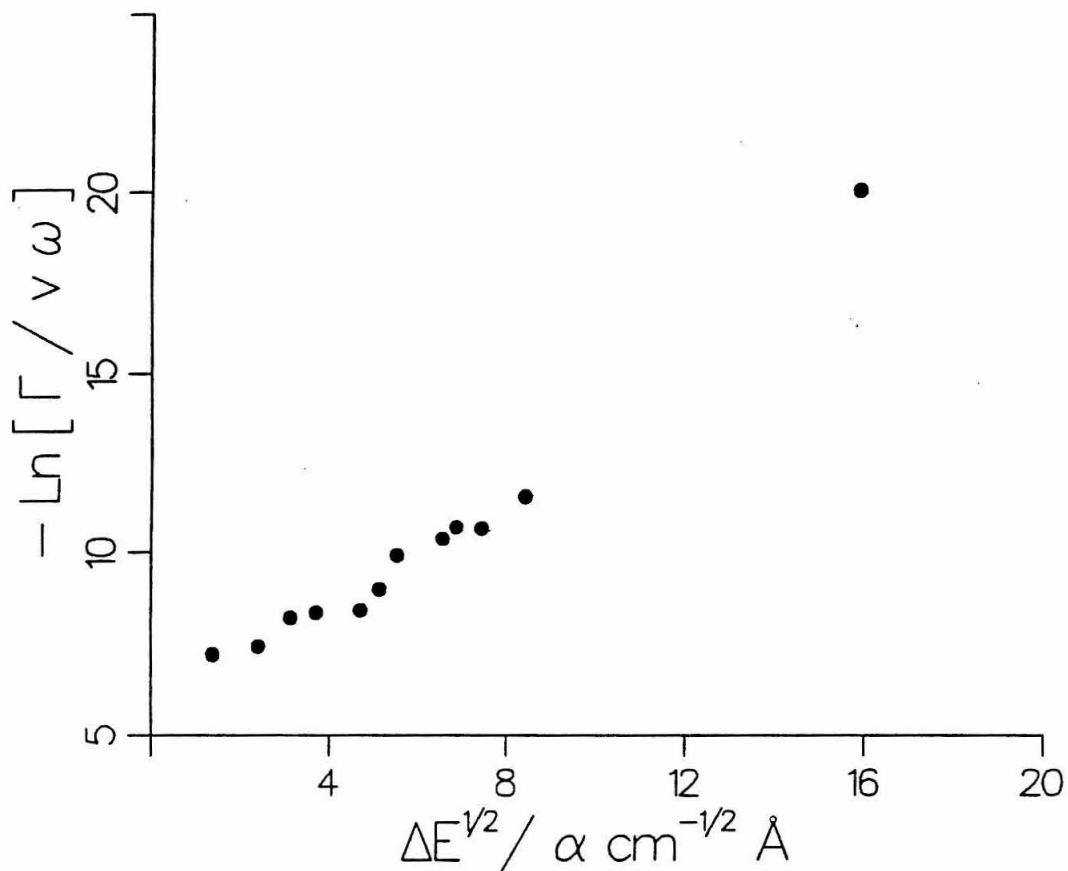


Figure 3. A plot of $-\ln[\Gamma/v\omega]$ versus $\Delta E^{1/2}/\alpha$ as a test of the energy gap model¹² for the vibrational predissociation of NeBr_2 . The points in the lower left are from the *B* state determined previously^{4,14} while the single point in the upper right is from the ground state determined in this paper.

$-\ln(\Gamma/\nu\hbar\omega)$ versus $\Delta E^{1/2}/\alpha$ to show the experimental agreement with Equation (4). Note that Equation (4) was proposed for the predissociation of a linear van der Waals molecule. The extrapolation from one vibrational frequency to another depends very sensitively on the range parameter, α . Although the form of the coupling for the T-shaped molecule is expected to be different from that assumed in the correlation, it is still instructive to compare the lifetimes in the B electronic state to the appropriate value of ΔE for NeBr_2 $\nu = 1$ in the ground electronic state. The value obtained, 0.6 microseconds, by extrapolating from the lifetimes in the B electronic state is nearly within an order of magnitude of the experimentally determined lifetime of 8 ± 3 microseconds. The variation in the two values may be explained by differences in the shape of the potentials in the ground and excited states. Further studies to determine the lifetimes of $\text{NeBr}_2(\nu = 2, 3)$ would help to clarify the question.

The analysis above assumes that all of the available energy, ΔE , goes into relative translational kinetic energy of the atom and diatom. The product $\text{Br}_2(B)$ vibrational and rotational quantum state distributions for the vibrational predissociation of the B state of NeBr_2 have been measured recently.¹³ Very little rotational excitation ($\approx 5\%$ of the available energy) of the Br_2 is observed, and thus the

mechanism is inferred to be a nearly pure $V \rightarrow T$ process. So far no measurements of the product state distribution for vibrational predissociation of rare gas-halogen van der Waals molecules on the ground electronic surface have been performed. Any significant participation of the rotational degree of freedom would be expected to increase the predissociation rate over that estimated from the energy gap law. Since the measured rate for the ground electronic surface is longer than predicted by extrapolating data from the B state, we conclude that rotation is probably not important in the vibrational predissociation process occurring on the the ground state surface. Instead it seems reasonable that the coupling between the covalent and van der Waals bonds is simply stronger on the excited state surface. The Morse range parameter must be 25% larger for the excited state potential energy surface to account for the entire difference found in extrapolating from the excited state to the ground state lifetimes. Along with the very similar van der Waals bond lengths measured for the two states¹⁴ this result suggests that both the van der Waals potential energy surface and the anharmonic terms between the covalent stretch and the van der Waals modes are quite similar for the X and B electronic states.

Conclusions

We have reported a value of 8 ± 3 microseconds for the vibrational predissociation lifetime of the $v = 1$ level of the ground electronic state of NeBr_2 . The lifetime measurement shows good agreement with a prediction based on the energy gap extrapolation of lifetimes of several vibrational levels of the *B* electronic state. Apparently, both the vibrational predissociation mechanism and the van der Waals potential energy surface are similar for the two electronic states.

Acknowledgement

We would like to acknowledge the financial support of the National Science Foundation (N.S., J.I.C., and K.C.J.) and the United States Department of Energy (D.D.E). We wish to thank Professor Alberto Beswick for helpful discussions and Professor Michael Golde for the loan of the KDP crystal.

References

1. D.H. Levy, *Adv. Chem. Phys.* **47**, 323 (1981).
2. J.A. Beswick and J. Jortner, *Adv. Chem. Phys.* **47**, 363 (1981).
3. D.E. Brinza, C.M. Western, D.D. Evard, F. Thommen, B.A. Swartz and K.C. Janda, *J. Phys. Chem.* **88**, 2004 (1984).
4. B.A. Swartz, D.E. Brinza, C.M. Western, and K.C. Janda, *J. Phys. Chem.* **88**, 6272 (1984).
5. D.D. Evard, F. Thommen, and K.C. Janda, *J. Chem. Phys.* **84**, 3630 (1986).
6. J.I. Cline, D.D. Evard, F. Thommen, and K.C. Janda, *J. Chem. Phys.* **84**, 1165 (1986).
7. L.J. van de Burgt, J.P. Nicolai, and M.C. Heaven, *J. Chem. Phys.* **81**, 5514 (1984).
8. J.C. Drobits, J.M. Skene, and M.I. Lester, *J. Chem. Phys.* **84**, 2896 (1986).
9. J.M. Skene, J.C. Drobits, and M.I. Lester, *J. Chem. Phys.* **85**, 2329 (1986).
10. R.F. Barrow, T.C. Clark, J.A. Coxon and K.K. Yee, *J. Mol. Spectrosc.* **51**, 428 (1974).
11. P. Berwanger, K.S. Viswanathan, and J. Tellinghuisen, *J. Mol. Spectrosc.* **91**, 275 (1982).
12. J. A. Beswick, and J. Jortner, *J. Chem. Phys.*, **68**, 2277 (1978).

13. J.I. Cline, D.D. Evard, B.P. Reid, N. Sivakumar, F. Thommen, and K.C. Janda, Proceedings of the NATO Advanced Research Workshop on Weakly Bound Molecular Complexes, Maratea, Italy, September, 1986, in press.
14. F. Thommen, D.D. Evard, and K.C. Janda, J. Chem. Phys. **82**, 5295 (1985).

Chapter VI

**The Structure and Dynamics of the ArCl₂
van der Waals Molecule**

The Structure and Dynamics of the ArCl_2
van der Waals Molecule

Dwight D. Evard, Joseph I. Cline, N. Sivakumar
and Kenneth C. Janda

Department of Chemistry
University of Pittsburgh
Pittsburgh, PA 15260

Abstract

The ArCl_2 van der Waals molecule was studied by a two laser pump-probe technique. The complex has a T-shaped geometry in both the ground and excited states, with a bond energy, D_0 , of $187.9 \pm 0.4 \text{ cm}^{-1}$ in the $X(v = 0)$ state and $178.4 \pm 0.3 \text{ cm}^{-1}$ in the $B(v = 7)$ state. The homogeneous linewidth of the ArCl_2 $B(v = 11)$ band was measured and indicates that the prepared state has a lifetime of 83 ± 10 psec. The one quantum predissociation process is the preferred channel when it is energetically accessible. The rotational distributions of the Cl_2 fragment formed in the two vibrational quantum dissociation are not smooth and are nonstatistical in nature. The distributions indicate relaxation to the intermediate bound level with one vibrational quantum transferred to the van der Waals modes.

Introduction

It has been over a decade since the pioneering work on HeI_2 was first published by Levy and coworkers.¹ In the past ten years a number of studies have been performed on the rare gas-halogen van der Waals molecules.^{2,3} The rare gas-halogen complexes provide a model system for the study of intramolecular energy transfer and are amenable to experimental and theoretical studies.²⁻⁴ Recent pump-probe studies of rare gas-halogen van der Waals molecules will be described to outline the application of this technique.

Lester and coworkers have used optical-optical double resonance techniques to study the vibrational predissociation of the NeICl van der Waals complex in the $A(^3\Pi_1)$ state.^{5,6} The pump laser excited the $A^3\Pi_1(v=14) \leftarrow X^1\Sigma^+(v=0)$ transition of NeICl formed in a free jet expansion. A second dye laser, delayed by 0 to 15 nsec from the pump laser pulse, was scanned through several $E \leftarrow A$ transitions while the E state fluorescence was detected. As the delay between the pump and probe lasers was increased, they observed increased intensity of a spectroscopic feature due to the dissociation fragment ICl $E \leftarrow A$ transitions. Simultaneously, they noted a decrease in intensity of several features attributed to direct excitation of the NeICl complex from the A state to the E state. The vibrational predissociation lifetime of NeICl in the $A(v=14)$ state is 3 ± 2 nsec.

The features attributed to direct excitation of the NeICl complex to the E state constitute a progression in the van der Waals stretching mode. The bond energy, D_0 , of NeICl in the $E(v = 1)$ state is $87.6 \pm 0.8 \text{ cm}^{-1}$ based on a Birge-Sponer analysis of the progression. The bond energy is $48.2 \pm 0.5 \text{ cm}^{-1}$ in the $X(v = 0)$ state and $43.3 \pm 0.9 \text{ cm}^{-1}$ in the $B(v = 15)$ state as determined by the shifts of the spectroscopic features. The progression observed in the van der Waals stretching mode indicates that there is a significant change in geometry in going from the A to the E states.

Skene et al. report rotational distributions of the ICl fragment in the predissociation of NeICl and HeICl van der Waals complexes excited to the $B(^3\Pi_0^+)$ state.⁷ These distributions are relatively narrow, are highly peaked and are nonstatistical. In the case of HeICl the rotational distribution is peaked at $j = 8$, while for NeICl the rotational distribution is peaked at $j = 17$, corresponding to 6.1 and 25.9 cm^{-1} of rotational energy in the ICl fragment, respectively. The classical impact parameter for the dissociation of HeICl and NeICl ranges from 0.7 to 2.1 \AA , which is quite reasonable for an impulsive model of dissociation.

Janda and coworkers have studied the vibrational predissociation of NeCl_2 and HeCl_2 using pump-probe techniques.^{8,9} The rotational distribution for Cl_2 formed

in the dissociation of NeCl_2 $B(v = 11)$ is peaked at low j , but has a flat tail extending out to high j . The highest Cl_2 fragment rotational state corresponds to the maximum allowed by the available energy. They were able to bracket the bond energy for Ne-Cl_2 between 44 and 52 cm^{-1} by subtracting the centrifugal barrier height and the fragment Cl_2 rotational energy from the energy of the Cl_2 vibrational quantum expended in the dissociation. They also observed an even/odd intensity alternation which depended upon the position of the pump laser.

Cline et al. studied the parity constraints of the dissociation of HeCl_2 .⁹ The relatively large rotational constants of HeCl_2 permitted excitation of a specific HeCl_2 rotational state, which decayed to give Cl_2 fragments which possessed the same symmetry with respect to exchange of the Cl atoms. The rotational distribution was peaked at $j = 2$ and had a second maximum near $j = 9, 10$ with a node at $j = 7$. The distribution extended out to $j = 14$, which is well below the limit which is energetically allowed. The node in the distribution may be due to a rotational rainbow or quantum interference effects in the dynamics.

In the present paper we report pump-probe spectra of several bands of the ArCl_2 van der Waals molecule. We have obtained parity-selected excitation spectra which reduce spectral congestion and allow a more accurate determination of the geometry of the complex. We report the ArCl_2 bond

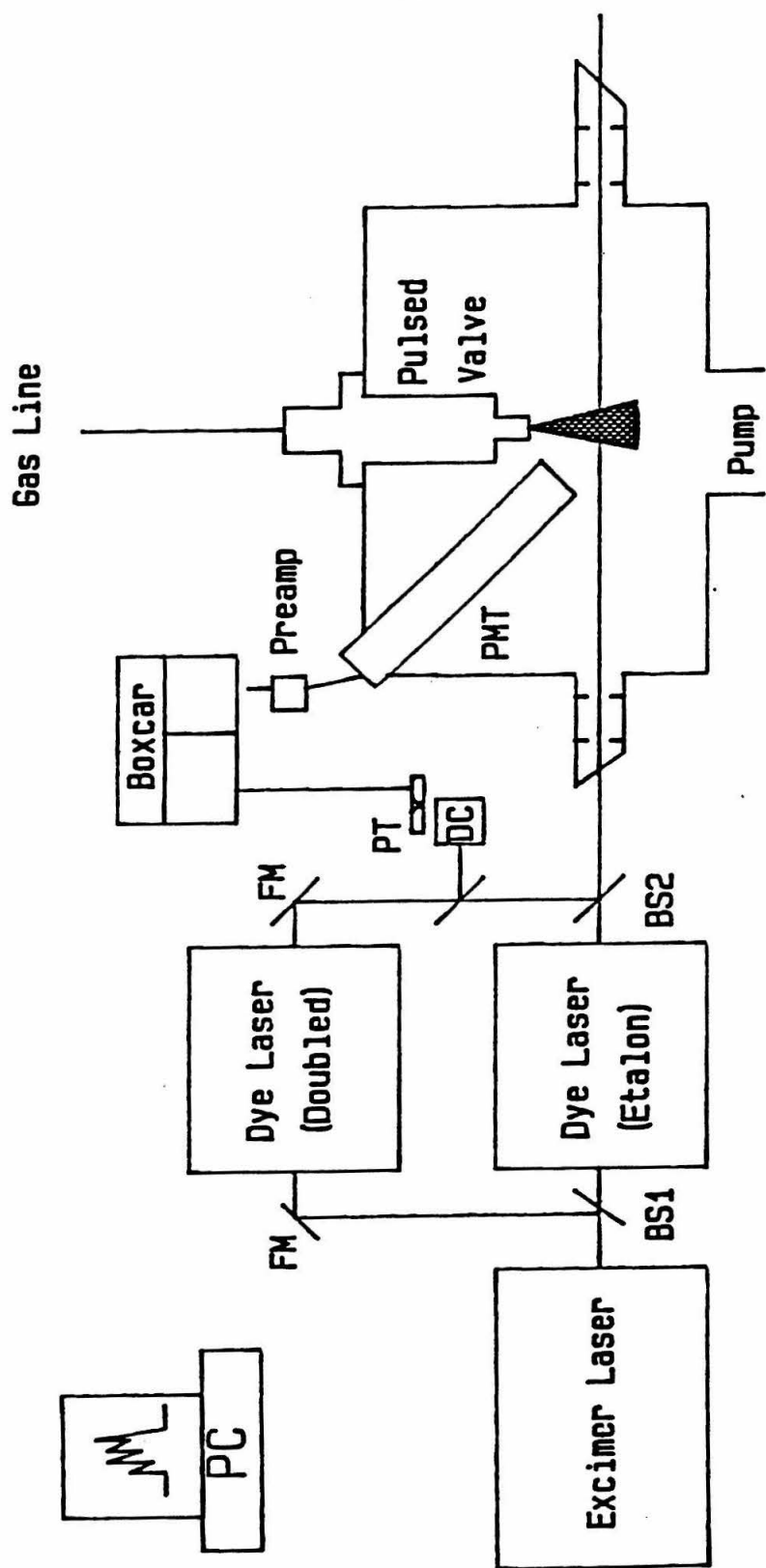
dissociation energy in the X and B states and rotational distributions of fragment Cl_2 formed in the dissociation. The dynamics of the vibrational predissociation process is discussed and is compared to previously reported work on other rare gas-halogen systems.

Experimental

A schematic representation of the experimental apparatus is shown in Figure 1. The pump laser is tuned through the $B \leftarrow X$ transitions of ArCl_2 , over the range 490 - 530 nanometers, preparing the complex in a particular level of the B state with ν quanta in the Cl_2 stretching mode.¹⁰ The weak van der Waals bond ruptures and the product Cl_2 is probed by tuning the second laser through the $E \leftarrow B$ transition in the range 250 - 260 nanometers.¹¹ The $E \rightarrow B$ fluorescence of Cl_2 is detected by a photomultiplier. An excitation spectrum may be obtained by scanning the pump laser while the probe laser is tuned to a particular $E \leftarrow B$ transition. Alternately, the rotational distribution of the Cl_2 product may be obtained by scanning the probe laser while the pump laser excites some initial levels of the complex in the B state.

The vacuum apparatus has been described previously.^{12,13} The backing gas is formed by passing 2.5% Ar in He over liquid Cl_2 held at -78 K. ArCl_2 van der Waals molecules are prepared in a pulsed, free jet

Figure 1. A schematic diagram of the experimental apparatus. The excimer beam is split by a beam splitter (BS1) coated to reflect 60% of the incident light at 308 nm. The pump and probe beams are combined by an optic (BS2) coated to reflect UV light and transmit visible light. Folding mirrors (FM) are used to direct the laser beams, and a portion of the probe pulse is sent through a dye cell (DC) and the fluorescence is detected by a phototransistor (PT). A UV sensitive photomultiplier (PMT) detects $E \rightarrow B$ fluorescence of Cl_2 . An IBM-PC controls the lasers and boxcars and accumulates the signal.



expansion through a 150 μm orifice (General Valve) at a stagnation pressure of 320 psi. The gas pulse is probed ≈ 5 centimeters downstream of the nozzle.

Two dye lasers, operating with Coumarin 503 dye, are pumped by a XeCl excimer laser to generate the pump and probe laser pulses. The first dye laser is equipped in some experiments with an angle tuned, air spaced Fabry-Perot etalon to reduce the linewidth to $\approx 0.05 \text{ cm}^{-1}$ from $\approx 0.2 \text{ cm}^{-1}$. The output of the second dye laser is doubled in KPB to generate the probe laser pulse, while the fundamental is rejected by a Schott UG-5 filter. The pump and probe beams are combined with an optic which reflects UV and passes visible radiation. The beams then propagate collinearly through Brewster windows into and out of the chamber. The probe laser is delayed approximately 10 nanoseconds from the pump pulse and the temporal width of each pulse is ≈ 20 nanoseconds. UV fluorescence is collected perpendicular to the laser and free jet axes by an imaging quartz lens with a 75 millimeter focal length ($f/0.7$). This lens focusses the fluorescence onto a UV sensitive photomultiplier tube (EMI 9558QA), while a Corning 7-54 filter attenuates the scattered visible laser light. The experiment is controlled by a microcomputer which scans the pump and probe lasers, triggers the excimer laser, pulsed valve and boxcar, and stores the data.

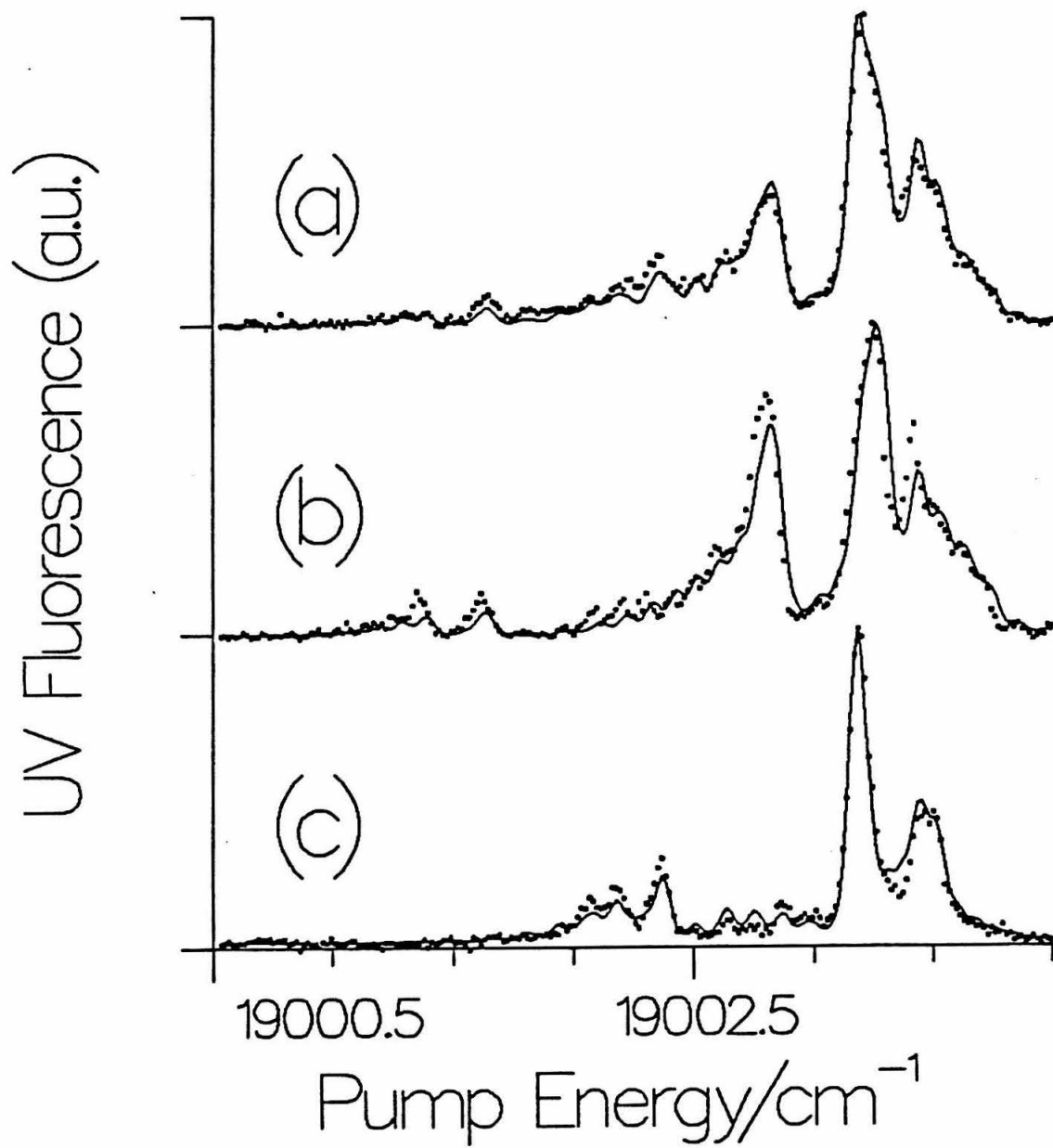
Results and Discussion

Structure: The rare gas-halogen van der Waals molecules provide a model system to compare the results of theory and experiment. In order to do quantitative theoretical calculations it is necessary to have a realistic potential energy surface. This potential must agree with experimentally determined parameters, such as the bond lengths and the dissociation energy. This section describes the determination of these two parameters for the ArCl_2 van der Waals molecule.

The NeCl_2 and HeCl_2 van der Waals molecules were both shown to have T-shaped structures in their equilibrium geometries.^{10,12} The ArCl_2 van der Waals molecule was studied at moderate resolution (0.06 cm^{-1}) of the pump laser and the spectrum of the $B \leftarrow X$ ($6 \leftarrow 0$) band is shown in Figure 2. The ArCl_2 spectrum contains a great deal of rotational structure which may be fit assuming a rigid asymmetric top model for both the ground and excited electronic states. The transition dipole lies along the Cl-Cl bond axis, which is parallel to the b inertial axis; thus ArCl_2 has a b-type asymmetric top spectrum.

The parity of the rare gas-homonuclear halogen complexes is conserved throughout the vibrational predissociation process.⁹ Cl_2 is produced with even j rotational quantum numbers when the initially prepared wavefunction of the ArCl_2 complex is symmetric with respect

Figure 2. Excitation spectrum of the ArCl_2 $B \leftarrow X$ ($6 \leftarrow 0$) transition detected using a pump-probe technique. The dots are the experimental data and the solid curves are the rigid rotor fits to the data. Trace (a) is the spectrum obtained by positioning the probe laser on the bandhead of the $E \leftarrow B$ ($0 \leftarrow 5$) Cl_2 transition. Trace (b) consists of transitions to odd parity states of ArCl_2 $B(v = 6)$ detected by positioning the probe laser on the P(5) line. Trace (c) consists of transitions to even parity states of ArCl_2 detected by positioning the probe laser on the P(6) line.



to a two-fold rotation about the figure axis, which exchanges the Cl atoms. Conversely, Cl_2 is produced with odd j when the initially excited state of ArCl_2 is antisymmetric with respect to an exchange of the Cl atoms. This greatly simplifies the otherwise complex spectrum of the ArCl_2 van der Waals molecule. Figures 2b and 2c show the ArCl_2 excitation spectra when the probe laser is positioned on $j = 10$ and $j = 9$, respectively. The three spectra in Figure 2 may all be fit assuming the same structure for ArCl_2 . During the fitting procedure the rotational temperature, the natural linewidth and the band origin were allowed to vary. The Ar to Cl_2 center of mass distance in both the X and B states was varied over a wide range to find the minimum, and the Cl_2 bond length was allowed to vary from the literature values for uncomplexed Cl_2 .¹⁰ Recent work by Reid et al. suggests that the Ar atom changes the effective Cl-Cl bond length in the complex.¹⁵

The most well resolved rotational structure was observed for the ArCl_2 $B \leftarrow X$ ($6 \leftarrow 0$) band. The rotational constants for the $X(v = 0)$ state were determined by fitting the spectra shown in Figure 2. For fitting vibrational bands, other than the ($6 \leftarrow 0$) band, the ground state rotational constants were fixed at the values determined in the fit to the ($6 \leftarrow 0$) band while the excited state parameters were allowed to vary. The final values for each

band are given in Table I. These distances represent the vibrationally averaged structure of the ArCl_2 complex.

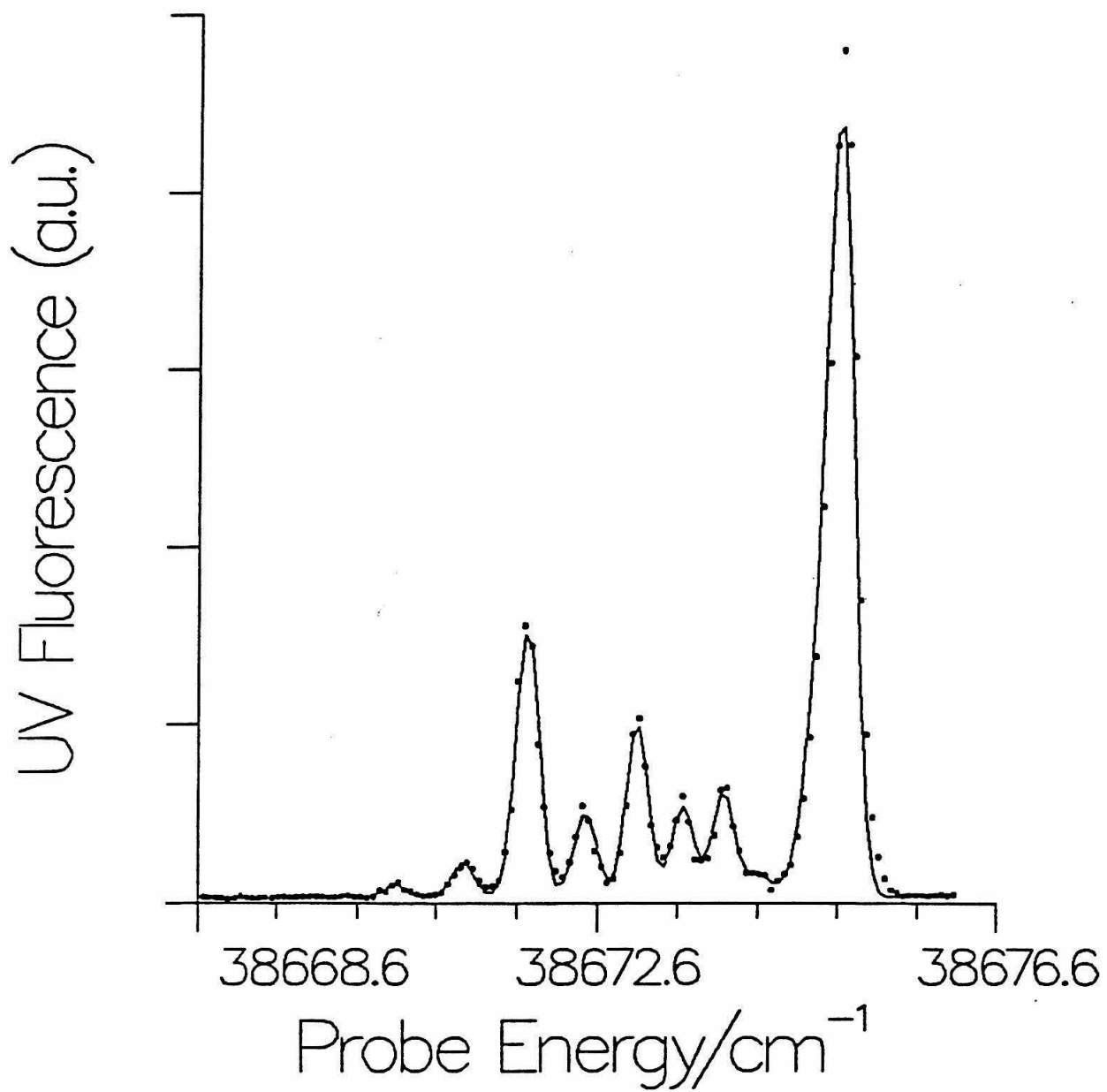
Bond Energy: The bond energy of the ArCl_2 van der Waals molecule may be determined by analysis of the rotational distribution of Cl_2 and the excitation spectra. Figure 3 shows the rotational distribution of Cl_2 $B(v = 6)$ formed in the dissociation of ArCl_2 $B(v = 7)$. The spectrum has an R branch head, and an extended P branch. The P(6) line is the last line with significant intensity, however there is some measurable intensity in the P(7) and P(8) lines. Excitation spectra obtained by setting the probe laser on the P(5) and P(7) lines of product Cl_2 and scanning the pump laser are shown in Figure 4. Similar spectra obtained with the probe laser positioned on the P(6) and P(8) lines are shown in Figure 5. In each parity-selected excitation spectrum we are detecting only those initial odd/even symmetry states which have sufficient energy to populate that particular j state of Cl_2 .

The spectra in Figures 4 and 5 provide the basis for an accurate determination of the Ar-Cl_2 bond energy. By examination of the spectra in Figure 5, it is clear that many more metastable states of ArCl_2 decay to the $j = 6$ level of the Cl_2 fragment than to the $j = 8$ level. However, in Figure 4, most lines in the excitation spectrum which contribute to the intensity of the P(5) line are seen

Table I. ArCl_2 Bond Lengths

State	$r(\text{Cl}_2)$ (Å)	$R(\text{Ar}-\text{Cl}_2)$ (Å)
$B(v = 11)$	2.81 ± 0.05	3.72 ± 0.05
$B(v = 9)$	2.68 ± 0.05	3.61 ± 0.05
$B(v = 7)$	2.53 ± 0.05	3.67 ± 0.05
$B(v = 6)$	2.55 ± 0.05	3.70 ± 0.05
$X(v = 0)$	1.98 ± 0.05	3.72 ± 0.05

Figure 3. The rotational distributions of the fragment Cl_2 $B(v = 6)$ formed in the dissociation of ArCl_2 $B(v = 7)$. The spectrum is obtained by scanning the probe laser while positioning the pump laser on the bandhead of the ArCl_2 $B \leftarrow X$ ($7 \leftarrow 0$) transition. The P(8) line is the highest product rotational state which is populated.



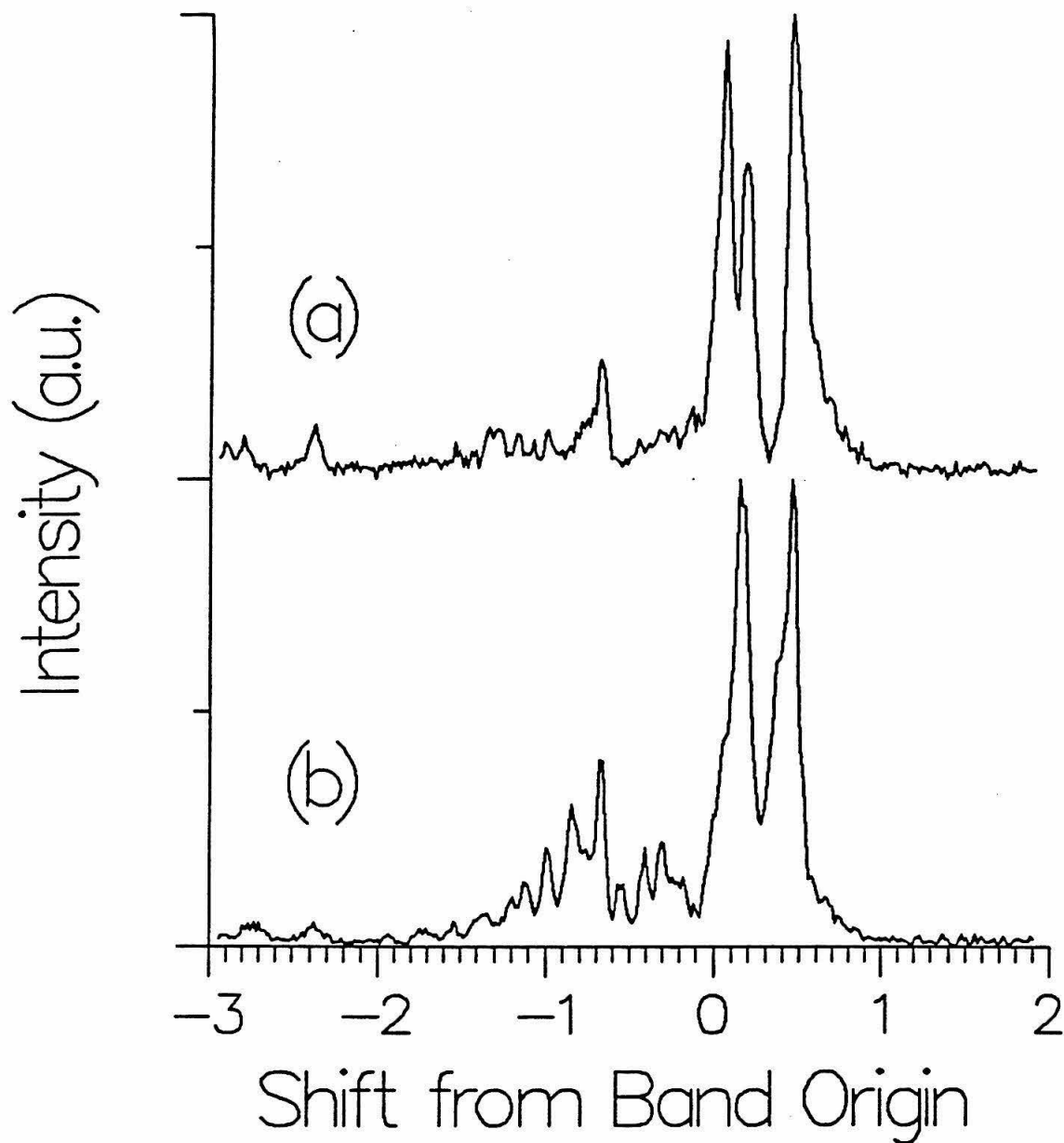


Figure 4. Excitation spectra of the ArCl_2 $B \leftarrow X$ ($7 \leftarrow 0$) transition with the probe laser positioned on the (a) P(7) and (b) P(5) lines in the Cl_2 $E \leftarrow B$ ($0 \leftarrow 6$) transition.

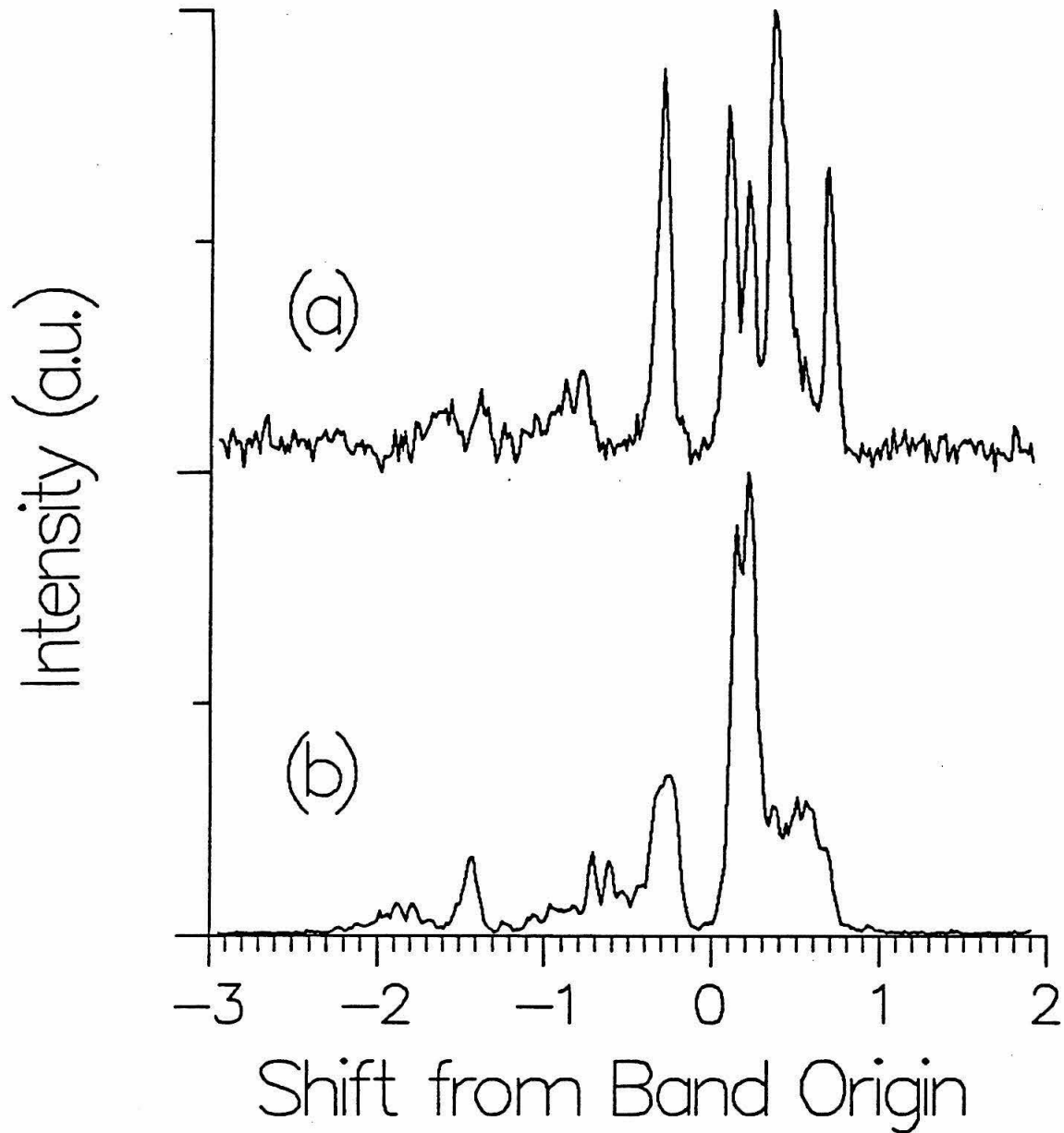
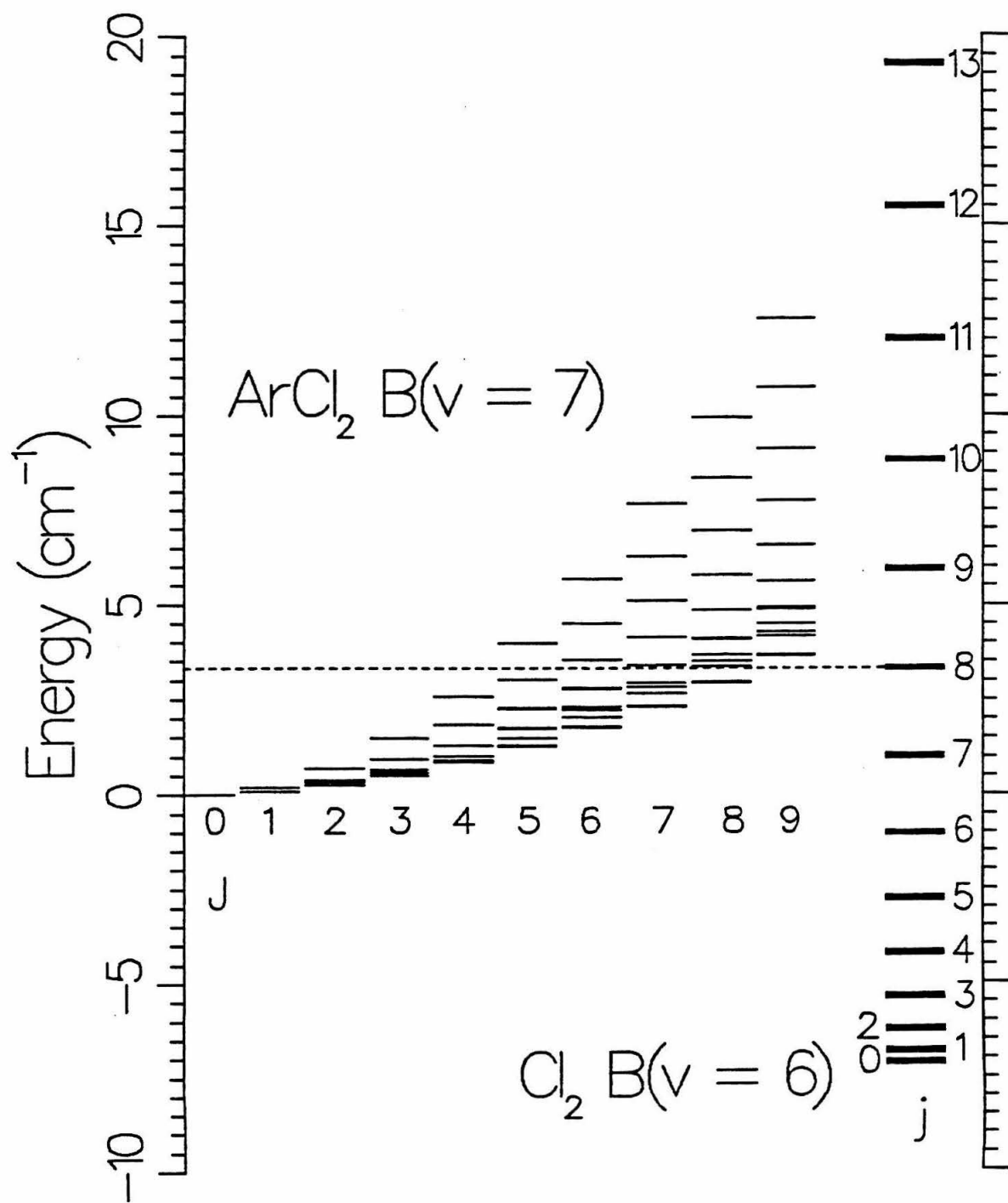


Figure 5. Excitation spectra of the ArCl_2 $B \leftarrow X$ ($7 \leftarrow 0$) transition with the probe laser positioned on the (a) P(8) and (b) P(6) lines of the Cl_2 $E \leftarrow B$ ($0 \leftarrow 6$) transition. These spectra are due to even parity states of ArCl_2 .

also in the excitation spectrum detecting Cl_2 P(7). The ArCl_2 B($\nu = 7$) rigid asymmetric top energy levels are shown in Figure 6, along with the fragment Cl_2 B($\nu = 6$) rotational energy levels. The ArCl_2 B 0_{00} state does not have sufficient energy to populate $j = 7$ of Cl_2 . As the ArCl_2 internal energy is increased the threshold is reached where sufficient energy is available to produce fragment Cl_2 with $j = 7$. The transition to the lowest energy rotational state of ArCl_2 B($\nu = 7$) which was observed in the P(7) excitation spectrum was determined. The bond energy, D_0 , is then the energy of the Cl_2 vibrational quantum expended in the dissociation, 185.222 cm^{-1} , minus the rotational energy of the Cl_2 ($j = 7$) product, 8.112 cm^{-1} , plus the lowest internal rotational energy of the ArCl_2 complex that gives Cl_2 , $j = 7$, as a product, $1.0 \pm 0.3 \text{ cm}^{-1}$. D_0 for ArCl_2 B($\nu = 7$) is $178.4 \pm 0.3 \text{ cm}^{-1}$, where the uncertainty derives from assignment of the transitions and from the rigid rotor energy levels. The relative translational energy between the Ar and fragment Cl_2 ($j = 7$) is given by the height of the centrifugal barrier and is less than 0.04 cm^{-1} . The dotted line in Figure 6 corresponds to the energy of fragment Cl_2 B($j = 8$). Since the centrifugal barrier is very small the ArCl_2 rotational levels which lie above this line may dissociate to produce Ar + fragment Cl_2 B($j = 8$). The Cl_2 free rotor states are imbedded in the Ar + Cl_2 continuum,

Figure 6. The light lines are the ArCl_2 rigid rotor energy levels in the $B(v = 7)$ state. The rotational constants were determined by fitting excitation spectra similar to those shown in Figure 2. The dark lines depict free rotor states of fragment Cl_2 $B(v = 6)$ formed in the dissociation of ArCl_2 $B(v = 7)$. ArCl_2 $B(v = 7, J = 0)$ can produce Cl_2 $B(v = 6, j = 6)$ but does not have sufficient energy to produce $\text{Cl}_2(v = 6, j = 7)$. The ArCl_2 rotational energy levels above the dotted line can produce fragment Cl_2 with $j = 8$, provided the symmetry of the initial state is correct, since parity is conserved in the dissociation.



since the relative translational energy of the dissociated complex is not quantized.

The shift of the ArCl_2 band origin relative to the uncomplexed Cl_2 band origin is a measure of the relative binding energy in the two electronic states. The ArCl_2 $B \leftarrow X$ ($6 \leftarrow 0$) transition is blue-shifted $9.5 \pm 0.2 \text{ cm}^{-1}$ from the free Cl_2 $B \leftarrow X$ ($7-0$) band origin, which indicates that the van der Waals bond is $9.5 \pm 0.2 \text{ cm}^{-1}$ stronger in the X state than in the B state. A series of measurements, as reported in Table II, for bands originating from the $X(v = 0)$ level provides information concerning the bond energy in the excited state. The bond energies for the bands other than the ($7 \leftarrow 0$) are determined as described elsewhere,⁸ and the centrifugal barriers are taken into account. The data in Table II show that the measured bond energies and band shifts are all consistent within the experimental error of the measurements. The band shift is a nearly linear function of v , as was seen with the HeI_2 van der Waals molecule.¹⁶

Lifetime: The excitation spectra were fit with a Voigt lineshape function. The inhomogeneous width was fixed at the instrumental linewidth and the natural linewidth was varied during the fitting procedure. No measurable lifetime broadening was observed for the ($6 \leftarrow 0$) or ($7 \leftarrow 0$) transitions. Lifetime broadening was observed for the

Table II. ArCl_2 Bond Energies and Band Shifts

State	D_0 (cm^{-1})	Band Shift
$B(v = 11)$	176 ± 4	13 ± 0.5
$B(v = 9)$	176 ± 5	11.3 ± 0.5
$B(v = 7)$	178.4 ± 0.3	9.5 ± 0.4
$B(v = 6)$	177.8 ± 1.8	9.3 ± 0.4
$X(v = 0)$	187.9 ± 0.4	-----

($11 \leftarrow 0$) transition, which was also studied at moderate resolution (0.06 cm^{-1}) of the pump laser. The inhomogeneous width includes the contributions of the Doppler ($\approx 0.01 \text{ cm}^{-1}$) and the laser ($\approx 0.05 \text{ cm}^{-1}$) widths. The natural linewidth of the ArCl_2 ($11 \leftarrow 0$) transition was determined to be $0.064 \pm 0.018 \text{ cm}^{-1}$, which corresponds to a vibrational predissociation lifetime of 83 ± 10 picoseconds.

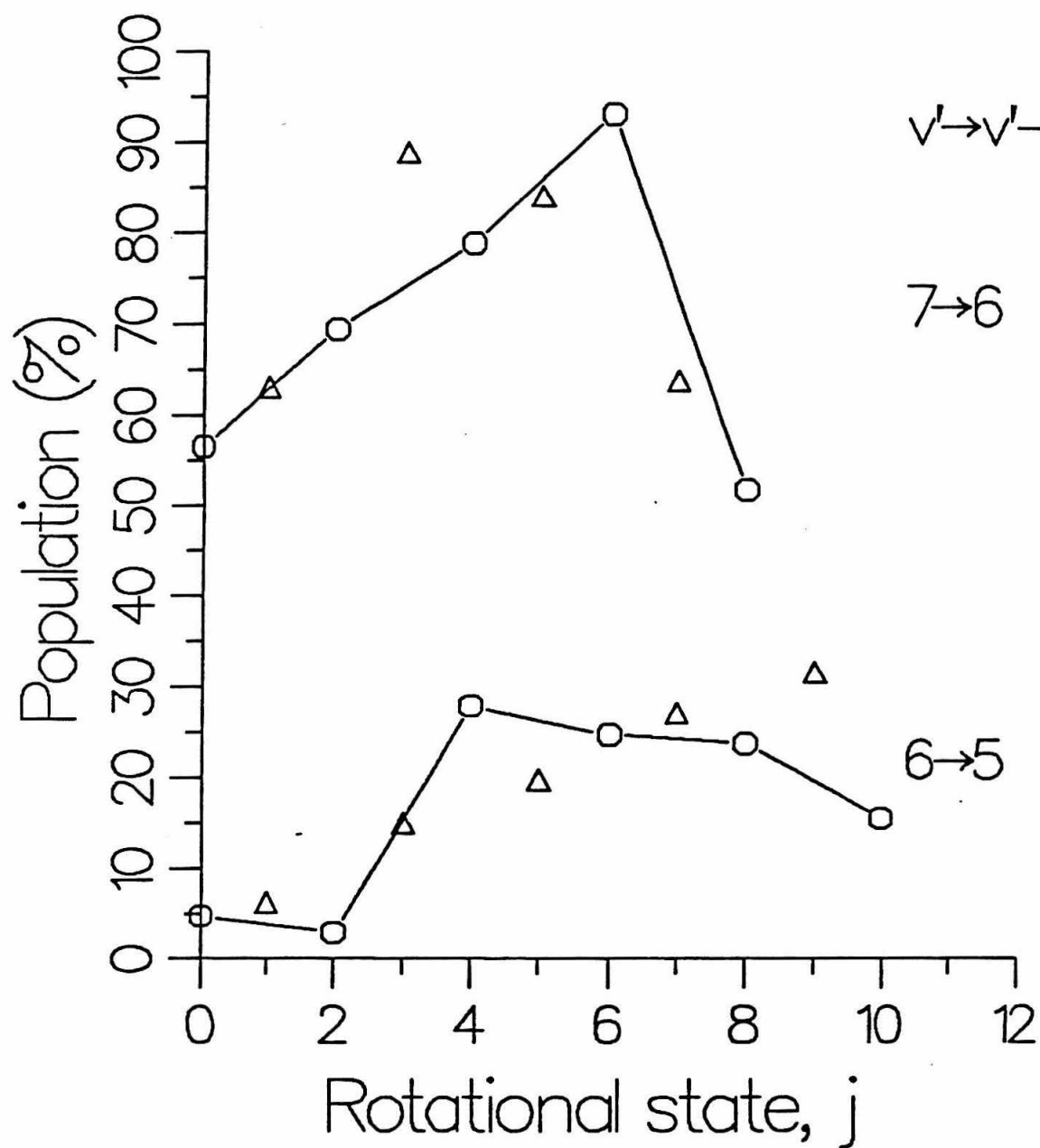
Dynamics: The rotational distributions which are observed using the pump-probe technique give a great deal of information on the dynamics of the vibrational predissociation process. Levy et al. observed that the channel in which one quantum of the halogen stretch is transferred to the van der Waals modes to dissociate the complex ($\Delta v = -1$) was dominant when this process was energetically accessible.² This result was explained by Beswick and Jortner in terms of an energy gap model which predicted that the most efficient channel would be the one which put the least amount of energy into rotation and relative translation of the products.⁴

The $\Delta v = -1$ channel is open for the $v < 8$ levels of the B state of ArCl_2 . A typical Cl_2 fragment rotational spectrum is shown in Figure 3, where Cl_2 B($v = 6$) was formed in the predissociation of ArCl_2 B($v = 7$). There is a sharp cut off in the rotational distribution, which

indicates the energetic limit of fragment rotational excitation. The highest observed Cl_2 rotational quantum number, j_{max} , is typically quite low for the $\Delta v = -1$ channel because breaking the Ar-Cl_2 bond accounts for nearly all of the energy of the Cl_2 stretching vibrational quantum. The rotational energy in $j = 6$ is nearly 90% of the available energy and corresponds to a classical impact parameter of 5.2 Å. For the NeCl_2 van der Waals molecule in the $B(v = 11)$ state, the product Cl_2 $B(v = 10)$ has a rotational distribution extending out to $j = 24$, corresponding to $\approx 85\%$ of the available energy and a classical impact parameter of 7.2 Å.⁸ The inverted distribution for ArCl_2 ($\Delta v = -1$) implies that the kinematically preferred j is much higher than is energetically allowed. The rotational distribution of fragment Cl_2 in the $\Delta v = -1$ dissociation of ArCl_2 for two initial states is shown in Figure 7. The $\Delta v = -2$ channel accounts for $< 10\%$ of the product Cl_2 formed in the dissociation of ArCl_2 $B(v = 7)$ and is closed completely for ArCl_2 $B(v = 6)$.

The energy of a Cl_2 vibrational quantum decreases with v and the $\Delta v = -1$ channel is energetically closed between $v = 7$ and $v = 8$ for ArCl_2 with $J = 0$. Since ArCl_2 $B(v = 9)$ cannot dissociate through the loss of one quantum we would expect to see the two quantum channel dominate the vibrational predissociation process and this is the case.

Figure 7. $^{35}\text{Cl}_2$ fragment rotational state populations for the $\Delta v = -1$ channels. The circles and triangles are the distributions for the even and odd parity rotational states of ArCl_2 , respectively. The populations for the upper trace were determined by fitting the spectrum in the Cl_2 $E \leftarrow B$ ($0 \leftarrow 6$) spectrum trace in Figure 3 using the spectroscopic constants of Ref. 10 and 11. The baseline for the upper trace is at 50%.



The Cl_2 $E \leftarrow B$ ($0 \leftarrow 7$) rotational distribution obtained by exciting the ArCl_2 $B \leftarrow X$ ($9 \leftarrow 0$) transition is shown in Figure 8. The cut off in the rotational distribution is quite sharp and, as was observed for NeCl_2 , the distribution extends out to the highest energetically accessible j . The highest j observed in Figure 8 is $j_{\text{max}} = 32$, which accounts for over 90% of the available energy. This corresponds to a classical impact parameter of 7.2 Å for the dissociation. This is similar to the NeCl_2 distributions, but distinctly different from HeCl_2 , where kinematic constraints limit the transfer of vibrational energy into rotational energy. The fragment Cl_2 rotational distributions from the two quantum dissociation of ArCl_2 are shown in Figure 9. The distributions show rotational state populations which are not smooth and are populated out to the energetically allowed limit.

The product rotational state distributions can be compared to those reported for HeCl_2 , NeCl_2 , HeICl and NeICl .⁵⁻⁹ The vibrational predissociation of each of these complexes is dominated by the $\Delta v = -1$ channel. The rotational distributions of ICl in the $B(v = 1)$ state following vibrational predissociation of the complexes HeICl and NeICl $B(v = 2)$ show different behavior. Both distributions are quite narrow and the peak of the distribution is at $j = 8$ for HeICl and at $j = 17$ for NeICl .

Figure 8. Pump-probe spectrum obtained by scanning the probe laser through the $E \leftarrow B$ ($1 \leftarrow 7$) transition while positioning the pump laser on the band head of the ArCl_2 $B \leftarrow X$ ($9 \leftarrow 0$) transition. The intensities of rotational lines are not a smooth function of j , which is typical of the $\Delta v = -2$ spectra observed for ArCl_2 .

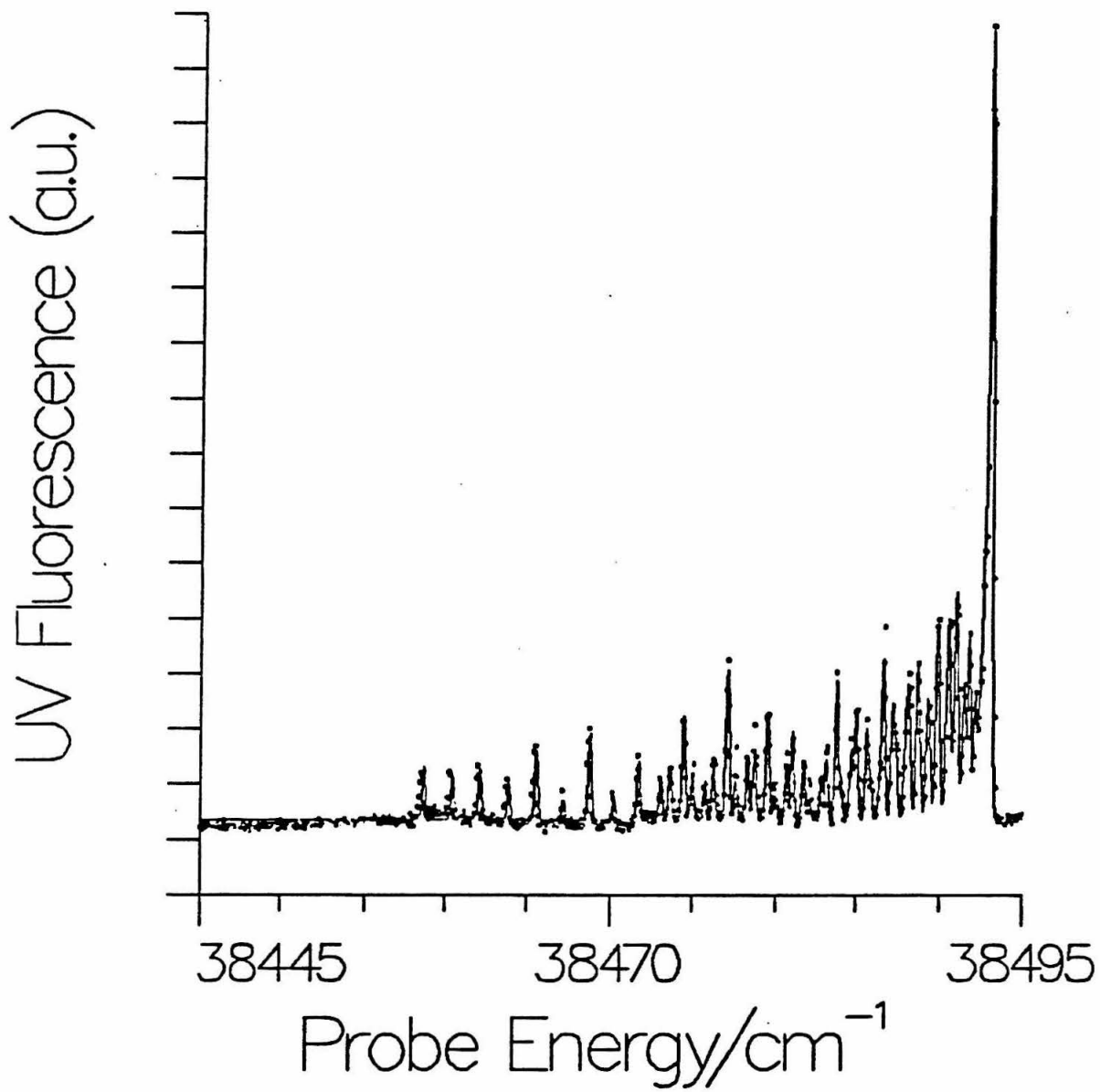
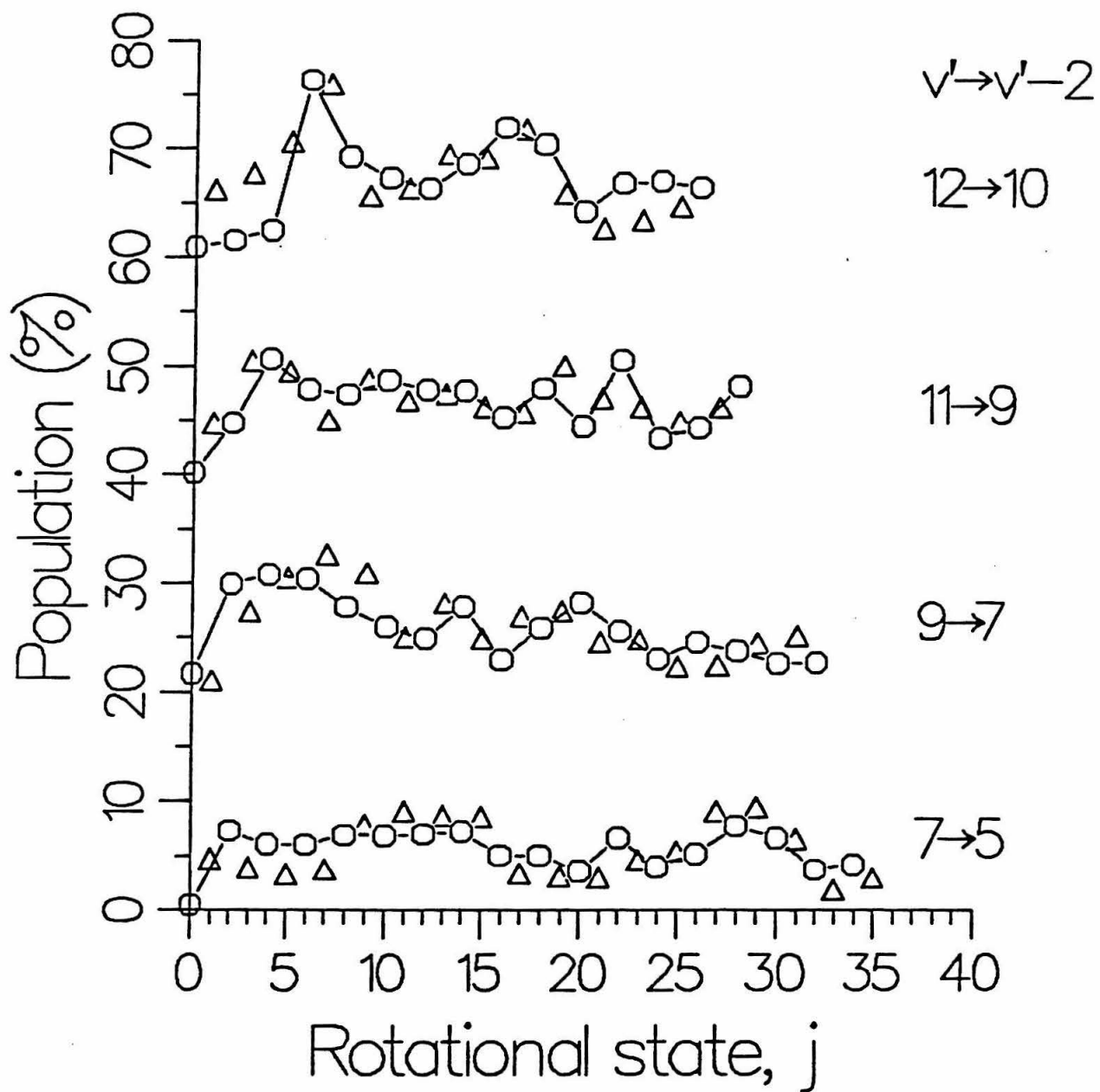


Figure 9. $^{35}\text{Cl}_2$ fragment rotational state populations for the $\Delta v = -2$ channels. The circles and triangles are the population of the even and odd j states of fragment Cl_2 , respectively. The highest fragment Cl_2 j state which is observed is determined by the available energy, rather than kinematic constraints. The baseline for each plot is offset by 20% on the vertical axis.



The impact parameter for the dissociation of the ICl complexes ranges from 0.7 - 2.1 Å. The HeCl₂ rotational distribution shows a gradual decrease in intensity out to $j_{\max} = 16$, which accounts for nearly 24% of the available energy, and corresponds to an impact parameter of 3 Å. Only for NeCl₂ are all fragment rotational states consistent with conservation of energy and angular momentum populated. For NeCl₂ B←X (11←0), detecting Cl₂ E←B (3←10) $j_{\max} = 24$, which is approximately 85% of the available energy and corresponds to a classical half-collision impact parameter of $\approx 7.2\text{Å}$. The ArCl₂ $\Delta v = -2$ distributions are most similar to the NeCl₂ distributions in that every energetically allowed j is populated and the distribution shows a sharp cut off above that limit.

The large impact parameters for the $\Delta v = -2$ dissociation of ArCl₂ indicate that the vibrational predissociation mechanism may not be a direct V→T,R process. A possible explanation for this behavior is an indirect half collision mechanism in which there is preliminary intramolecular vibrational relaxation (IVR) from the Cl₂ stretching mode to the van der Waals modes followed by predissociation. The major difference between the ArCl₂ and the NeCl₂ product rotational distributions is that the NeCl₂ distribution is smooth while the ArCl₂ distributions are quite structured and complex. This complex structure is observed when the $\Delta v = -1$ channel for

ArCl_2 is closed, where preliminary IVR leading to ArCl_2 in a metastable state of highly excited van der Waals modes becomes possible.

These unusual distributions cannot be explained through any simple analysis, and additional theoretical work will be necessary to fully understand the dynamics of the system. One possible explanation for the interesting behavior of this complex is as follows. In order to simplify the discussion, consider initially the case where the total angular momentum $J = 0$. For ArCl_2 $B(v = 9)$, the one quantum channel is closed, having 12 cm^{-1} less energy than needed to dissociate the complex. The predissociation process may then be described as a two step process in which the spectroscopically prepared state decays via IVR into highly excited, metastable stretching and bending levels of the ArCl_2 $B(v = 8)$ complex van der Waals modes. The number of vibrational states for ArCl_2 is shown in Figure 10. The region of interest is shown in detail in Figure 11, where only the $J = 0$ stretching and bending levels are shown. The density of ($J = 0$) vibrational states near the top of the ArCl_2 $B(v = 8)$ potential well is approximately 1 state/cm^{-1} . In general, the initially prepared state can couple to a limited number of rotational states, such as those shown in Figure 6, having the same overall J , for each of the bending and stretching vibrational levels. The unusual rotational state population distribution of the Cl_2 ($v = 7$) fragment may

Figure 10. Energy levels for ArCl_2 $B(v = 7, 8, 9)$ and Cl_2 $B(v = 7, 8, 9)$. The dotted lines are the vibrational energy levels for ArCl_2 , which were calculated using the techniques of Reid et al.¹⁵ Only the $J = 0$ levels of ArCl_2 are shown. The solid lines are the Cl_2 free rotor states in the $\text{Ar} + \text{Cl}_2$ continuum. The energy scale is relative to the energy of the prepared $J = 0$ state of ArCl_2 $B(v = 7)$.

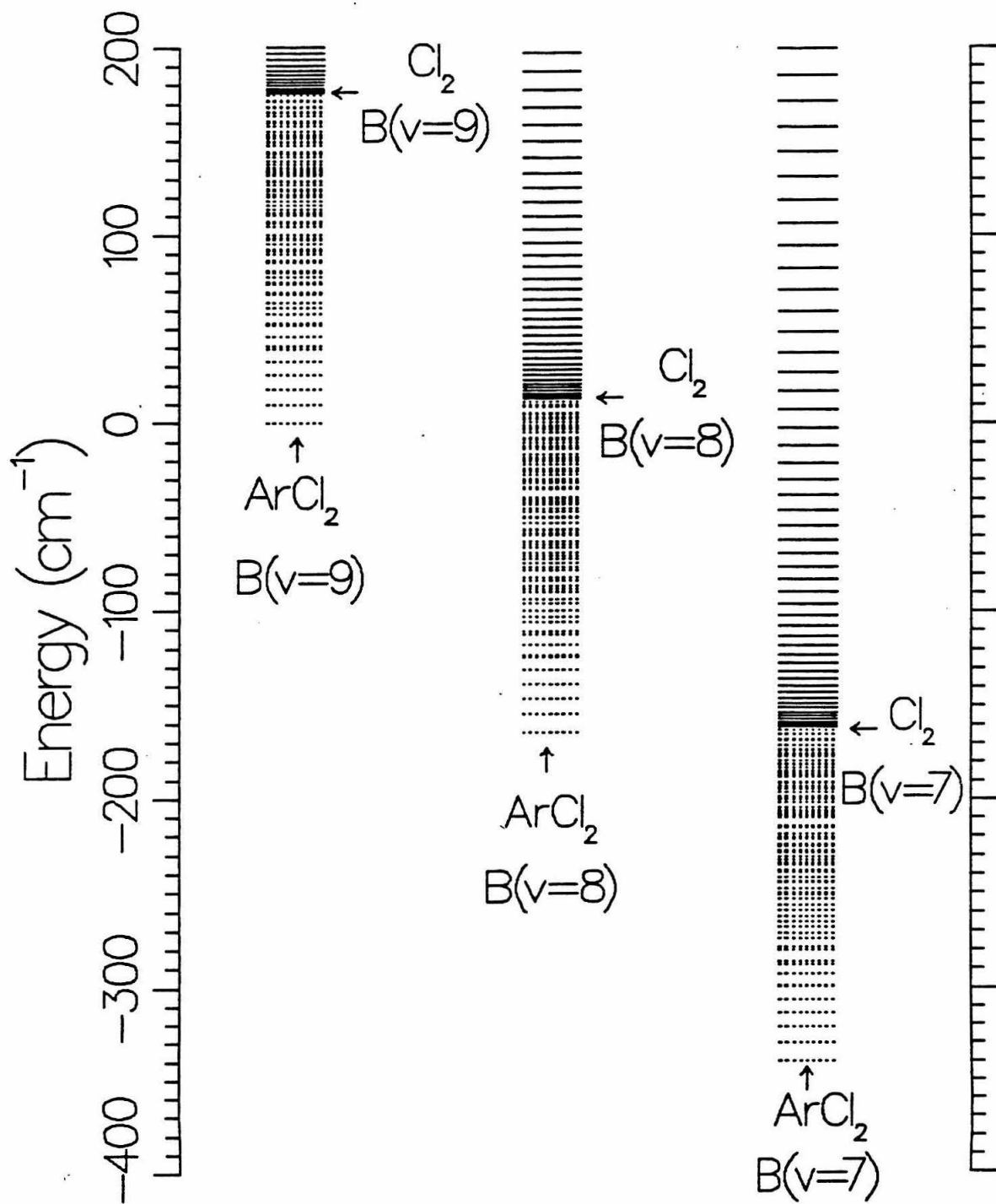
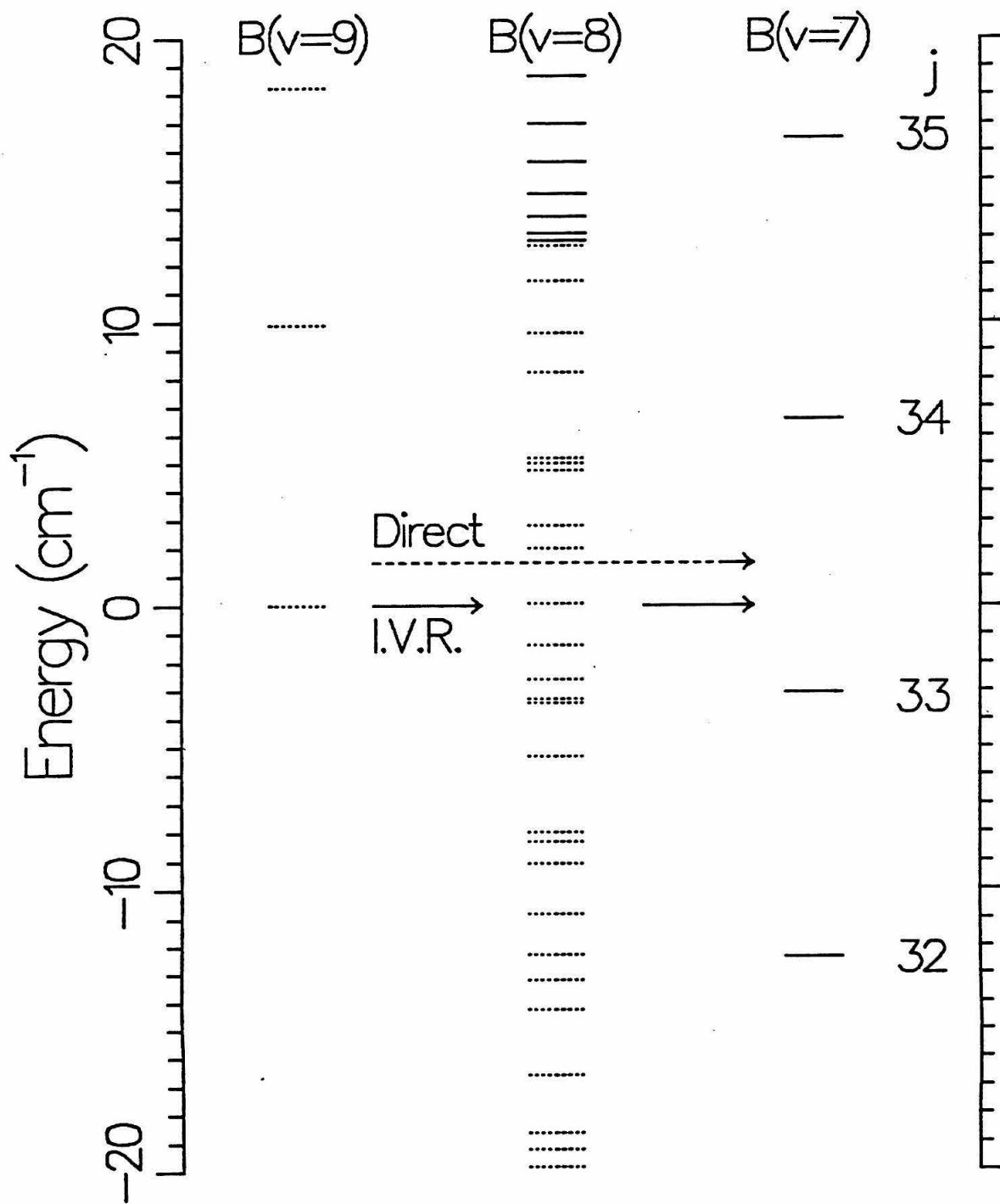


Figure 11. Energy levels for ArCl_2 $B(v = 8, 9)$ and Cl_2 $B(v = 7, 8)$. The dotted lines are the ArCl_2 $B(v = 8, 9; J = 0)$ energy levels, while the solid lines indicate the energy of the Cl_2 free rotor states imbedded in the $\text{Ar} + \text{Cl}_2$ continuum. The $\Delta v = -1$ dissociation channel is closed, however preliminary IVR to highly excited vibrational levels of ArCl_2 $B(v = 8)$ may occur, followed by coupling to the $\text{Ar} + \text{Cl}_2$ $B(v = 7)$ continuum. Alternatively, the ArCl_2 $B(v = 9)$ complex may dissociate by coupling directly to the $\text{Ar} + \text{Cl}_2$ $B(v = 7)$ continuum, or both processes may occur competitively.



reflect the relative coupling between the initially prepared ArCl_2 $B(v = 9)$ rotational states and the highly excited van der Waals vibrational levels of ArCl_2 $B(v = 8)$. Following the preliminary IVR the second Cl_2 vibrational quantum is transferred to the van der Waals modes and the highly excited ArCl_2 $B(v = 8)$ complex decays to the $\text{Ar} + \text{Cl}_2$ $B(v = 7)$ continuum. Alternatively, the initially prepared state may decay directly into the ArCl_2 $B(v = 7)$ continuum.

Halberstadt et al. have performed a three dimensional quantum mechanical study for vibrational predissociation of NeCl_2 .¹⁷ The lifetimes and product Cl_2 rotational distributions were calculated from the wave functions using the Fermi golden rule. The calculated lifetimes and rotational distributions were in qualitative agreement with experimental results. Similar calculations could be performed on ArCl_2 which might serve to explain the interesting results which we have reported here. This would be a good model system to study with exact close coupling methods, and then test various approximations which would allow calculations to be performed on more complex systems.

Conclusions

The ArCl_2 van der Waals complex has been studied using a pump-probe technique to obtain excitation spectra of the ArCl_2 and rotational distributions of Cl_2 following predissociation of the complex. The ArCl_2 geometry is T-shaped with an Ar to Cl_2 center of mass distance of $3.72 \pm 0.04 \text{ \AA}$ and $3.70 \pm 0.04 \text{ \AA}$ in the ground and excited states, respectively. The bond energy, D_0 , of the complex is $187.9 \pm 0.4 \text{ cm}^{-1}$ in the X state and varies with v in the B state. The lifetime of the spectroscopically prepared $B(v = 11)$ state is 83 ± 10 picoseconds. It is not clear whether this corresponds to an IVR rate, or the lifetime of this complex. The rotational distributions of Cl_2 formed in the predissociation process are very complex, non statistical in nature. The distributions extend out to the energetically allowed limit and, for $\Delta v = -2$, the highly structured distributions indicate that IVR may occur prior to dissociation.

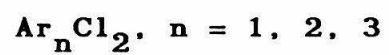
References

1. R.E. Smalley, D.H. Levy, and L. Wharton, *J. Chem. Phys.* **64**, 3266 (1976).
2. D.H. Levy, *Adv. Chem. Phys.* **47**, 323 (1981).
3. K.C. Janda, *Adv. Chem. Phys.* **60**, 201 (1985).
4. J.A. Beswick and J. Jorter, *Adv. Chem. Phys.* **47**, 323 (1981).
5. J.C. Drobits, J.M. Skene, and M.I. Lester, *J. Chem. Phys.* **84**, 2896 (1986).
6. J.C. Drobits, and M.I. Lester, *J. Chem. Phys.* **86**, 1662 (1987).
7. J.M. Skene, J.C. Drobits, and M.I. Lester, *J. Chem. Phys.* **86**, 2329 (1986).
8. J.I. Cline, N. Sivakumar, D.D. Evard, and K.C. Janda, *J. Chem. Phys.* **86**, 1636 (1987).
9. J.I. Cline, N. Sivakumar, D.D. Evard, and K.C. Janda, *Phys. Rev. A* **36**, 1944 (1987).
10. J.A. Coxon, *J. Mol. Spectrosc.* **82**, 264 (1984).
11. T. Shinzawa, A. Tokunaga, T. Ishiwata, and I. Tanaka, *J. Chem. Phys.* **83**, 5407 (1985).
12. D.E. Brinza, C.M. Western, D.D. Evard, F. Thommen, B.A. Swartz, and K.C. Janda, *J. Phys. Chem.* **88**, 2004 (1984).
13. N. Sivakumar, D.D. Evard, J.I. Cline, and K. C. Janda, *Chem. Phys. Lett.* **137**, 403 (1987).

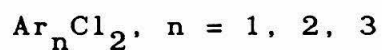
14. J.I. Cline, D.D. Evard, F. Thommen, and K.C. Janda, J. Chem. Phys. **84**, 1165 (1986).
15. B.P. Reid, K.C. Janda, and N. Halberstadt, J. Chem. Phys., in press.
16. J.E. Kenny, K.E. Johnson, W. Sharfin, and D.H. Levy, J. Chem. Phys. **72**, 1109 (1980).
17. N. Halberstadt, J.A. Beswick, and K.C. Janda, J. Chem. Phys., in press.

CHAPTER VII

A Test of Atom-Atom Additive Interactions:



A Test of Atom-Atom Additive Interactions:



Dwight D. Evard, Joseph I. Cline,
N. Sivakumar and Kenneth C. Janda

Chemistry Department, University of Pittsburgh
Pittsburgh, Pennsylvania 15260, U.S.A.

Abstract

We have determined dissociation energies for the van der Waals molecules Ar_nCl_2 , where $n = 2, 3$. These values are compared to those obtained from the approximation that the intermolecular potential is given by the sum of the Ar-Ar and Ar- Cl_2 interactions. Within experimental error the Ar_2Cl_2 bond energy is identical to the predicted value. The measurements are precise enough to illustrate a slight deviation from simple bond-bond additivity for the Ar_3Cl_2 complex.

Introduction

A simple approach to constructing an intermolecular potential for a weakly bound cluster is to employ a set of additive atom-atom potentials. This model is attractive because accurate atom-atom potentials are often available.¹ However, there has been some debate as to whether this model is correct for all van der Waals molecules. Klemperer and coworkers have studied the ArClF^2 and KrClF^3 van der Waals molecules using molecular beam electric resonance spectroscopy. The structure of each of these complexes is linear with the rare gas atom on the Cl end of the halogen. This structure is predicted by considering the rare gas atom to be a Lewis acid which donates electrons into the halogen σ orbital, which is the the lowest unoccupied molecular orbital (LUMO) of the ClF . This model does not correctly predict the structure of the rare gas-homonuclear halogen complexes. These van der Waals molecules are T-shaped, indicative of an atom-atom additive model of the binding.

The dissociation energy of the van der Waals bond is indicative of the type of bonding which is important in the complex.⁴ Levy and coworkers have studied HeI_2 and were able to bracket the dissociation energy of the van der Waals bond because of the anharmonicity of the I_2 potential. By dispersing the fluorescence of fragment I_2 they were able to determine the last I_2 stretching quantum

which had sufficient energy to dissociate the complex. The energy of that quantum served as an upper limit to the bond energy while the next smaller quantum determined the lower limit.

Janda and coworkers have studied the ArCl_2 van der Waals molecule at 0.05 cm^{-1} resolution using a pump-probe technique.⁵ They determined the rotational distribution of fragment Cl_2 formed in the vibrational predissociation of the complex by scanning the $E \leftarrow B$ transition of Cl_2 . Every rotational state was populated, as allowed by conservation of energy. The initial internal energy of the ArCl_2 complex allowed two additional Cl_2 rotational states to be populated. By analysing the spectra and adding the blue shift from Cl_2 they determined the bond energy of ArCl_2 to be $187.9 \pm 0.4 \text{ cm}^{-1}$ in the $X(v = 0)$ state.

We have determined dissociation energies for the van der Waals molecules Ar_nCl_2 , where n ranges from 2 to 3, to test the approximation that the intramolecular potential is given by the sum of Ar-Ar and Ar-Cl_2 potentials. The determination is performed by interpreting the fragment Cl_2 rotational distribution produced in the vibrational predissociation of Ar_nCl_2 .

Experimental

A gas mixture was prepared by passing 2.5% Ar in He over liquid Cl_2 at -77 C . The van der Waals molecules were

formed in a free jet expansion of the gas mixture from a stagnation pressure of 320 psi. The rotational temperature of the clusters was approximately 1.5 K. The $\text{Ar}_n^{35}\text{Cl}_2$ molecules were detected using a laser pump-probe technique.^{6,7,8} For $n = 1, 2, 3$ the $B \leftarrow X$ ($11 \leftarrow 0$) transitions for Ar_nCl_2 lie approximately 12, 24 and 33 cm^{-1} to the blue of the associated $B^3\Pi(0_u^+) \leftarrow X^1\Sigma_g^+$ transitions of uncomplexed Cl_2 .⁹ The band shift is dependent upon the vibrational level excited. The product rotational distribution is obtained by setting the visible pump laser on an Ar_nCl_2 transition and scanning the UV probe laser through the region of the Cl_2 $E(0_g^+) \leftarrow B^3\Pi(0_u^+)$ transition.¹⁰

Results

Narrow limits can be placed on the dissociation energy of the complexes by measuring the internal energies of the products. The van der Waals bond energy is the difference between the total cluster energy and the energy remaining in the highest fragment Cl_2 rotational state following dissociation.⁸ Since in the Ar_nCl_2 case the cut off between the highest observed fragment level and the lowest unobserved fragment level is very sharp, we believe that the cutoff is due strictly to conservation of energy and not due to kinematic constraints. There are two small, but significant corrections to this argument. First, the clusters have some distribution of rotational energy (< 5

cm^{-1}) before excitation. Second, there is a centrifugal barrier to dissociation on the order of 2 cm^{-1} or less which is approximately incorporated into the calculations below.

Figure 1 shows the $E \leftarrow B$ ($1 \leftarrow 8$) spectrum of fragment Cl_2 produced by vibrational predissociation of Ar_2Cl_2 ($B, v = 11$). Three quanta of the halogen stretch are necessary to dissociate the complex. An upper limit may be placed on the Ar_2Cl_2 bond energy by subtracting the rotational energy of Cl_2 ($B, v = 8, j = 12$) (21.52 cm^{-1}) and the height of the centrifugal barrier ($\approx .25 \text{ cm}^{-1}$) from the available energy (458.39 cm^{-1}). The centrifugal barrier in Ar_2Cl_2 is estimated by adding the centrifugal potential to the long range van der Waals potential which is calculated from the polarizabilities of Ar and Cl_2 .¹¹ Calculation of the centrifugal barrier for Ar_2Cl_2 is ambiguous because the dissociation mechanism is unknown, but a good estimate can be made. The lower limit for the dissociation energy is obtained by doing the same for the first unobserved rotational level of fragment Cl_2 . Using this method the ArCl_2 $B(v = 11)$ bond energy is determined to be $434 \pm 2 \text{ cm}^{-1}$.

The Ar_2Cl_2 van der Waals molecule may dissociate through two processes to produce different products;

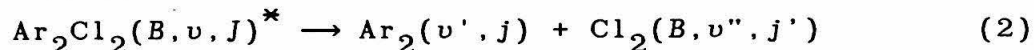
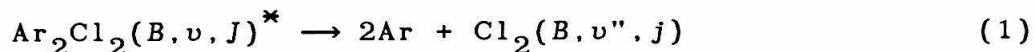
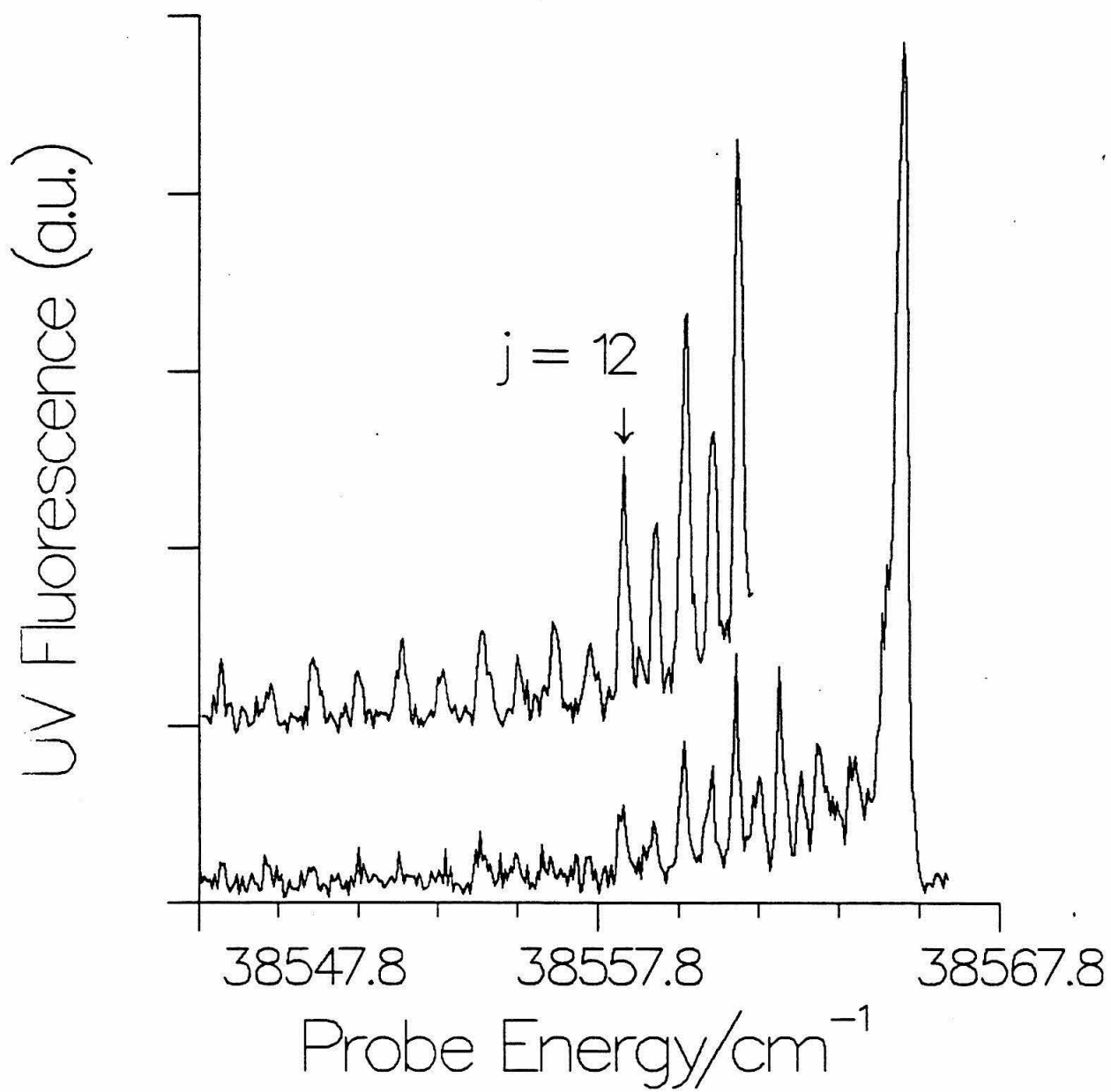


Figure 1. Pump-probe spectrum of fragment Cl_2 $B(v = 8)$ formed in the dissociation of Ar_2Cl_2 $B(v = 11)$. The spectrum was obtained by scanning the probe laser while positioning the pump laser on the bandhead of the ArCl_2 $B \leftarrow X$ ($11 \leftarrow 0$) band. In this figure $j = 12$ is the maximum j allowed energetically to produce $2\text{Ar} + \text{Cl}_2$ as the products in the dissociation process.



where v and j represent the vibrational and rotational excitation of the products. The Cl_2 product state spectrum shown in Figure 1 suggests that both of these processes are important. A sharp decrease in intensity is observed above $j = 12$ due to the closing of channels for the process shown in Equation 1, but there is a small probability of producing states to at least $j = 22$. The Cl_2 fragments possessing $j > 12$ appear to be products of the dissociation shown in Equation 2 for which the Ar-Ar bond remains intact so that extra energy can be released to Cl_2 rotation.

The rotational state distribution of fragment Cl_2 $B(v = 6)$ produced in the vibrational predissociation of Ar_3Cl_2 $B(v = 11)$ is shown in Figure 2. The sharp cut off which was observed for Ar_2Cl_2 is also visible in this distribution. The population decreases gradually and then drops off steeply above $j = 20$. There is no evidence for the different decay processes which were observed for Ar_2Cl_2 . The bond energy for the Ar_3Cl_2 complex may be determined by using the procedure which was outlined above. The total cluster binding energy for the Ar_3Cl_2 complex in the $B(v = 11)$ state is $754 \pm 4 \text{ cm}^{-1}$.

In Table I, the experimental total cluster binding energies are compared with values obtained by simple bond-bond additivity, where D_0 for Ar-Ar is taken to be 84.8 cm^{-1} .^{12,13} It is observed that, within experimental error, the total binding energy of Ar_2Cl_2 is identical to

Figure 2. Pump-probe spectrum of fragment Cl_2 $B(v = 6)$ formed in the dissociation of Ar_3Cl_2 $B(v = 11)$. The spectrum was obtained by scanning the probe laser while positioning the pump laser on the bandhead of the ArCl_2 $B \leftarrow X (11 \leftarrow 0)$ band.

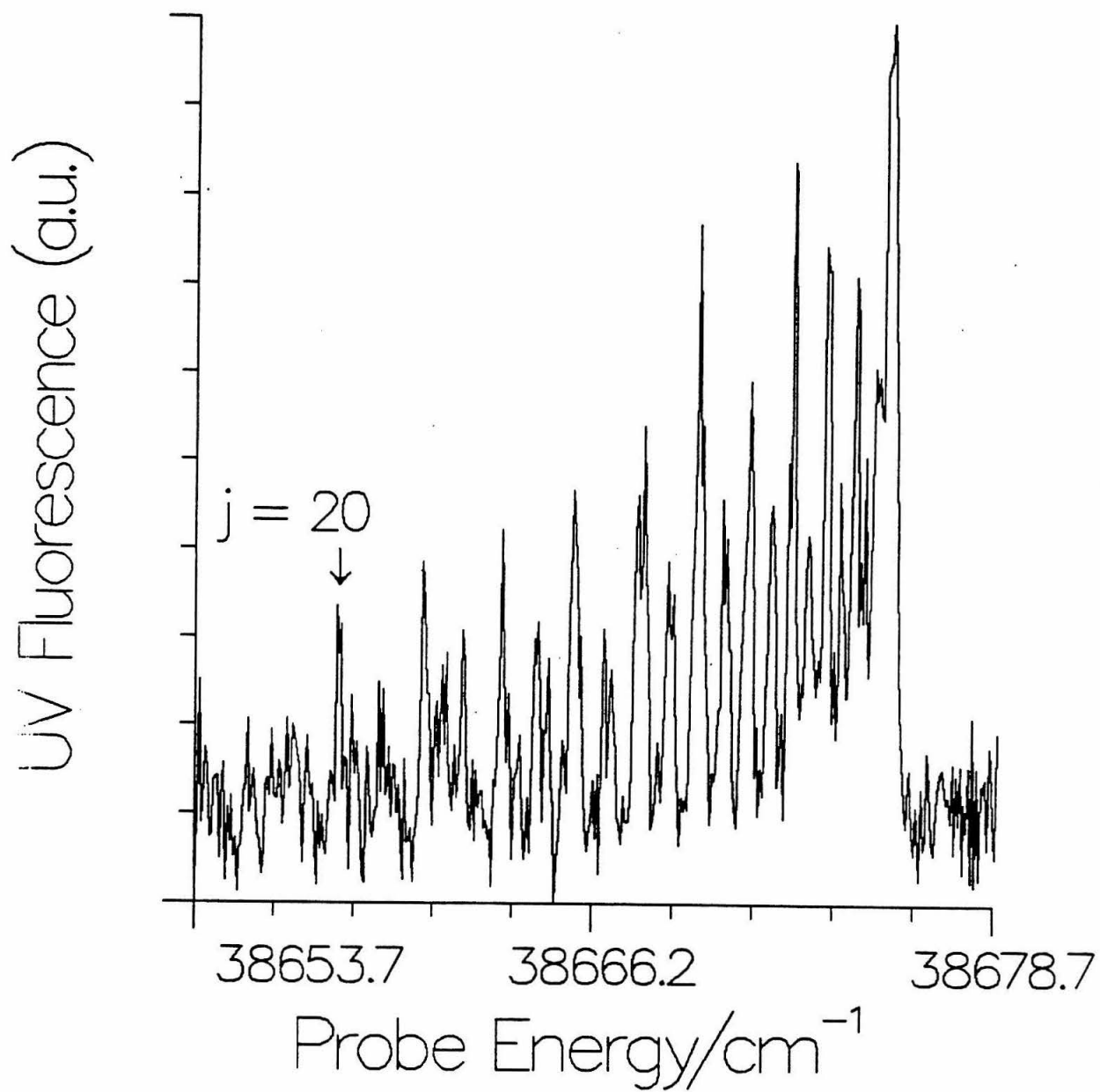


Table I. Ar_nCl_2 Bond Energies (cm^{-1})

n	m	State	$E_{\text{dissoc}}(\text{exp})$	$E_{\text{dissoc}}^{\text{a)}}(\text{calc})$
1	0	X(v=0)	$187.9 \pm 0.3^{\text{b)}}$	- - -
1	0	B(v=7)	$178.4 \pm 0.3^{\text{b)}}$	- - -
2	1	X(v=0)	458 ± 3	460.6 ± 0.4
2	1	B(v=11)	434 ± 2	- - -
3	3	X(v=0)	787 ± 5	818.1 ± 0.5
3	3	B(v=11)	754 ± 4	- - -

a) $E_{\text{dissoc}}(\text{calc}) = nD_0(\text{Ar-Cl}_2) + mD_0(\text{Ar-Ar})$.

b) From reference 5.

$2D_0(\text{Ar-Cl}_2) + D_0(\text{Ar-Ar})$ while that of Ar_3Cl_2 is 4% less than $3D_0(\text{Ar-Cl}_2) + 3D_0(\text{Ar-Ar})$.

Discussion

The band shift of Ar_nCl_2 from free Cl_2 measures the difference in binding energies of the complex between the X and the B states. We have determined the bond energy for the Ar_nCl_2 complexes in the B state, but we can obtain the bond energy in the ground state if we know the band shift. The spectroscopic features attributed to the Ar_nCl_2 van der Waals complexes are blue shifted from free Cl_2 , which implies that the potential well is deeper in the ground state. In Table I, we also list the bond energies for the X state of the complexes, which were obtained by adding the band shift to the B state binding energy.

Kenny et al.¹⁴ observed a constant band shift for Ne_nI_2 , for $n = 1 - 6$, from which they inferred a geometry which has six equivalent sites in the first shell. One consistent structure, the "belt" model, has equivalent sites in equatorial positions about the Cl_2 bond axis. We observe that Ar_1Cl_2 and Ar_2Cl_2 have approximately 12 cm^{-1} shifts while Ar_3Cl_2 has only a 9 cm^{-1} blue shift from Ar_2Cl_2 . Ar_1Cl_2 is T-shaped,⁵ and the Ar_2Cl_2 bond energy is consistent with the "belt" model which would predict a distorted tetrahedral arrangement of the four atoms. A "belt" model for Ar_3Cl_2 , however, would allow for two Ar-Ar

bonds, while the experiment indicates that there may be three. There is no structure which allows three Ar-Ar bonds while maintaining perpendicular Ar-Cl₂ configurations. The total van der Waals attraction is maximized by allowing the Ar atoms to form a triangle clustered perpendicular to the Cl₂ axis. The total binding energy of such a structure will be slightly less than predicted by simple bond-bond additivity.

Conclusion

In conclusion, the bond energies for the complexes Ar_nCl₂ have been measured. The results are precise enough to illustrate slight deviations from simple bond-bond additivity relationships. The "belt" model suggested by Levy and coworkers¹⁴ for NeI₂ correctly predicts the structure of Ar₂Cl₂, but not Ar₃Cl₂.

Acknowledgments

This work was supported by the United States Department of Energy (D.D.E.) and the National Science Foundation (J.I.C., N.S., and K.C.J.). Acknowledgement is made to the donors of the Petroleum Research Fund, for partial support of this research.

References

1. K.P. Huber, and G. Herzberg, *Constants of Diatomic Molecules* (Van Nostrand Reinhold, New York, 1979).
2. S.J. Harris, S.E. Novick, W. Klemperer, and W.E. Falconer, *J. Chem. Phys.* **61**, 193 (1974).
3. S.E. Novick, S.J. Harris, K.C. Janda, and W. Klemperer, *Can. J. Phys.* **53**, 2007 (1975).
4. J.A. Blazy, B.M. DeKoven, T.D. Russell, and D.H. Levy, *J. Chem. Phys.* **72**, 2439 (1980).
5. D.D. Evard, N. Sivakumar, J.I. Cline, and K.C. Janda, manuscript in preparation.
6. J.C. Drobits, J.M. Skene, and M.I. Lester, *J. Chem. Phys.* **84**, 2896 (1986).
7. J.M. Skene, J.C. Drobits, and M.I. Lester, *J. Chem. Phys.* **85**, 2329 (1986).
8. J.I. Cline, N. Sivakumar, D.D. Evard, and K.C. Janda, *J. Chem. Phys.* **86**, 1636 (1987).
9. J.A. Coxon, *J. Mol. Spectrosc.* **82**, 264 (1980).
10. T. Ishiwata, T. Shinzawa, T. Kusayanagi, and I. Tanaka, *J. Chem. Phys.* **82**, 1788 (1985).
11. B.P. Reid, N. Halberstadt, and K.C. Janda, *J. Chem. Phys.*, in press.
12. J.M. Parson, P.E. Siska, and Y.T. Lee, *J. Chem. Phys.* **56**, 1511 (1972).

13. R.A. Aziz, and H.H. Chen, J. Chem. Phys. 67, 5719 (1977).
14. J.E. Kenny, K.E. Johnson, W. Sharfin, and D.H. Levy, J. Chem. Phys. 72, 1109 (1980).

APPENDIX

SHAPE: A Working Manual

Introduction

The rotational structure of electronic excitation spectra of rare gas-halogen van der Waals molecules can be very complex. Although HeCl_2 has the least complicated spectrum, because of its large rotational constants, as the mass of the rare gas atom increases the rotational constants decrease and the number of accessible rotational states increases rapidly, even in a supersonic expansion. Also, homogeneous and inhomogeneous broadening tend to smooth the spectra and eliminate the possibility of making definitive frequency assignments to individual transitions. It would be very difficult to try to fit NeBr_2 or ArCl_2 spectra simply by line positions. Instead, an automated spectrum fitting program is essential to interpretation of the spectra.

Colin Western, a postdoctoral fellow, assembled such a spectrum fitting program for our research group. He used routines which he obtained from Herb Pickett, at the Jet Propulsion Laboratory, and made the necessary additions and modifications. These routines, known collectively as SHAPE, are the basis of the spectrum fitting program. This appendix first provides a theoretical basis for the routines in SHAPE by outlining the quantum mechanics of the asymmetric rigid rotor. Following this are operating instructions for SHAPE, as well as a few suggestions for

common modifications to this program. Beyond this, you are on your own.

Quantum Mechanics of the Asymmetric Rigid Rotor

The rare gas-halogen van der Waals molecules are not actually rigid rotors, but a reasonable description of the system may be made by assuming that the deviations from the equilibrium geometry are small. This assumption appears to be valid for complexes of Ne and Ar as with the halogens Cl_2 and Br_2 . In these cases the interaction of vibration and rotation may be treated quite accurately by perturbation theory. We have been quite successful treating these molecules as rigid rotors¹ and thus a brief discussion of the quantum mechanics of rigid asymmetric rotors will follow. There are several very good references for the description of asymmetric tops,^{2,3} so the following discussion will not be in complete detail.

The van der Waals molecule ArCl_2 is a good example of an asymmetric top. The excitation spectra of the $B \leftarrow X$ system of ArCl_2 in a free jet expansion have been obtained by a laser pump-probe technique.⁴ Analysis of the spectra indicate that the ArCl_2 complex has a T-shaped geometry in both the ground and excited states. The spectra can be reproduced using a rigid rotor Hamiltonian for both states. The ArCl_2 van der Waals molecule will serve as an example for this discussion.

The geometry of the ArCl_2 van der Waals molecule is shown in Figure 1. If we take the z axis as the symmetry axis, then the three principal moments of inertia are

$$I_z = \mu_m r^2 \quad (1a)$$

$$I_x = \mu_M R^2 \quad (1b)$$

$$I_y = I_x + I_z \quad (1c)$$

where μ_m is the Cl_2 reduced mass and μ_M is the Ne-Cl_2 reduced mass. The standard notation defines $I_a \leq I_b \leq I_c$ and correlation of a, b, and c with x, y and z depends upon the values of the moments of inertia. If none of the three moments of inertia are equal then the molecule is an asymmetric top. The rotational constants, A, B and C, may be obtained from the moments of inertia by the expression

$$A = \frac{h}{4\pi I_a} \quad (2)$$

and analogous expressions for B and C. The asymmetry of the molecule is quantified by an asymmetry parameter expressed as

$$\kappa = \frac{2A - B - C}{B - C} \quad (3)$$

where κ ranges from a value of -1 in the case of a prolate symmetric top ($B = C$) to a value of +1 for an oblate top ($A = B$). The rotational constants and κ are given for ArCl_2 X($v = 0$) and B($v = 7$) in Table I. It can be seen that ArCl_2 is a near prolate top in the ground state and is more asymmetric in the B state.

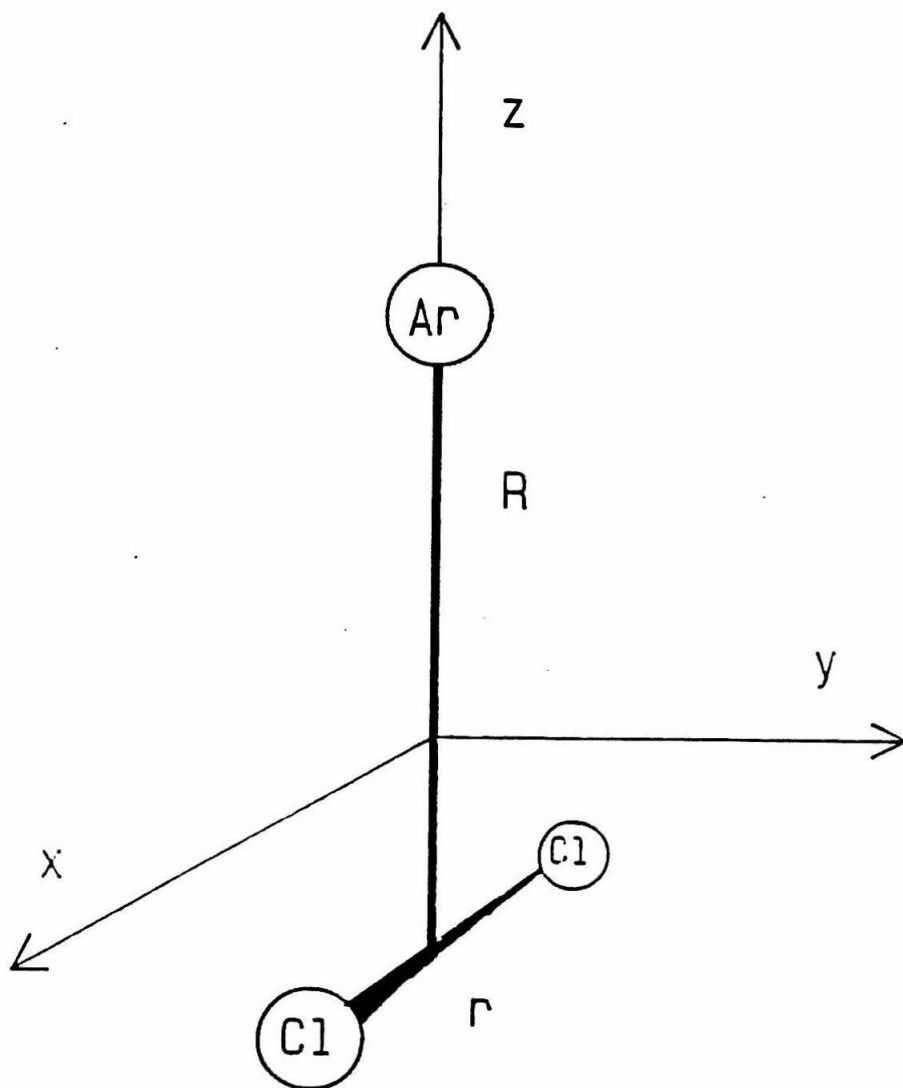


Figure 1. This is the axis system for the ArCl_2 van der Waals molecule in the body-fixed frame. The symmetry axis is taken to be the z axis and a right handed coordinate system is used.

Table I. Rotational Constants for ArCl_2

	$X(v = 0)$	$B(v = 7)$
A	0.2461 cm^{-1}	0.1500 cm^{-1}
B	0.0479 cm^{-1}	0.0493 cm^{-1}
C	0.0410 cm^{-1}	0.0371 cm^{-1}
κ	-0.933	-0.784

The next issue to address is the problem of calculating the energy levels of an asymmetric rotor. First select a body fixed axis system as shown in Figure 1, with the origin at the center of mass of the molecule and the axes coinciding with the principle axes of inertia. The quantum mechanical Hamiltonian for the rotation of a rigid asymmetric top is then

$$H_R = AJ_a^2 + BJ_b^2 + CJ_c^2 \quad (4)$$

where J_n is the angular momentum about a particular axis. The energy levels are obtained by solution of the Schrodinger equation

$$H_R \psi_{JM} = E \psi_{JM} \quad (5)$$

where ψ_{JM} are the wave functions and E , the corresponding eigenvalues, are the rigid asymmetric top energies. The rotational Hamiltonian is such that Equation (5) cannot be solved directly, so there are no analytical expressions for the wavefunctions. The asymmetric rotor wavefunctions may be expressed as a linear combination of symmetric rotor wavefunctions,

$$\psi_{JM}(\phi, \theta, \chi) = \sum_k c_k |JKM\rangle \quad (6)$$

$|JKM\rangle$, the symmetric rotor wavefunctions are

$$|JKM\rangle = \left[\frac{2J+1}{8\pi^2} \right]^{1/2} D_{MK}^J(\phi, \theta, \chi) \quad (7)$$

and D_{MK}^J are the Wigner functions.⁵ In both Equations (6) and (7) ϕ , θ , and χ are the Euler angles describing the rotation of the body fixed axes with respect to some set of

space fixed axes. Substituting Equation (6) into Equation (5), left-multiplying by $\langle JK'M |$ and integrating we can see that the energy levels may be determined by solving the $2J+1$ by $2J+1$ secular determinant

$$\left| \langle JK'M | H_R | JKM \rangle - E \delta_{K'K} \right| = 0 \quad (8)$$

where $\delta_{K'K}$ is the Kronecker delta. This is the brute force method to determine the energy levels of the asymmetric rotor, but the problem can be greatly simplified by taking advantage of the symmetry inherent in the rotational Hamiltonian.

The Hamiltonian describing the rotation of a rigid asymmetric rotor has symmetry properties which can be determined by considering its ellipsoid of inertia. The ellipsoid of inertia belongs to the D_2 point group, which consists of the identity element and two-fold rotations, C_2^a , C_2^b and C_2^c , about each of the three principal axes. The character table of the D_2 group is given in Table II. Ideally, the basis set which is used should have wave functions with the same symmetry as the species A, B_a , B_b and B_c of the D_2 group. This will simplify the entire problem because the only nonvanishing matrix elements would arise between states of the same symmetry. This result occurs because the symmetry species are orthogonal to each other and the Hamiltonian has A symmetry, thus the integral $\langle \psi_i | H_R | \psi_f \rangle$ is zero when $\langle \psi_i |$ and $| \psi_f \rangle$ do not have the same

Table II. Character Table of the D_2 point group

Symmetry Species	Symmetry Element			
	E	C_2^a	C_2^b	C_2^c
A	1	1	1	1
B_a	1	1	-1	-1
B_b	1	-1	1	-1
B_c	1	-1	-1	1

Table III.

Submatrix	K	γ	Symmetry Species ($K_{-1}K_1$)	
			J_{even}	J_{odd}
E^+	e	0	A (ee)	B_a (eo)
E^-	e	1	B_a (eo)	A (ee)
O^+	o	0	B_c (oe)	B_b (oo)
O^-	o	1	B_b (oo)	B_c (oe)

symmetry. Thus the secular determinant factors into four separate subdeterminants.

The symmetric rotor wave functions belong to the D_∞ point group and thus are an inappropriate choice for the basis set for this problem. Wang suggested an appropriate linear combination of symmetric rotor wave functions,⁶

$$|JKM\gamma\rangle = 2^{-1/2} [|JKM\rangle + (-1)^\gamma |J-KM\rangle] \quad \text{for } K > 0 \quad (9)$$

$$|JKM\gamma\rangle = |JKM\rangle \quad \text{for } K=0, \gamma=0 \quad (10)$$

where K is now non-negative. These linear combinations do belong to the D_2 point group. The four blocks are labeled E or O , depending upon the Even or Odd nature of K , and also $+$ or $-$, depending upon the value of γ . The correlation of the four symmetry species of D_2 is given in Table III.

The energy levels of the asymmetric top may be written as $J_{K_{-1}K_1}$, where K_{-1} and K_1 represent the K value in the prolate and oblate top limits, respectively. K is not a quantum number, but this labeling is convenient because the symmetry of the state may be determined easily. The K_{-1} value corresponds to the symmetry of the wave function with respect to a C_2 rotation about the a inertial axis, since this is the symmetry axis in the prolate top limit. If K_{-1} is odd, then the wave function is antisymmetric with respect to the two-fold rotation about the axis, which is denoted by the label "o," while the symmetric species is labeled "e." Similarly K_1 corresponds to the symmetry of

the wave function with respect to a rotation about the c axis, while the product of K_{-1} with K_1 corresponds to a rotation about the b axis. By examination of the character table of the D_2 point group given in Table II, correlations may be made regarding the nature of the $K_{-1}K_1$ labels and the associated symmetry species. Table III lists the appropriate submatrix and symmetry species for the combinations of $K_{-1}K_1$ for the prolate top. The most appropriate representation for the oblate top will change the entries in this table.

The next step is the calculation of the individual elements in each submatrix. The diagonal matrix elements in the right handed prolate top basis are given by the expression

$$\langle JKM\gamma | H_R | JKM\gamma \rangle = 1/2(B+C)[J(J+1)^2 - K^2] + AK^2 \quad (11)$$

while the off diagonal elements are expressed as

$$\begin{aligned} \langle JKM\gamma | H_R | JK\pm 2M\gamma \rangle = & 1/4(B-C)[J(J+1) - K(K\pm 1)]^{1/2} \\ & \times [J(J+1) - (K\pm 1)(K\pm 2)]^{1/2} \end{aligned} \quad (12)$$

Since we are working in the prolate top basis the K in the matrix element expressions is the K_{-1} value which is associated with K in the limit of the prolate top.

The energy levels may be calculated from the equations which are given here. The first step is to determine the symmetry of the particular energy level, which defines the determinant subblock to be used to calculate the energy. The energy may be calculated using Equations (11) and (12)

when the wave functions have been correctly written as shown in Equations (9) and (10). If there are two or more energy levels of the same symmetry, then the secular determinant is a 2x2 or larger matrix. For example, for $J = 3$, there are 3 2x2 secular determinants and one 1x1. This represents a great simplification from solving the 7x7 matrix which results if we do not take advantage of the symmetry inherent in the Hamiltonian.

The spectrum of the asymmetric rotor is determined not only by the energy levels of the ground and excited states, but is also governed by the selection rules that determine which transitions are allowed. If the integral $\langle \psi_i | \mu | \psi_f \rangle$ is non-zero, then the transition is allowed. In this integral ψ_i and ψ_f are the initial and final wave functions and μ is the transition dipole which carries the oscillator strength for the transition. The transition moment for the diatomic molecule Cl_2 lies along the Cl-Cl bond axis. This is the axis for the transition moment in ArCl_2 as well and since it is the b inertial axis, μ transforms as B_b in the D_2 character table. Thus the allowed transitions are $\langle A | B_b | B_b \rangle$ and $\langle B_a | B_b | B_c \rangle$ since these products give the totally symmetric A representation. The selection rules are written as

$$ee \longleftrightarrow oo \quad \text{and} \quad eo \longleftrightarrow oe$$

$$\text{or} \quad \Delta K_{-1} = \pm 1 \quad \text{and} \quad \Delta K_1 = \pm 1$$

with $\Delta J = 0, \pm 1$. The line frequencies of the transitions

may be used to assign the spectrum or the spectrum may be simulated by calculating the intensities and convoluting the transitions with the laser and homogeneous linewidths.

In summary, there are a number of steps which must be performed to generate the spectrum of an asymmetric top. A structure must be assumed and the rotational constants calculated for the ground and excited states. The symmetry of each energy level is determined, then the matrix elements for each subdeterminant are calculated and each submatrix is diagonalized. The energy levels are ordered according to the J and K labels and the allowed transitions are determined. The intensities are calculated and the spectrum is generated by convoluting the individual lines with a Voigt profile.

SHAPE

The routines which make up the SHAPE spectrum fitting package are currently found in the directories of `USR4:[11742.210165.SHAPE]` on the PITTVMs VAX cluster. The subdirectories `[...SPECOPT]`, `[...V2OPT]`, `[...SPLBOPT]` and `[...SLIB]` contain the source code for the respective object libraries which are necessary to link to `SHAPE.OBJ` in making an executable file. At the present time, in order to make an executable file you must submit a batch job because we do not have sufficient memory to link SHAPE interactively. The current file which will perform this

task is LINK.COM, and the important line is \$LINK SHAPE, SPECOPT/LIB,V2OPT/LIB,SPLBOPT/LIB,LIB/LIB,PRG:DISPLA/LIB.

The order in the library list is critical because of the way in which the linking routine performs its search for subroutines. We do not have any source code for the library PRG:DISPLA.OLB, which is supported by the VAX system.

In addition to the executable version of SHAPE, two files are necessary for fitting spectra. The first is the file which contains information about the Hamiltonian, atomic masses, frequencies, fitting regions, etc., as well as initial guesses for the parameters to be fit. The format of this file is outlined in the reference file SHAPE.DOC and is different when fitting diatomics or van der Waals complexes. Samples of each are given in DIATSMP.DAT and VDWSMP.DAT in the [..SHAPE] directory.

The second file which is necessary to run the SHAPE program is a file which contains the experimental parameters and the spectrum you want to fit. Samples of this file are given in DIATSMP.SPC and VDWSMP.SPC. The format of this file is determined by the subroutine RSPCT.FOR, which reads the spectrum from the _____.SPC file. The data is obtained on the free jet machine using a program written in PC-FORTH by Colin Western. There have been a number of modifications to the original PC program, most recently by Joe Cline to allow use of two dye lasers.

one doubled and the other with an angle-tuned etalon. The ____SPC file, generated by the data collection routines, can be transferred from the experimental files to the VAX using the FORTH emulator program entitled VAX. The file which is transferred to the VAX contains only the number of data points, the beginning and ending wavelengths and the data. A file header can be constructed from an existing example which fits the current RSPCT format. You must modify the header with the number of data points, the beginning and ending wavelengths and the first and last points, e.g., 0, 299 near the end of the ____SPC file.

The program is ready to be run once the ____SPC and ____DAT files are in the correct form. On the VAX system, the files must be assigned to FORTRAN logical unit numbers before program can be run. The first assignments are made using the A.COM and AP.COM command files which are in the [..COM] subdirectory. The following are the necessary commands.

```
$ assign __ plotdev (__ is the graphics output device
    number in the graphics routine GSTART. $ PC
    defines the PC running one of the FORTH emulator
    routines.)
$ a ____spc 4 (assigns ____SPC to FOR004)
$ ap ____ (assigns ____DAT to FOR009 and various
    output devices as necessary.)
$ rshape (RUN USR4:[11742.210165.SHAPE]SHAPE)
```

The first thing that SHAPE asks for as input is sigma, which is a linewidth for artificially broadening the experimental spectrum to help obtain an initial fit. If you do not want to use this feature simply hit return, <cr>. The spectrum is read from FOR004, then the number of points and the wavelength (cm^{-1}) of the maximum intensity point is displayed. Following a <cr> the entire spectrum is displayed on the screen, after which the twelve parameters which may be varied are printed out. These are the rotational temperature, the natural linewidth, the experimental (laser and Doppler) linewidth, the band shift, a scaling factor, the band origin and six parameters for the structure. These parameters can be either bond distances or rotational constants, depending on which of these the program is intended to vary. Any parameter may be changed by typing the appropriate number of commas, to leave the intermediate parameters unchanged, and then typing in the new value of that parameter followed by / <cr>. The rotational temperature, which is negative initially, must be changed to a positive value, greater than 1., for the first pass. On subsequent iterations the temperature may be set less than 1.

The second set of numbers which is displayed on the screen controls the fitting of parameters by the SHAPE program. The first value is the number of parameters to vary when fitting the experimental spectrum. The remaining

spaces are the parameters listed which are to be varied. For example, to float the rotational temperature, the natural linewidth and the band origin one would input 3,1,2,6/ <cr>. The final three numbers which can be changed are the accuracy required in fitting the spectrum, the initial step size to be used when varying the parameters and the maximum step.

The fitting process begins by fitting the spectrum by eye, varying the band origin (6) or the experimental offset, parameter (4). After the experimental and calculated spectra overlap, the SHAPE fitting routine may be used to vary the structural parameters to fit the experimental spectrum. The fitting process may be repeated as many times as necessary to obtain a satisfactory fit. The rotational temperature should be varied manually to obtain the best sum of the squares of the deviations, because SHAPE is unwilling to vary this parameter widely from its initial value. The entire process is an iterative one, employing some manual fitting as well as computer fitting. The program is terminated by entering a negative rotational temperature. This is the correct way to stop SHAPE and is essential to close the files created when using SHAPE to generate a plot file or a data file.

There are several problems which occur commonly that can be easily solved. The first is a difference in the header between the file in FOR004 and RSPCT, the routine

which reads this file. The two must be compatible and it is simply a matter of editing the _____.SPC file to be sure that the header has the correct format. The next problem is that the experimental spectrum and the calculated spectrum do not overlap at all, i.e., the calculated spectrum is being generated over an entirely different frequency region. This is a fatal error and causes the program to stop. This may be remedied easily by checking that the band origin of the calculated spectrum, parameter (6), minus the offset, (4), is near the maximum of the experimental spectrum as printed at the start of the run. Finally, the rotational temperature must be greater than one degree, and yes that means it must be positive.

There are several modifications which can be made to the SHAPE program. The first is to modify RSPCT if the _____.SPC file format is changed and someone feels the need to make the process more convenient. This is done by simply modifying the READ statement of RSPCT to be compatible with the header of the _____.SPC file. The parameters which are currently used are TITLE, SPCTSI, START, ENDSPC, FIRSTP, LASTP and the spectrum is read into SPCT. The title is not essential, but is printed out when running SHAPE. If a new version of RSPCT is prepared then the object module must be placed in the object library SPECOPT.OLB for linking with SHAPE.

Another modification which has been made is to allow fitting the spectra by varying the rotational constants rather than the structural parameters. This new version of SHAPE is entitled ROTCON.FOR and the source code is in the [..SHAPE] directory. You may peruse that program to see the changes which were necessary. This was a fairly simple modification, but I think that any other changes may end up being quite complex, so I wish you the best. Finally, the source code for all of the subroutines is somewhere in the laboratory, compiled in a notebook entitled, oddly enough, SHAPE.

References

1. D.D. Evard, F. Thommen, and K.C. Janda, *J. Chem. Phys.* **84**, 3630 (1986).
2. W. Gordy, and R.L. Cook, *Microwave Molecular Spectra*, 3rd Ed. (John Wiley & Sons, Inc., New York, 1984).
3. R.N. Zare, *Angular Momentum in Quantum Mechanics* (manuscript in preparation).
4. D.D. Evard, J.I. Cline, N. Sivakumar, and K.C. Janda, manuscript in preparation.
5. E.P. Wigner, *Group Theory* (Academic Press, Inc., New York, 1959).
6. S.C. Wang, *Phys. Rev.* **34**, 243 (1929).